

TRANSLATING OPHTHALMOLOGIC DRUG DELIVERY SYSTEMS  
FROM THE BENCH TO CLINICAL TRIALS

AN ABSTRACT

SUBMITTED ON THE TWENTY FOURTH DAY OF NOVEMBER 2020

TO THE BIOINNOVATION PROGRAM

IN PARTIAL FULFILLMENT OF THE REQUIREMENTS

OF THE SCHOOL OF SCIENCE AND ENGINEERING

OF TULANE UNIVERSITY

FOR THE DEGREE OF

DOCTOR OF PHILOSOPHY

BY

  
\_\_\_\_\_  
Mitchell L Fullerton

APPROVED:



Diane A. Blake, Ph.D., Director



Ramesh S. Ayyala, M.D.



Vijay T. John, D.Eng.Sc.



Louise B. Lawson, Ph.D

## **Abstract**

Glaucoma is a debilitating and insidious disease and is the world's leading cause of irreversible blindness. There have been many proposed innovations in the ophthalmology space though few have successfully been implemented in humans. The gap between proof of concept studies and market launch has been termed the "valley of death." The Blake, Ayyala, and John research group have been endeavoring to bring two drug delivery systems through this "valley of death" for the last ten years. These products aim to solve a common problem in glaucoma surgery: post-surgical fibrosis resulting in the need for revision surgery. The two drug systems are a poly(hydroxyl ethyl methacrylate) hydrogel loaded with mitomycin C and a biodegradable poly(lactic-co-glycolic acid) matrix loaded with 5-fluorouracil and mitomycin C. These anti-fibrotics, when released into the surgical site, successfully reduced scar tissue formation in animal models. To translate these technologies to market, we created methods to interrogate their synthesis, studied their properties after sterilization, and performed longitudinal studies to determine their stability.

For the pHEMA-based drug delivery system, we introduced a new casting method and compared it to previous studies. This new method reduced casting time two-fold and increased lot-to-lot reproducibility. We also developed an assay for quantifying the amount of drug loaded into each hydrogel. Using this assay, we reduced the loading time of the hydrogels two-fold by more than 5 days. The product was then gamma and e-beam sterilized to determine how sterilization would affect the hydrogel. We showed that the hydrogel releases mitomycin C more slowly after gamma irradiation than after e-beam and that both releases were slower than unsterilized material. This indicates that the hydrogel has cross-linked during the sterilization process.

For the PLGA-based drug delivery system, we developed a solvent extraction method for quantifying the amount of drug in each piece. We then used this assay to interrogate different steps in the manufacturing process. We discovered the need for a new casting method using a positive displacement pipette. We tested the homogeneity of the 5-fluorouracil within the polymer matrix and discovered that drug distribution in our films was uniform. We ensured that we could reproducibly create lots of these films. Then, we tested the stability of this drug delivery system after gamma irradiation. We performed a longitudinal shelf-life study to see how temperature and the presence of air could affect the system during 3 months of storage. We then lyophilized our product and compared e-beam and gamma sterilization techniques. These studies contributed to an investigational new drug filing with the FDA which is the next milestone for a drug product before first-in-human trials.

TRANSLATING OPHTHALMOLOGIC DRUG DELIVERY SYSTEMS  
FROM THE BENCH TO CLINICAL TRIALS


A DISSERTATION  
SUBMITTED ON THE TWENTY FOURTH DAY OF NOVEMBER 2020  
TO THE BIOINNOVATION PROGRAM  
IN PARTIAL FULFILLMENT OF THE REQUIREMENTS  
OF THE SCHOOL OF SCIENCE AND ENGINEERING  
OF TULANE UNIVERSITY  
FOR THE DEGREE OF  
DOCTOR OF PHILOSOPHY

BY

  
\_\_\_\_\_  
Mitchell L Fullerton

APPROVED:

  
\_\_\_\_\_  
Diane A. Blake, Ph.D., Director

  
\_\_\_\_\_  
Ramesh S. Ayyala, M.D.

  
\_\_\_\_\_  
Vijay T. John, D.Eng.Sc.

  
\_\_\_\_\_  
Louise B. Lawson, Ph.D



## **Acknowledgments**

There are many who deserve credit for the completion of this document either for moral, scientific, or technical support. First and foremost, I would like to thank my parents, Jon and Tyra Fullerton, who managed to raise twin boys to adulthood despite our predilections toward losing our swim floaties mid-swim, biking in traffic, and starting small fires. Being raised in an environment with ample play and exploration led me to my field of study and I owe you an innumerable debt for all you gave to ensure my success. My sister, Hannah Hanegan, and her family shared the city of New Orleans with me during my studies. It has been a joy to see my niece and nephew grow into precocious future scientists. My brother, Garrett Fullerton, and sister-in-law were able to stay in New Orleans and gifted me one of the best years of my education. Thank you, Hannah, Kevin, Laena, Caleb, Garrett, and Ana. I'll never again take for granted a family visit. Thank you to my late grandfather, Bruce Fullerton, whose gifted yearly subscriptions to Popular Science magazine had a more lasting impression than I think he ever realized. I'd like to thank my scientific mentors, Dr. Diane Blake, Dr. Ramesh Ayyala, and Dr. Vijay John who have afforded me opportunities to learn in and out of the lab. I'd like to thank John Christie, Shafin Kahn, Greg Stein, and the Tulane Office of Technology Transfer for the opportunity to intern for you and your introduction to my career field. Thank you to the Bioinnovation Program and for Dr. Don Gaver, Rosie, and Dr. Anne-Marie Job's dedication and passion, which keeps the program running. Thanks to my undergraduate mentors, Dr. Mark Batzer and Dr. Vladimir Reukov, who encouraged me early to take the dive into graduate school. Thank you to my community of friends who kept me sane with game nights, ice cream runs, hammock days, and meals shared. Particular thanks to Peter Lawson and Jessica Motherwell,

our soul-roommates; Erika and Garrett Broadnax; Dan Guidice, and Cameron Williams. Being around you is a joy, and Devon and I are so grateful for your friendship. Finally, I'd like to thank my brilliant wife, Devon Bowser. We started and finished this PhD journey together. Thank God it's not the end of our travels.

## Table of Contents

Abstract.....	
Acknowledgments.....	i
Table of Contents.....	iii
List of Figures .....	vii
Chapter 1 Introduction .....	1
1.1 Glaucoma .....	1
1.1.1 Anatomy of Structures Involved in Glaucoma .....	2
1.1.2 Aqueous Humor .....	3
1.1.3 Intraocular Pressure.....	3
1.1.4 Glaucoma Characterization.....	3
1.1.5 Glaucoma Treatment .....	4
1.2 Fibrosis .....	6
1.3 Wound healing.....	9
1.3.1 Inflammation.....	9
1.3.2 Proliferation .....	9
1.3.3 Maturation .....	10
1.4 Antifibrotic Agents .....	11
1.4.1 5-Fluorouracil (5-FU) .....	11
1.4.2 Mitomycin C (MMC).....	12
1.5 Polymers as Drug Delivery Systems .....	14
1.5.1 Hydrogels .....	15
1.5.2 Biodegradable Polymers .....	15
1.5.3 Poly(hydroxyethyl methacrylate) (pHEMA) .....	16
1.5.4 Poly(lactic-co-glycolic acid) (PLGA) .....	17
1.6 Previous Work.....	18
1.6.1 pHEMA Drug Delivery System.....	18
1.6.2 PLGA Drug Delivery System .....	19
1.6.3 In Vivo Studies of Drug Delivery Systems .....	21



1.7 Bench-to-Bedside Translation.....	23
1.7.1 Sterilization .....	24
1.7.2 Stability .....	26
1.7.3 Current Good Manufacturing Practice.....	26
1.7.4 Clinical Trials .....	27
1.8 Aims of the thesis project .....	28
Chapter 2 - AIM 1: Translating a p(HEMA)-based drug delivery system for good manufacturing practice (GMP) .....	30
2.1 Introduction .....	30
2.2 Materials and Methods.....	33
2.2.1 Materials .....	33
2.2.2 Casting Hydrogel Disks.....	34
2.2.3 p(HEMA) Disk Weight.....	35
2.2.4 Drug Loading .....	35
2.2.5 Drug Quantification.....	35
2.2.6 PBS Release .....	35
2.2.7 Cytotoxicity .....	36
2.3 Results.....	37
2.3.1 Sheet vs Mold Cast Loading Efficiency.....	37
2.3.2 6-hour vs 12-hour Weight.....	37
2.3.4 6-hour vs 12-hour Ethanol Quantification .....	38
2.3.5 6-hour vs 12-hour PBS Release .....	38
2.3.6 6-hour v 12-hour Cytotoxicity .....	38
2.4 Discussion.....	39
2.5 Conclusion.....	41
Chapter 3 - Aim 2: Translating a PLGA-based drug delivery system to a good manufacturing practice (GMP) facility .....	43
3.1 Introduction .....	43
3.2 Materials and Methods.....	45
3.2.1 Materials .....	45
3.2.2 Drug Quantification.....	46
3.2.3 Pipette Test .....	47
3.2.4 Casting the Films .....	48

3.2.5 Homogeneity.....	49
3.2.6 Kinetics of drug release into PBS .....	50
3.2.7 Cytotoxicity .....	50
3.3 Results.....	51
3.3.1 Determining the best pipetting technique for casting PLGA films .....	51
3.3.2 Lot-to-Lot Drug Quantification.....	52
3.3.4 Homogeneity Study.....	52
3.3.5 Kinetics of drug release into PBS .....	53
3.3.6 Cytotoxicity .....	54
3.4 Discussion.....	54
3.6 Conclusion.....	56
Chapter 4 - Aim 3: Sterilization and storage considerations for novel pHEMA and PLGA-based drug delivery systems .....	58
4.1 Introduction .....	58
4.2 Materials and Methods.....	60
4.2.1 Materials .....	60
4.2.2 Casting of p(HEMA) Disks.....	61
4.2.3 Casting of PLGA Wafer .....	61
4.2.4 Comparison of UV and Gamma Sterilization of PLGA.....	62
4.2.5 Longitudinal Study Storage Conditions and Sterilization.....	62
4.2.6 GMP Manufacturing and Packaging.....	63
4.2.7 GMP Product Gamma vs. E-Beam Sterilization Run .....	63
4.2.8 PBS Release Studies .....	64
4.2.9 Cytotoxicity Study .....	64
4.2.10 Statistical Analysis and Curve Fit.....	65
4.3 Results.....	66
4.3.1 Preliminary UV and Gamma Irradiation Test.....	66
4.3.2 Longitudinal Storage Study in vitro Release after Gamma Irradiation .....	68
4.3.3 Longitudinal Storage Study Cytotoxicity Assay after Gamma Irradiation.....	69
4.3.4 GMP Manufactured and Sterilized PLGA Wafers.....	72
4.3.5 GMP Manufactured and Sterilized p(HEMA) Disks.....	74
4.4 Discussion.....	75
4.4.1 Comparison of UV and Gamma Sterilized PLGA Wafers.....	75

4.4.2 Longitudinal Storage Study of Gamma Sterilized PLGA Wafers .....	76
4.4.3 Comparison of Gamma and E-beam Sterilization Techniques with GMP Manufactured PLGA Wafers .....	77
4.4.4 Comparison of Gamma and E-beam sterilization with GMP Manufactured p(HEMA) 77	
4.5 Conclusion.....	79
Chapter 5 - Glaucoma Market Landscape and Challenges .....	81
Chapter 6 - Conclusion and Future Work .....	85
References .....	88
Supplementary Information .....	97
Appendix - Injectable drug delivery systems .....	106
A.1 Hyaluronic acid particles.....	106
A.2 Physical conjugation of MMC to hyaluronic acid .....	108
Biography .....	111

## List of Figures

Figure 1.1 Anatomy of structures involved in glaucoma .....	2
Figure 1.2 Anatomy of filtering surgery .....	4
Figure 1.3 Glaucoma drainage device .....	5
Figure 1.4 Image of a bleb .....	6
Table 1.1 Organs affected and disease states of fibrosis.....	7
Figure 1.5 Progression of fibrosis .....	8
Figure 1.6 Six modes of fibrosis .....	9
Figure 1.7 Timeline of wound healing .....	10
Figure 1.8 Structures of Uracil, 5-Fluorouracil, and Thymine. ....	12
Figure 1.9 Reductive alkylation of MMC .....	13
Figure 1.10 Routes of drug release in biodegradable system .....	14
Figure 1.11 Structure of pHEMA .....	16
Figure 1.12 Structure of PLGA and its monomers .....	17
Figure 1.13 Ayyala pHEMA drug delivery system .....	19
Figure 1.14 Ayyala PLGA drug delivery system .....	20
Figure 1.15 A breath figure formed on PLGA .....	21
Figure 1.16 Results of p(HEMA) rabbit study .....	22
Figure 1.17 Bleb thickness results of <i>in vivo</i> rabbit study .....	23
Figure 1.18 The “valley of death” for translational research .....	24
Figure 2.1 New molding method .....	33
Figure 2.2 Drug loading set-up of p(HEMA) disks .....	34
Figure 2.3 The percent theoretical yield for sheet and mold-cast pHEMA disks .....	36
Figure 2.4 Weights of 6 and 12-hour p(HEMA) disks .....	37
Figure 2.5 Drug yield of 6 and 12-hour p(HEMA) disks .....	38
Figure 2.6 PBS release of 6 and 12-hour p(HEMA) disks .....	39

Figure 2.7 A representative plate of COS-1 staining .....	40
Figure 2.8 12 and 6-hour disks loaded with 6.5 $\mu$ g of MMC .....	41
Figure 3.1 Determining the best pipetting method for use in casting a PLGA solution .....	46
Figure 3.2 Drug quantification study with lots compared and lots averaged .....	47
Figure 3.3 5-FU is homogeneously dispersed in the films .....	48
Figure 3.4 The 5-FU is homogeneously dispersed in the films .....	49
Figure 3.5 The release profiles of films n=9 with the lots compared and the lots averaged .....	52
Figure 3.6 Cytotoxicity of 5-FU and 5-FU with MMC in PLGA films .....	53
Figure 4.1 Theoretical <i>in vitro</i> release of the MMC from the p(HEMA) fitted to the exponential decay equation .....	64
Figure 4.2 Example of Hill equation for release analysis .....	65
Figure 4.3 UV and gamma-sterilized films shown immediately after and 6 months after sterilization .....	67
Figure 4.4 The sigmoidicity coefficients from the releases decrease as the films are stored for longer .....	68
Figure 4.5 This graph depicts the C coefficient (day of 50% release) from the curve fits of each data set .....	69
Figure 4.6 The release profile of the PLGA wafers in PBS changes after 3 months in storage .....	70
Figure 4.7 The sigmoidicity from the curves of the releases decrease as the films are stored for longer .....	70
Figure 4.8 The curves show the time in the 50% release happening earlier with longer storage. ....	71
Figure 4.9 Cytotoxicity data from PLGA wafers stored under the most stringent storage conditions (4°C under vacuum) .....	72
Figure 4.10 The release profile of the PLGA wafers in PBS changes under three sterilization conditions, unsterilized, gamma sterilized and e-beam sterilized. ....	73
Figure 4.11 The sigmoidicity from the curves of the unsterilized, gamma sterilized, and e-beam sterilized films. ....	73
Figure 4.12 The day of 50% drug release for the unsterilized, gamma sterilized and e-beam sterilized films. ....	74
Figure 4.13 <i>In vitro</i> release of MMC from pHEMA disks .....	78
Table 5.1 Competitors.....	82

## Chapter 1 Introduction

The thesis describes the process of translating a polymer-based drug delivery system for use in glaucoma surgery from an academic setting to a commercially available product.

Glaucoma surgeries suffer from a lack of consistency between surgeons with respect to administering antimetabolites during and after surgery. These antimetabolites help prevent the non-functional fibrosis and scarring that limit the efficacy of the surgery. Here, we introduce the anatomy and physiology of glaucoma, glaucoma surgery, the mechanisms of fibrosis and wound healing, and the hurdles for these drug delivery systems in their last steps toward use in patients.

### 1.1 Glaucoma

Glaucoma is a group of disease states characterized by damage to the optic nerve. It is the leading cause of irreversible blindness in the world.<sup>1</sup> Increased intraocular pressure (IOP) is the most common underlying optic neuropathy, but not all glaucomas exhibit this as a risk factor.<sup>2</sup> **Figure 1.1** illustrates the flow of aqueous humor in the anterior chamber and indicates where the drainage is occluded in glaucomatous eyes. The dynamics surrounding the aqueous humor and its role in increased IOP are well understood compared to the underlying causes of glaucoma. Thus, techniques for modulating aqueous humor flow have emerged as the leading approaches for preventing glaucoma. It is likely that as our understanding of the causes of glaucoma changes, our classification and treatment of these disease states will also change. According to the 2014 Cheng et al. meta-analysis, an estimated 64.3 million people between the ages of 40 and 80 have glaucoma.<sup>3</sup> That number is projected to increase to 76 million by the end

of 2020 and 111.8 million by 2040. Asia is the most heavily impacted with approximately 60% of cases.<sup>3</sup>

### 1.1.1 Anatomy of Structures Involved in Glaucoma

The structures most relevant to aqueous humor dynamics are located in the limbus, the transitional section between the cornea and the sclera in the eye. The scleral sulcus is an indentation on the limbus that contains the trabecular meshwork. The trabecular meshwork bridges the scleral sulcus and creates a tube called Schlemm's canal. Aqueous humor flows from the anterior chamber in front of the iris through the trabecular meshwork into Schlemm's canal.

Intrascleral channels then connect Schlemm's canal to the episcleral veins where the aqueous humor is circulated. These three structures, the trabecular meshwork, Schlemm's canal, and the intrascleral channels constitute the

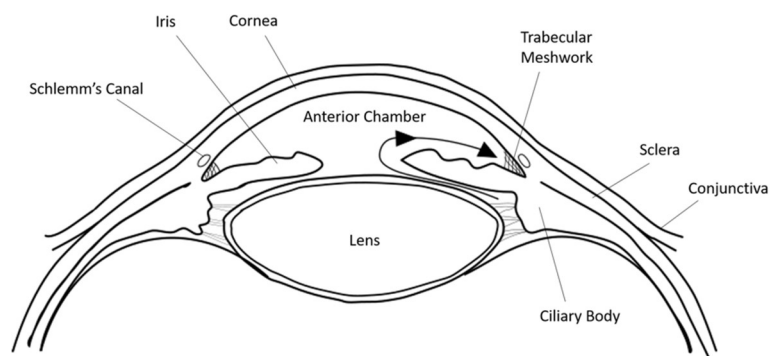


**Figure 1.1:** Anatomy of structures involved in glaucoma. The arrows indicate flow of aqueous humor from the ciliary body, through the pupil, and out of the trabecular meshwork. In many glaucomas, this flow has been disrupted which results in increased intraocular pressure. (Adapted from Shields Textbook of Glaucoma)<sup>1</sup>

primary route of outflow for aqueous humor.<sup>2</sup>

In the posterior chamber, behind the iris is the ciliary body. This structure attaches to a protrusion of the scleral sulcus, the scleral spur. The innermost portion of the ciliary body is known as the ciliary processes and is where aqueous humor production takes place.

The iris inserts on the anterior side of the ciliary body and separates the aqueous humor compartment into anterior and posterior chambers. The angle formed by the iris and the cornea

is called the anterior chamber angle.<sup>3</sup> **Figure 1.1** shows an anatomical cross-section of the anterior chamber and the direction of normal aqueous flow.

#### *1.1.2 Aqueous Humor*

The aqueous humor maintains proper intraocular pressure, provides nutrients, and removes waste products within the eye while remaining optically colorless and transparent. Approximately 1-1.5% of the aqueous humor volume is recycled every minute in typical flow.<sup>4</sup> This flow rate is subject to changes in the circadian rhythm. If this flow is obstructed, the IOP begins to elevate.<sup>5 6</sup>

#### *1.1.3 Intraocular Pressure*

Intraocular pressure (IOP) is the most utilized measurement in the detection and prevention of glaucoma. It is a complex variable that is determined by inflow and outflow of the aqueous humor as well as venous pressure in the episcleral vasculature. Normal IOP is around 13-17 mmHg while IOPs above 20 mmHg often indicate a likelihood of glaucoma development and require further examination by the physician.<sup>7,8</sup>

#### *1.1.4 Glaucoma Characterization*

As previously stated, glaucoma is a group of diseases resulting in optic nerve damage. Most glaucomas are characterized by an increase in IOP, which causes damage to the optic nerve leading to irreversible blindness. Glaucoma can be characterized anatomically as open-angle or closed-angle glaucoma. The angle in question is formed by the iris and the cornea with the vertex comprising of the trabecular meshwork. In open-angle glaucoma, the anterior chamber angle of the eye is unobstructed so aqueous humor can flow through the pupil but the trabecular meshwork is obstructed. Open-angle glaucoma is the most prevalent type of glaucoma in the United States. In closed-angle glaucoma, the anterior chamber angle is obstructed restricting flow to the trabecular meshwork.



### 1.1.5 Glaucoma Treatment

The first line of defense against glaucoma is topical pharmacologic therapy. Many of these topical agents work by targeting the aqueous humor dynamics to reduce the IOP;  $\beta$ -blockers and carbonic anhydrase inhibitors reduce the secretion of aqueous humor from the ciliary body while prostaglandins increase the flow of aqueous humor out of the trabecular meshwork. These medications

require application up to three times daily. Additionally, these medications have adverse side effects including ocular irritation, conjunctivitis, hypertrichosis of the eyelashes, and iris pigmentation. These adverse side

effects, especially ocular irritation, can lead to decreased patient compliance. For glaucoma that is unresponsive to therapeutics, or for patients that are unwilling to comply with a treatment regimen, the next option is surgical intervention.<sup>4</sup>

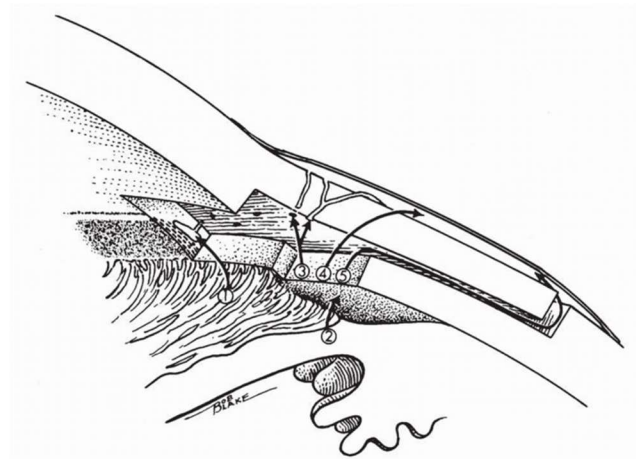


**Figure 1.2:** Anatomy of filtering surgery. Here you see a cross section of the trabecular meshwork, the scleral spur, the scleral flap that remains after filtration surgery, and routes of filtration after surgery. 1. Aqueous flow into the cut ends of Schlemm's canal, which is rare; 2. Cyclodialysis can happen if the tissue is dissected posterior to the scleral spur; 3. Filtration through outlet channels in scleral flap; 4. Filtration through connective tissue of scleral flap; 5. Shows filtration through the margins of the scleral flap. (Adapted from Shields Textbook of Glaucoma)<sup>1</sup>

Filtering surgery is used to divert the flow of aqueous from the anterior chamber into the subconjunctival space to reduce the IOP. In a trabeculectomy, an opening called a fistula is made at the transition between the sclera and the cornea known as the limbus. This incision bypasses the trabecular meshwork, allowing aqueous humor to flow out into the subconjunctival space. This reduces IOP by reducing the volume of aqueous humor in the eye.

**Figure 1.2** is an anatomical drawing of the scleral flap and routes of aqueous drainage following filtering surgery.

An alternative mechanism used to remove aqueous from the anterior chamber and divert flow into the subconjunctival space is glaucoma drainage device (GDD) surgery. In this technique, flow from the anterior chamber is facilitated by a tube that is used to shunt the trabecular meshwork and divert flow through a plate in the subconjunctival

space.<sup>5,6</sup> Glaucoma drainage device surgery seeks to maintain the drainage fistula by implanting a material to shunt the opening. These devices span the length of the fistula from the anterior chamber to the subconjunctival space. Usually, a tube is used to divert the aqueous humor from the anterior chamber to a plate or other flat disk that prevents obstruction of the tube and permits flow into the subconjunctival space. **Figure 1.3** shows a typical placement of a glaucoma drainage device and the flow of the aqueous out of the plate.

Most filtering and glaucoma drainage device surgeries create an elevation of the conjunctiva at the surgery site, known as a bleb, with glaucoma device surgery forming thicker encapsulating blebs. **Figure 1.4** shows a bleb following device surgery.<sup>10</sup> The different morphologies of these encapsulating blebs are thought to be caused by the chronic wound healing process that occurs due to a foreign body response or micromotion of the GDD plate on the sclera. Functioning blebs have normal epitheliums with few tight junctions between cells, which would restrict flow, and loose subepithelial connective tissue. Failed blebs have dense networks of collagen at the subepithelial level. This collagen deposition is due to overactive

Tube is placed through the  
Trabecular meshwork

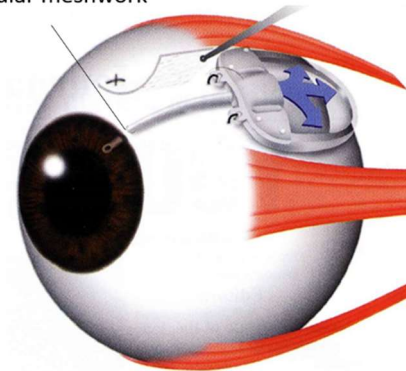


**Figure 1.3:** Glaucoma drainage device. This is an image of the Ahmed Valve, one of several glaucoma drainage devices currently in use. (Adapted from New World Medical)<sup>9</sup>

wound healing. The factors that indicate an individual predisposition towards excess scarring are disparate and varied but include race, age, genetics, and previous medical history.

Despite their differences, both filtering surgery and glaucoma drainage device surgery have been recommended as viable options for managing glaucoma. Although, one study reported higher failure rates in trabeculectomy than in glaucoma drainage device surgery.<sup>11</sup>

## 1.2 Fibrosis

Fibrosis is the deposition of excess extracellular matrix during aberrant wound healing that leads to impaired organ function. Forty-five percent of deaths in the west are caused by or comorbid with fibrosis. Fibrosis can occur in any organ and is a component of many disease states.

**Table 1.1** lists the various disease states affected by fibrosis organized by organ.

Fibrosis is caused when the wound healing process fails. **Figure 1.5** shows a typical route to fibrosis. As a result of an insult to the epithelium, transforming growth factor-beta

(TGF $\beta$ ), matrix metalloproteases (MMPs), interleukins, and other cytokines are released, which leads to fibroblast recruitment and differentiation. In fibrosis, this cascade does not cease with the repair of the original damage. Instead, the release of growth factors leads to epithelial-mesenchymal transition, increasing the presence of myofibroblasts and leading to increased extracellular matrix deposition and decreased reabsorption of ECM. The six modes of fibrosis (**Figure 1.6**)<sup>12</sup> are profibrotic inflammation, profibrotic signaling, myofibroblast activation, extracellular matrix assembly, cell loss via apoptosis, and the generation of reactive oxygen species. These modes are all interwoven and collectively contribute to greater scarring and ECM

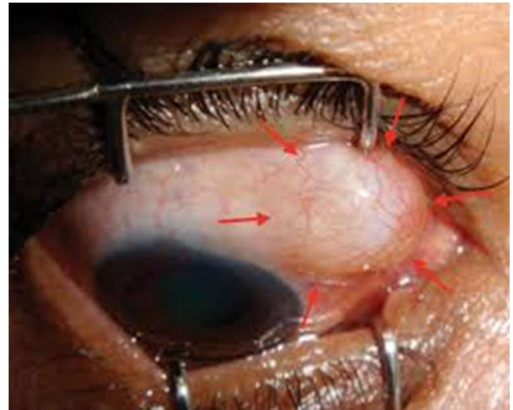


**Figure 1.4:** Image of a bleb. (Adapted from Suzuki et al)<sup>10</sup>

maturation. In profibrotic inflammation, the innate immune system is activated and responds to the initial injury. Profibrotic signaling is initiated by platelets releasing cytokines, including TGF $\beta$  and PDGF. Additional cytokines and MMPs also contribute to profibrotic inflammation. Immune cell production of reactive oxygen species leads to necrotic cell death and apoptosis of surrounding cells. Myofibroblasts are activated during the immune response and the endothelial to mesenchymal transition is spurred by profibrotic signaling and inflammation.

<b>Table 1.1 Organs affected and disease states of fibrosis</b>	
<b>Organ</b>	<b>Disease State</b>
Lung	Idiopathic Pulmonary Fibrosis, Cystic Fibrosis
Liver	Non-Alcoholic Fatty Liver Disease/Non-Alcoholic Steatohepatitis (NAFLD/NASH), Primary Sclerosing Cholangitis, Cirrhosis
Skin	Scleroderma, Keloid scars
Kidney	Chronic Kidney Disease
Heart	Heart Failure, Atrial Fibrosis, Endomyocardial Fibrosis
Intestine	Irritable Bowel Disease, Crohn's
Brain	Glial Scar
Eye	Corneal scarring, lens fibrosis, certain glaucomas
Other	Fibrous cancers, excessive wound healing

There are only two drugs currently on the market for fibrosis: Nintedanib and Pirfenidone.<sup>13</sup> Nintedanib targets both receptor tyrosine kinases (RTK), including PDGFR and FGFR, and non-receptor tyrosine kinases (nRTK). Nintedanib competitively inhibits these RTKs and nRTKs, which reduces fibroblast proliferation. Pirfenidone inhibits transforming growth factor beta (TGF $\beta$ ). Many extracellular matrix molecules have regions in their promotor that are

activated by TGF $\beta$ .<sup>14</sup> Thus, pirfenidone reduces the deposition of collagen, fibroblast proliferation, and the levels of other inflammatory cytokines.

In the eye, fibrosis is seen after filtration surgery to treat glaucoma. After one to six weeks post-surgery, a thick-walled bleb with prominent vascularity called Tenon's cyst is formed. This is known as

the hypertensive phase. Scarring of the filtering bleb is the most common cause of failure in filtering surgery.

Aqueous humor constituents, age, and genetics all play a role in the wound healing process in the eye.<sup>15</sup> A typical cascade of fibrosis in the eye would see the

damaged conjunctiva and sclera releasing cytokines to recruit inflammatory cells. A

breakdown of the blood-aqueous barrier would cause a release of growth factors. Then

Inflammatory cells would migrate and proliferate. This would cause the activation, migration,

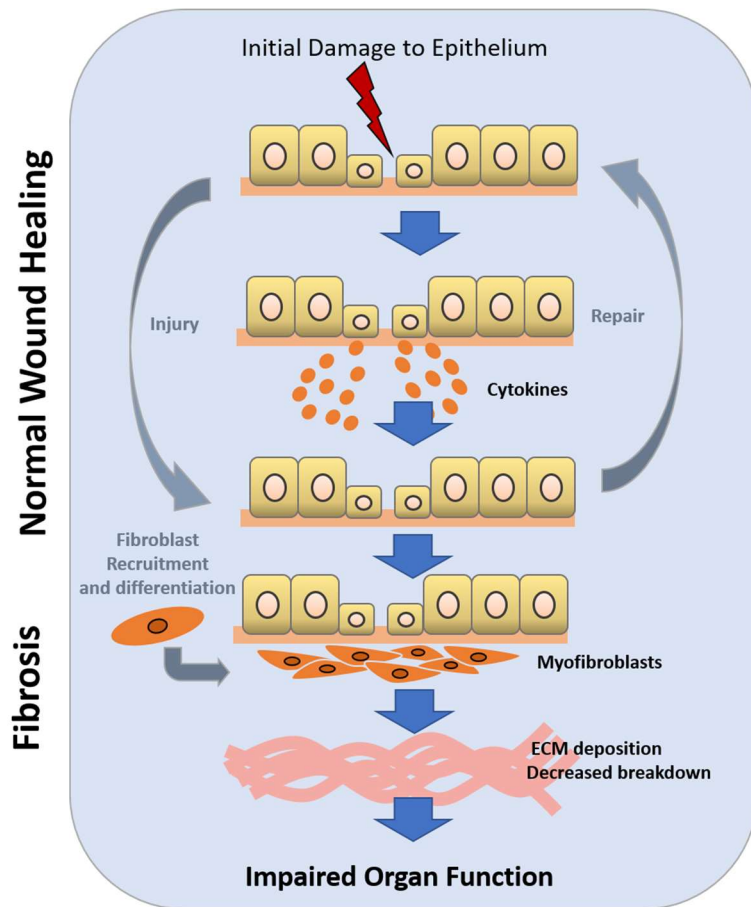


**Figure 1.5:** Progression of fibrosis. The process of normal wound healing response is exacerbated, and the inflamed organ undergoes aberrant wound healing. In glaucoma surgery, it is possible that the presence of the glaucoma drainage device causes prolonged wound healing and scar tissue formation. (Adapted from Atkinson et al)<sup>12</sup>

and proliferation of fibroblasts, which would differentiate into myofibroblasts that contract the wound. If unchecked, the fibroblast can create a fibrous subconjunctival scar.

### 1.3 Wound healing

Normal wound healing is divided into three stages: inflammation, proliferation, and maturation. **Figure 1.7** graphs a timeline of wound healing with the migration of immune cells to the wound.<sup>16</sup> Here, we describe these stages from the perspective of glaucoma surgery.

#### 1.3.1 Inflammation

After tissue damage, the body attempts hemostasis by constricting the blood vessels at the surgery site. The ruptured cells release cytokines including transforming growth factor-alpha and beta (TGF $\alpha$ , TGF $\beta$ ) and platelet-derived growth factor (PDGF) that recruit neutrophils, lymphocytes, and monocytes to the wound site. These immune cells remove foreign bodies and release cytokines to facilitate wound healing. Profibrotic plasma proteins such as fibrinogen, fibronectin, and plasminogen leak into the tissue to form a clot.

#### 1.3.2 Proliferation

Fibroblasts, activated by TGF $\beta$ , migrate and proliferate in the surgery site around five days post-surgery as indicated in animal models. This migration is shown to return to baseline

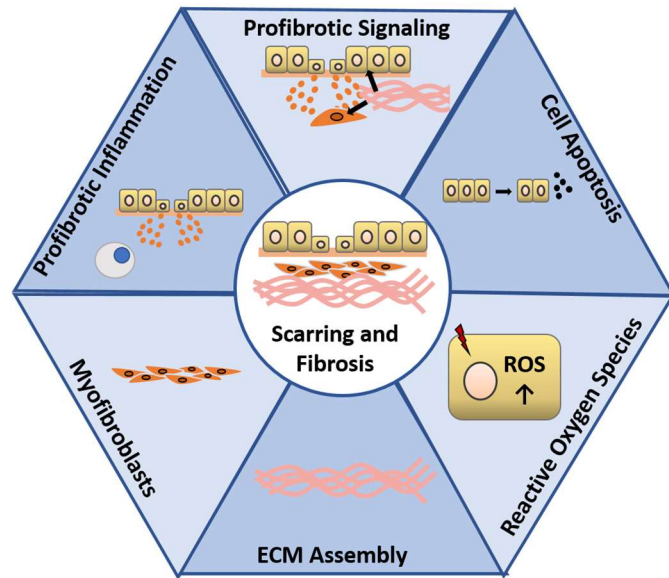


**Figure 1.6:** Six modes of fibrosis. The six modes of fibrosis are Profibrotic Inflammation, Profibrotic Signaling, Cell Apoptosis, Reactive Oxygen Species, and ECM assembly. Each mode affects the others and ultimately leads to ECM maturation, scarring and fibrosis. An effective fibrosis treatment would treat each of these six modes. (Adapted from Atkinson et al)<sup>12</sup>

levels eleven days after surgery. These fibroblasts, originating in the subconjunctival tissue and the episcleral tissue<sup>17</sup>, deposit new extracellular matrix proteins including collagens I and III, fibronectin, and glycosaminoglycans; type III collagen is deposited within the first three days of healing and later replaced by type I collagen. Additionally, the release of vascular endothelial growth factor (VEGF) initiates the growth of new capillaries towards the wound site. During this time, wound contraction begins to occur as activated myofibroblasts pull the wound margins together.

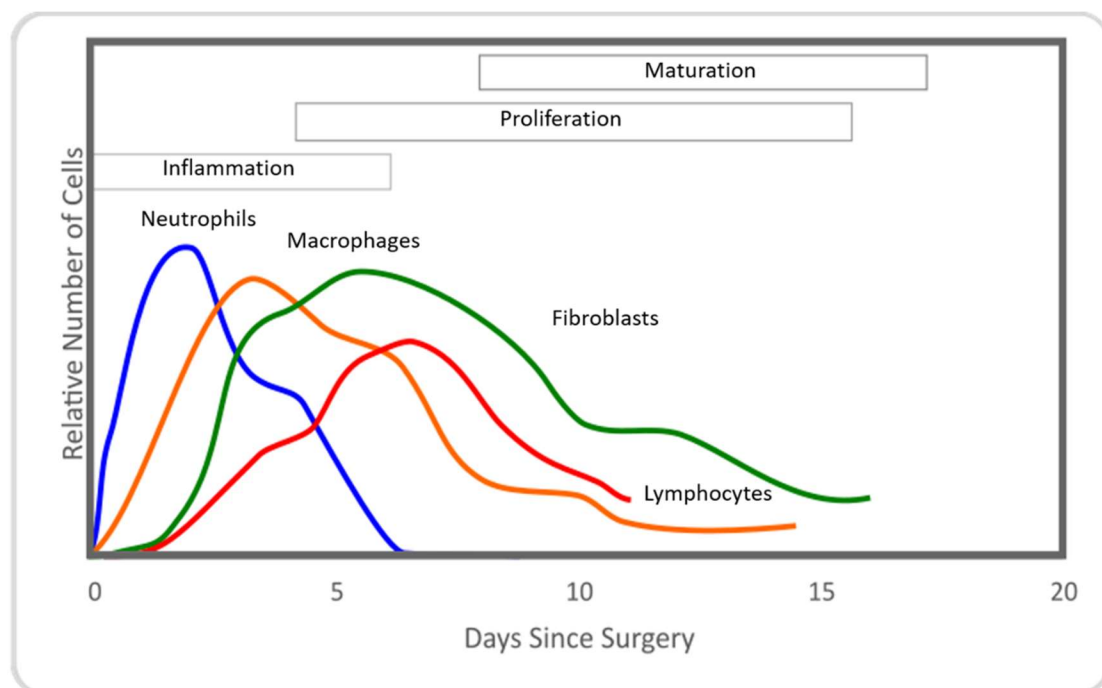


**Figure 1.7:** Timeline of wound healing. In normal wound healing, cytokines released by damaged tissue recruit immune cells to the site of injury. Fibroblasts typically enter the wound healing cascade after day two with maximum presence around day 5 before migrating away after the wound has been closed around day 15. In aberrant wound healing, the fibroblasts continue to proliferate and deposit excess collagen. (Adapted from Witte et al.)<sup>16</sup>

### 1.3.3 Maturation

Collagen deposited in the proliferation phase crosslinks over several months into a collagenous scar. Wound healing is concluded when the fibroblasts undergo apoptosis and the

blood vessels begin to be reabsorbed. It has been suggested that inducing early apoptosis in fibroblasts can modulate the scarring response and reduce collagen deposition thereby reducing scar tissue.

#### **1.4 Antifibrotic Agents**

The antimetabolites 5-fluorouracil (5-FU) and mitomycin C (MMC) have been used in glaucoma filtering surgery as antifibrotic agents for many years<sup>15,18</sup>. The goal of their administration is to prevent bleb failure in glaucoma filtering surgery by modulating the wound healing process. Below, we discuss the mechanisms of action for these therapeutics and their modes of administration.

##### *1.4.1 5-Fluorouracil (5-FU)*

5-FU (**Figure 1.8**) was developed in the 1950s as an antimetabolite for chemotherapy.<sup>19</sup> It is an analog of uracil with a fluorine atom at the c5 position instead of a hydrogen atom. Once in the cell, 5-FU is metabolized into three active metabolites that disrupt the synthesis of RNA and inhibit the synthesis of thymidylate. The enzyme thymidylate synthase catalyzes the reduction of deoxyuridine monophosphate into deoxythymidine monophosphate, which is the sole source of thymidylate in the cell.<sup>20</sup> Thymidylate is used for DNA replication and repair. The 5-FU metabolite fluorodeoxyuridine monophosphate competitively inhibits the binding of deoxyuridine monophosphate to thymidylate synthase and inhibits the production of deoxythymidine monophosphate. Additionally, fluorouradine triphosphate is incorporated into RNA which disrupts transcription.<sup>19</sup>

5-FU reduces fibroblast proliferation in cell culture and is used extensively in glaucoma filtering surgery to improve outcomes. Originally, 5 mg of 5-FU was injected twice daily into the subconjunctival space for 7 days and then once daily for 7 more days. Complications with bleb leakage and corneal epithelial defects led to a reduction of the dose to 5 mg once daily which



has demonstrated success. Additionally, it is not agreed upon whether the treatment is better to start on the first postoperative day or to start 3 to 15 days after the surgery. 5-FU has also been administered intraoperatively by soaking a sponge in 25-50 mg/mL of 5-FU and applying it to the surgical site for 5 minutes. These practices vary from surgeon to surgeon and often from patient to patient.

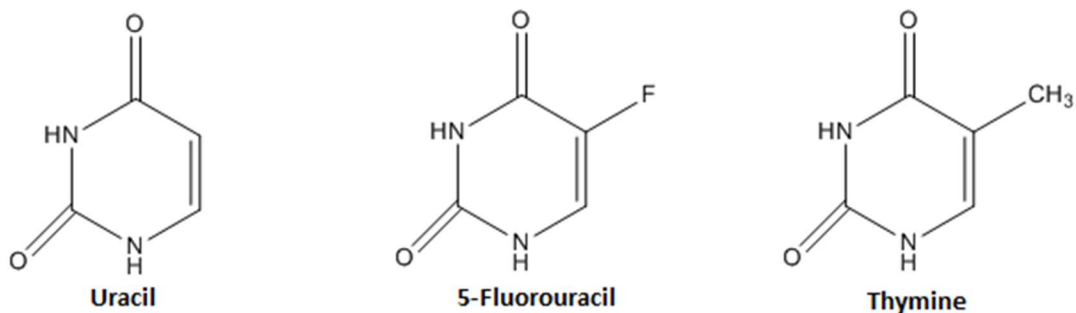


**Figure 1.8:** Structures of Uracil, 5-Fluorouracil, and Thymine.

#### 1.4.2 Mitomycin C (MMC)

In 1958, Wakaki and co-workers first isolated MMC from *Streptomyces caespitosus* (**Figure 1.9 A**)<sup>21</sup>. Its structure was first reported in 1960 by Sato et al<sup>22</sup>. The mechanism of action of MMC has been described as bioreductive alkylation. In this process, MMC is enzymatically reduced at the c5 oxygen, which causes a spontaneous chain of reactions resulting in the opening of the aziridine ring following cleavage of the c9a-methoxy group. This creates two functional groups on MMC that selectively alkylate DNA at guanine residues in the sequence 5'-CpG-3'. (**Figure 1.9**) It has been suggested that this selectivity has been caused by natural selection optimizing the lethality of the crosslink. A single crosslink in the bacterial genome is sufficient to cause cell death.<sup>23</sup>

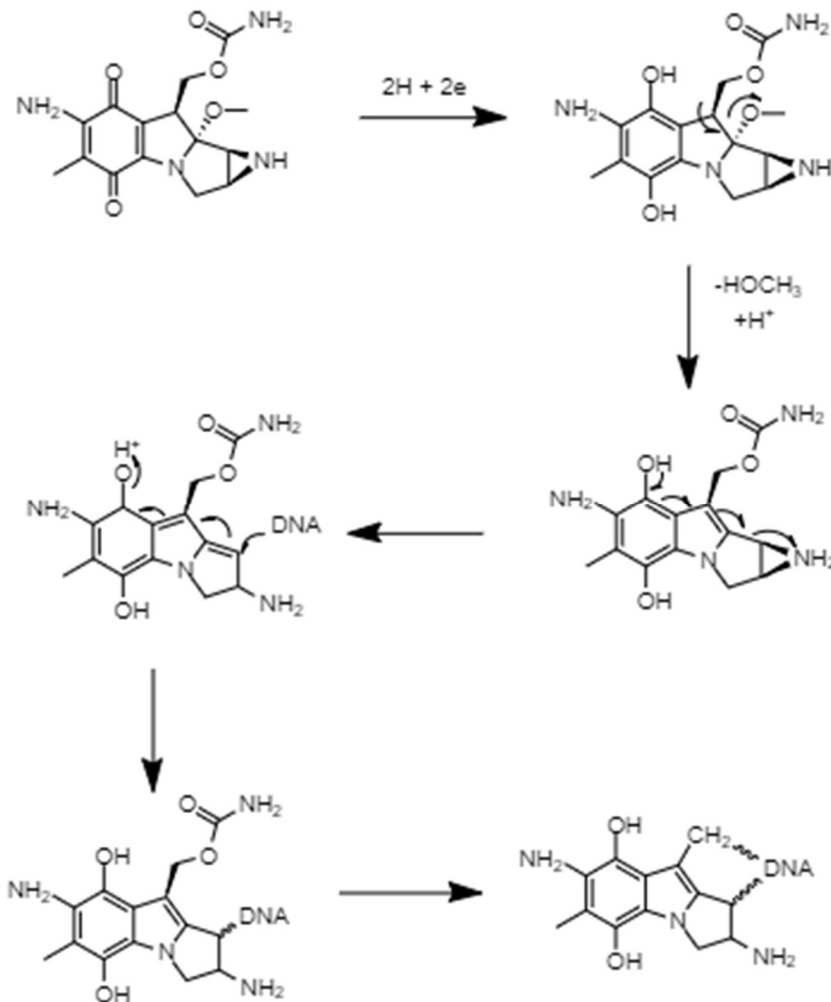


**Figure 1.9:** Reductive alkylation of MMC (A) as it crosslinks DNA. Adapted from Stevens et al.<sup>22</sup>

MMC's use in glaucoma filtering surgery was first reported in 1983<sup>24</sup>. It has been shown to inhibit fibroblast proliferation in cell culture. Protocols for applying MMC intraoperatively use a sponge soaked with MMC applied to the site of surgery. MMC concentration, exposure time, sponge type, and sponge shape all vary from practice to practice.<sup>25</sup> While adjunctive use of MMC is less likely to cause complications when compared to 5-FU, it can cause more serious postoperative complications.<sup>26</sup> Over-filtering blebs, which reduce the IOP below normal physiologic levels (a condition known as hypotony), can result from MMC application and lead

to loss of visual acuity. Additionally, at least one case has been reported where MMC application damaged the ciliary body and led to a lowered secretion of the aqueous humor.<sup>24</sup>

### 1.5 Polymers as Drug Delivery Systems

Polymers are organic materials composed of long-chain macromolecules formed by covalent bonds between repeat units. Polymers can be natural such as collagen, fibrin, and hyaluronic acid, or synthetic such as polyethylene or polytetrafluoroethylene. Polymers are sought after in biomedical applications because they are easily tailored for specific applications. For example, changing the molecular weight of a polymer can drastically change its physical, mechanical, and degradative properties. Depending on the characteristics of the polymer backbone and sidechains, polymers can have a wide variety of properties in the body.

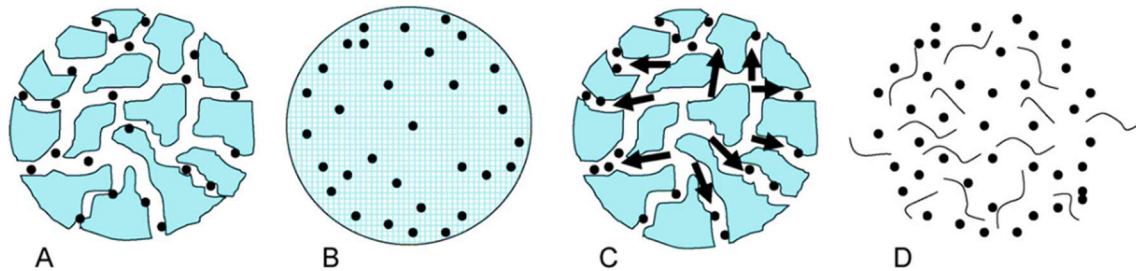


**Figure 1.10:** Routes of Drug Release in Biodegradable System: A diffusion through pores in the polymer. B Diffusion through the bulk of the polymer. C Osmotic diffusion due to water ingress. D. Release of drug due to polymer degradation. (Adapted from Fredenberg et al)<sup>27</sup>

Many polymer types have been used as drug delivery systems. Methods for drug delivery include polymer micro and nanoparticles for injection, topical gels and films for transdermal drug delivery, and contact lenses for topical delivery.<sup>28</sup> A polymer for a drug delivery system must be carefully selected based on the criteria of biocompatibility, route of administration, length of the release, and ease of manufacture. Here we describe two popular polymer types for drug delivery, hydrogels, and biodegradable polymers.

### 1.5.1 Hydrogels

Polymers can be crosslinked to form large networks. If the crosslinks and sidechains of the polymer are hydrophilic, this network will swell in the presence of water to form a hydrogel. Hydrogels were the first biomaterials designed specifically for use in the clinic<sup>29</sup>. The vitreous humor in the eye is a natural hydrogel comprised of collagen fibers and hyaluronic acid.<sup>30</sup> The ability of hydrogels to retain large amounts of water has made them sought after for soft tissue applications. Additionally, hydrogels can be loaded with hydrophilic drugs, which are then diffused as the material swells in the presence of water.

### 1.5.2 Biodegradable Polymers

Natural polymers such as collagen or proteins degrade enzymatically. It is also possible to design synthetic polymers that degrade in aqueous environments via hydrolysis. Hydrolysis is the cleavage of bonds within the polymer and subsequent reduction in the molecular weight. This form of degradation is common in polymers formed by condensation reactions. Amide, anhydride, and ester bonds are all susceptible to hydrolysis. Of these, polyesters are the majority of studied biodegradable polymers. Biodegradable polymers have been used in tissue engineering, wound closure, and drug delivery.<sup>31</sup> Two different methods of biodegradation can occur in polymers susceptible to hydrolysis: bulk and surface degradation. In bulk degradation, water penetrates the polymer network faster than the polymer degrades. Surface degradation happens when the hydrolysis of the polymer occurs faster than the ingress of water into the polymer. The method of degradation depends on the lability of the bonds, and the hydrophobicity/hydrophilicity of the polymer chains. **Figure 1.10** shows the possible routes of drug release from biodegradable polymers.<sup>27</sup> Most polymeric drug delivery systems will exhibit many of these routes leading to diverse release kinetics.

### 1.5.3 Poly(hydroxyethyl methacrylate) (pHEMA)

pHEMA was invented in Czechoslovakia in the 1950s and reported in 1960 in Nature (Figure 1.11).<sup>61</sup> Two scientists, Otto Wichterle and Drahoslav Lim were attempting to create biocompatible polymers for use in ophthalmology. Crosslinked pHEMA was a proper candidate because it formed a hydrogel with suitable mechanical and optical properties. pHEMA is hydrophilic and forms a porous sponge-like macromolecular structure in the presence of water. It has been used for soft contact lenses in the US since 1966 with minimal complications.<sup>29</sup>

The porous structure of pHEMA can be measured on the scale of nanometers. This allows for the diffusion of small molecules through the hydrogel. In drug delivery, the

hydrogel is loaded by placing a dried gel into a solution containing a drug of interest. After the material has reach equilibrium, the gel can be dried and the drug will be entrapped in the macromolecular meshwork. Drug delivery is governed by diffusion driven by the concentration gradient of the drug and is generally considered to follow Fick's Law:  $f = -D\nabla C$ , where  $f$  is the flux,  $D$  is the diffusion coefficient and  $C$  is the concentration.<sup>32</sup> The release of the drug through pHEMA can be tailored by decreasing the pore size, which can be done by altering the amount of crosslinker present during the polymerization.

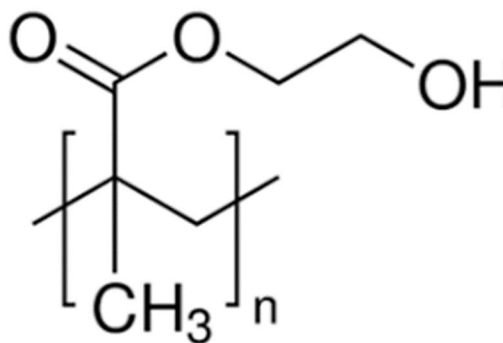


Figure 1.11: Structure of pHEMA

#### 1.5.4 Poly(lactic-co-glycolic acid) (PLGA)

PLGA is a copolymer of poly(lactic acid) (PLA) and poly(glycolic acid) (PGA) (**Figure 1.12**). PLGA is biodegradable by hydrolysis of the ester bond. PLGA undergoes bulk erosion as it is relatively hydrophilic and as a result is hydrated rapidly. Hydrolysis begins after contact with water and creates acids within the bulk of the polymer. It has been shown that PLGA will autocatalyze degradation by reducing the local pH. As the polymer degrades and the molecular weight decreases, it becomes more hydrophilic with the oligomers becoming soluble at 1100 Da. PLGA degrades to form both lactic acid and glycolic acid.<sup>33</sup> The lactic acid is further degraded into water and carbon dioxide by the tricarboxylic acid cycle. The glycolic acid is broken down by enzymes and excreted in the urine.<sup>34</sup> Degradation of PLGA can be tailored by modifying the molecular weight and lactide:glycolide ratio. For example, an 85:15 ratio will degrade much slower than a 50:50 ratio. Likewise, a higher molecular weight polymer will degrade more slowly than one of a lower molecular weight.<sup>34</sup>

PLGA has been used extensively as a drug delivery system.<sup>27,35</sup> Classically, the drug is encapsulated within the bulk of the polymer and then released as the polymer degrades. Typically, this follows a tri-phasic release pattern. Phase I consist of the drug on the surface or close to the surface of the polymer being released upon contact

with water. Phase II is a slow release phase where the drug diffuses through the polymer or through small pores that are formed during water ingress. Phase III is a final and faster release due to the onset of erosion. This occurs only when the polymer has degraded enough for the oligomers to dissolve and erode. The release of drugs depends on a variety of factors including

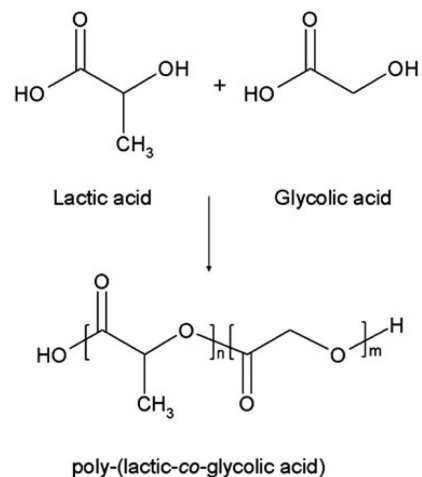


**Figure 1.12:** Structure of PLGA and its monomers

hydrophobicity of the drug, drug particle size, and dimensions of the drug delivery system. A hydrophobic drug will release more slowly causing a short phase I, longer phase II, and releasing the majority of product in phase III. A larger particle size would lead to a larger burst in phase I due to more drug being present at the surface and larger pores being formed by the drug's erosion. The dimensions of the drug delivery system greatly affect the release. A higher surface area to volume ratio will cause a higher burst release in phase I and an earlier phase III.<sup>27</sup>

## **1.6 Previous Work**

Due to the differences in administration of antimetabolites from physician to physician as well as surgery to surgery, it is difficult to understand the relationship of antimetabolites to the success or failure of a surgery. It would be beneficial to have a drug delivery system that metered the dose of these antimetabolites into the site of the surgery. As the wound healing cascade progresses, antimetabolites would reduce the number of fibroblasts in the surgical site and prevent ECM deposition.

Blake, Ayyala, and John et. al. have been working on drug delivery systems for glaucoma surgery for over a decade.<sup>36</sup> After recognizing the need to standardize MMC administration to glaucoma patients intraoperatively, they began to develop polymer-based drug delivery systems designed to release anti-metabolic drugs into the surgical site in a controlled fashion.

### *1.6.1 pHEMA Drug Delivery System*

The research group first studied a pHEMA-based system comprised of 1% crosslinked HEMA with methylene bisacrylamide (MBA) as the crosslinker (**Figure 1.13**). Polymerization was performed by redox reaction with ammonium persulfate and tetramethylethylenediamine (TEMED) as initiating reagents. MMC was loaded into the hydrogels by placing the desired amount of MMC in ethanol and then allowing the gels to swell in the solution while it evaporated. This process was repeated until the drug reached the desired concentration in the

pHEMA disc. The concentration gradient drives the diffusion of the MMC into the gels. The release of drugs from these hydrogel systems is sink-dependent, meaning that the larger the volume of medium the hydrogel is submerged in, the faster the drug will release. These hydrogels were tested in cell culture with human conjunctival fibroblasts as well as immortalized COS-1 fibroblasts. Future experiments relied solely on COS-1 cells due to increased reproducibility. It was shown that hydrogels that had been properly rinsed to remove unreacted or low molecular weight byproducts of the polymerization reaction did not affect the cells unless they were loaded with MMC. In vitro testing confirmed that the MMC was released over a period of 1-2 weeks.<sup>37,38</sup>

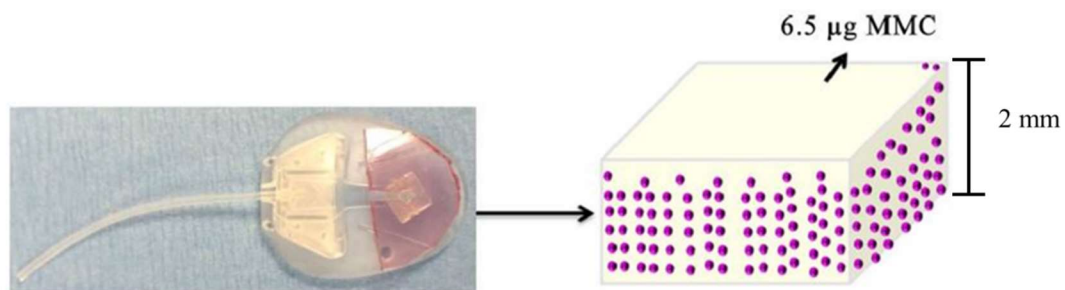


**Figure 1.13:** Ayyala pHEMA drug delivery system. The disks are 13 mm on the longest side when hydrated and 2 mm thick (Adapted from Schoenberg et al)<sup>39</sup>

### 1.6.2 PLGA Drug Delivery System

Further experiments were performed using biodegradable PLGA as there was concern over the long-term effect of implanting pHEMA at the surgical site. These PLGA systems relied on a breath figure morphology, which enables the dual loading of therapeutics. These drug delivery systems were designed to degrade after a month in the surgical site and release 5-FU as well as MMC (**Figure 1.14**)<sup>40</sup>.



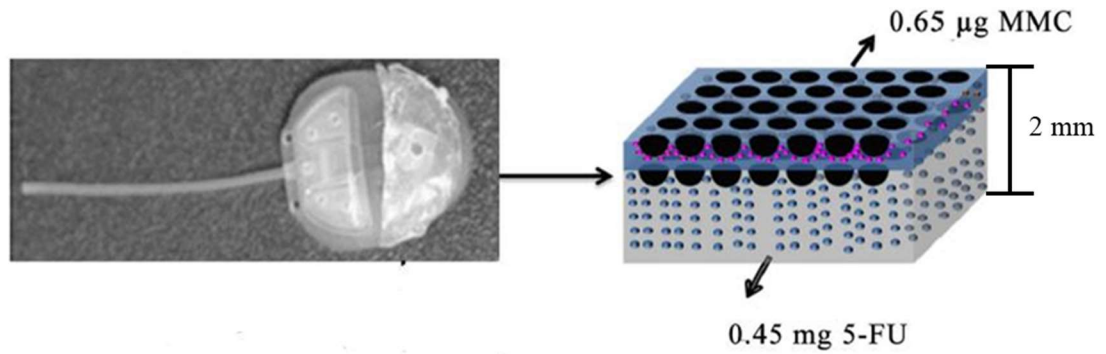


**Figure 1.14:** Ayyala PLGA drug delivery system. The wafers are 13 mm on its longest side and 2 mm thick. (Adapted from Schoenberg et al)<sup>39</sup>

Breath figures were first described by Aitken and were considered a natural phenomenon with little use for a century.<sup>41</sup> In 1994, Francois et al first reported the creation of a honeycomb porous polymer film using moist air.<sup>42</sup> The term “breath figure” refers to the condensation of moisture on a hydrophobic cold surface, akin to breathing on a cold piece of glass. In material science, breath figure arrays are made by exposing a rapidly evaporating substrate, such as polymer dissolved in an organic solvent, to humid air. The evaporation of the solvent rapidly cools the surface and the humid air condenses into a breath figure. The water droplets then form a patterned hexagonal array of pores after they evaporate. **Figure 1.15** shows a breath figure formed on PLGA. While the concept of creating breath figure arrays remains consistent, the setups can vary. Polymers can be solvent cast, dip-coated or spin-coated. The humid air can flow over the substrate in some experimental setups and in others, the humidity is controlled without airflow. These breath figure arrays can be used for templates in micropatterning, biosensors, tissue culture substrates, and drug delivery systems.<sup>43</sup> In our studies, breath figures are used as dual-loaded drug carriers.

In the present experiments, PLGA was solvent cast in dichloromethane with 5-FU suspended in the solution. Then, more PLGA without 5-FU was spin-coated on top of the disk and humid air was blown over the substrate while it evaporated from a breath figure array. The pores left on the surface of PLGA could be loaded with MMC, which

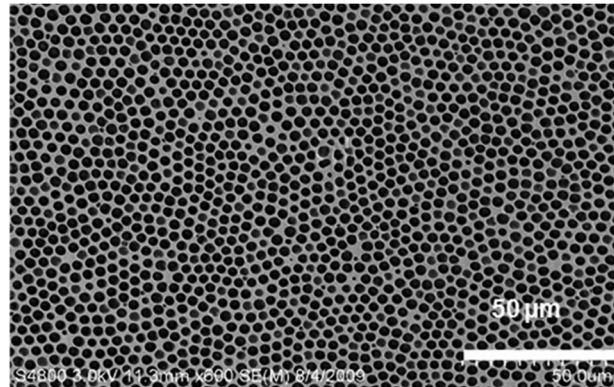


**Figure 1.15:** A breath figure formed on PLGA. (From Ponnusamy et al 2012)<sup>44</sup>

could not be loaded into the polymer with the organic solvent without deactivation. Meanwhile, 5-FU could be solvent cast as a powder within the polymer. This allowed for a dual release of anti-metabolites where the MMC was released in a burst in the first 2-4 days and the 5-FU followed in a tri-phasic release over thirty days. In vitro studies showed that the films were effectively cytotoxic to COS-1 fibroblasts for up to 24 days. Films without MMC took approximately one week to become fully cytotoxic while films with MMC loaded on top showed cytotoxicity after one day. This system was designed to combat the initial inflammation due to surgery, as well as the chronic fibrosis of bleb encapsulation caused by the implantation of a glaucoma valve.<sup>40,44</sup>

### 1.6.3 In Vivo Studies of Drug Delivery Systems

The pHEMA delivery system was tested in a New Zealand white rabbit model after in vitro testing. The right eye of each rabbit was implanted with a glaucoma valve. In group 1 (n=4), the valve had no hydrogel, the other three groups had hydrogels with dosages of 0.17, 0.35, and 0.8 mg MMC per gram of dried HEMA attached to the valve. After 3 months, the animals were

sacrificed, and the eyes were enucleated for histological analysis. It was shown that the fibrous capsule surrounding the glaucoma valve was thinner in animals treated with the MMC-loaded

hydrogel.<sup>38</sup> **Figure 1.16**

shows the results of the histological analysis of the bleb formed from these surgeries.

An additional study was completed to test determine the success of the biodegradable PLGA drug delivery system in trabeculectomy. In this study, 18

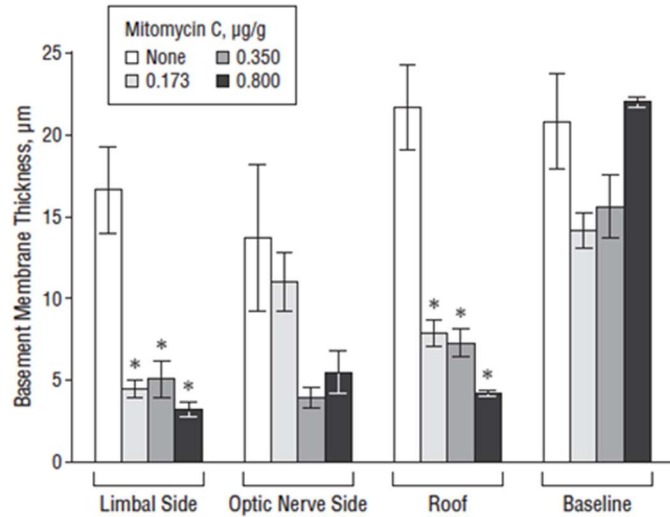


**Figure 1.16:** Results of p(HEMA) rabbit study. (from Sahiner et al 2009)<sup>38</sup>

New Zealand White rabbits were divided equally into three groups: A control group with no device treated with 0.4 mg/ml MMC solution applied by sponge for 45 seconds, PLGA with 0.45 mg of 5-FU and 0.65 µg of MMC, and PLGA with 0.23 mg of 5-FU and 0.33 µg of MMC.

Trabeculectomy was performed on the right eye of each rabbit. IOP was measured at one day after surgery, and again on months one, two, and three. After the third month, the rabbits were sacrificed, and their eyes were enucleated and examined histologically. It was concluded that the PLGA device was safe and effective with lower dosages than required using MMC applied by a surgical sponge. Additionally, the use of this device avoids the known side effects of MMC application during trabeculectomy.<sup>45</sup>

Both drug delivery systems were compared directly in a controlled New Zealand White Rabbit study. pHEMA hydrogel loaded with 6.5 µg of MMC per gel and PLGA films loaded with 0.45 mg of 5-FU and 0.65 µg of MMC were implanted with glaucoma valves. Forty-eight rabbits were equally divided into six groups: PLGA alone, pHEMA with 6.5 µg of MMC, PLGA with 0.45

mg 5-FU, PLGA with 1.35 mg 5-FU, PLGA with 0.45 mg 5-FU and 0.65  $\mu$ g of MMC, and PLGA with 1.35 mg of 5-FU and 0.65  $\mu$ g of MMC. After 3 months, rabbits were sacrificed, and the eyes enucleated for histological analysis. **Figure 1.17** shows the results of the microcaliper measurements of the bleb roof thickness from each of the treatment groups. There was a significant difference in bleb roof thickness in three of the six groups; treatment with pHEMA with 6.5  $\mu$ g of MMC or PLGA with 0.45 mg 5-FU and 0.65  $\mu$ g of MMC or PLGA with 1.35 mg of 5-FU and 0.65  $\mu$ g of MMC all resulted in bleb reduction. This study concluded that the pHEMA and PLGA drug delivery systems were a success but the decision of which system to ultimately move

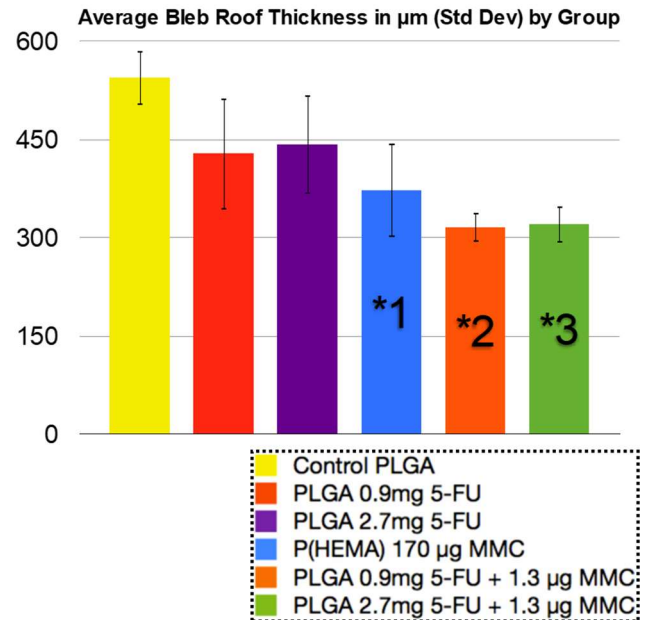


**Figure 1.17:** Bleb thickness results of *in vivo* rabbit study. Effect of PLGA and pHEMA drug delivery systems on bleb thickness in a rabbit (Adapted from Schoenberg et al)<sup>39</sup>

to market would depend on their respective compatibility with GMP manufacturing procedures and sterilization protocols and the long-term stability of the product.<sup>39</sup>

### 1.7 Bench-to-Bedside Translation

It has been suggested that the average lag time from evidence-based research to clinical practice is 17 years.<sup>46</sup> The toll of this lag time is evident. McGlynn et al. reported that 45% of patients from 12 metropolitan areas were not receiving recommended care.<sup>47</sup> This gap is even larger for new drug delivery systems when compared to new best practices in medicine. Clinical trials for a new pharmaceutical alone are expected to take 6-7 years. This results in a so-called

“valley of death” for products where there is a need for resources to overcome commercialization hurdles (**Figure 1.18**).<sup>48</sup>

Despite significant progress, the research group has made towards developing a new drug delivery system, several factors need to be carefully considered before moving on with a clinical trial. These include how the product is to be sterilized, the stability of the product and its active pharmaceutical ingredients during storage, how the product is to be made reproducibly, and the regulatory hurdles that need to be completed before reaching the market.

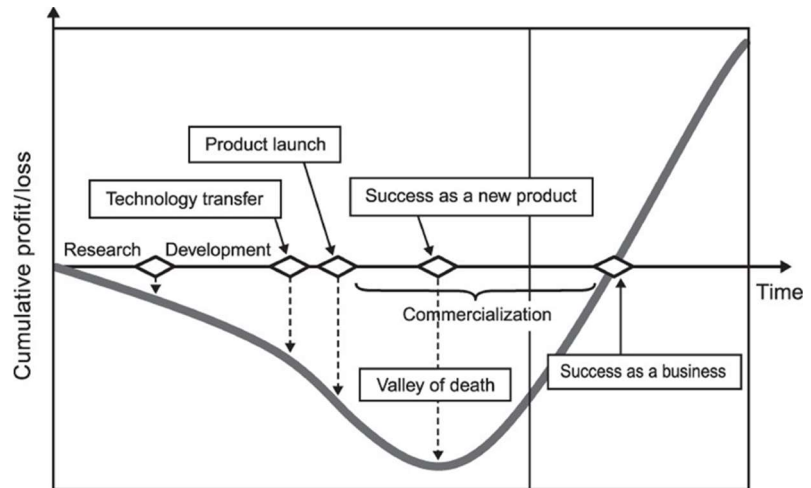


**Figure 1.18:** The “valley of death” for translational research. (Adapted from Osawa and Miyazaki)<sup>48</sup>

### 1.7.1 Sterilization

A factor in designing all medical implants is terminal sterilization after the product has been manufactured. Sterilization methods include dry and wet heat, gas, and radiation. Polymers can have different reactions to each of these techniques and it is important to choose the method of sterilization with care.

In wet sterilization, the product is placed in a chamber and the air is replaced with steam via a vacuum pump. The temperature is brought to 121-124°C for 15 minutes. These temperatures denature cell components, subsequently destroying microorganisms. Dry heat operates similarly to wet heat but excludes steam. Dry heat requires much higher temperatures

(170-190°C) and is only suitable for heat resistant materials. Dry and wet heat can affect active pharmaceutical ingredients reducing efficacy.

Gas sterilization typically used reactive agents (i.e. ethylene oxide) which damage cell components. This process requires humidity, which is unsuitable for biodegradable polymers. Gas sterilization also runs the risk of residue remaining on the product, which is increased in porous substrates such as hydrogels. Additionally, the need for sterilization-compatible packaging in gas sterilization adds to the cost.

For the pHEMA and PLGA drug delivery systems, radiation sterilization is the most feasible solution. Radiation sterilization relies on the radioactive decay of cobalt 60 or another gamma-ray source. The ionizing radiation causes the scission of the DNA. Typically, products are irradiated at 25 kilograys (kGy). This high dose can cause undesired alterations in polymer matrices including polymer chain scission or crosslinking. The dose and product environment can be modulated to reduce these undesired effects.<sup>49,50</sup>

It has been shown that under gamma irradiation, scission and crosslinking occur in pHEMA hydrogels<sup>51</sup>. Whether the chain scission or crosslinking dominates depends on the reagents used in casting the hydrogel as well as the environment in which the gel is irradiated. If the gel is well dried, there should be little impact on the release of the drug with a typical dose of irradiation.

PLGA undergoes chain scission as a result of gamma irradiation with average molecular weight being reduced an order of magnitude at doses around 20 kGy. This degradation of the polymer chain leads to a more rapid release of embedded drugs. Lower doses of up to 15 kGy with dose rates of 0.64 kGy/hr have been shown to mitigate this to create a stable product for up to 5 months<sup>52</sup>.

### *1.7.2 Stability*

It is also important to assess the degradation of polymer drug delivery systems over time to determine the stability and potential shelf-life. The stability of polymeric drug delivery systems is highly influenced by temperature and humidity<sup>53</sup>. Any water in the product during storage of biodegradable polymers will also lower the stability. It has also been shown that lyophilization can mitigate the instability of the polymer upon storage in drug delivery applications<sup>54</sup>. In this study, we have conducted studies to optimize lyophilization techniques for polymeric materials.

The introduction of free radicals during the irradiation process can negatively affect the shelf-life of the product. In one study, PLGA of 34,000 molecular weight degraded only 10% in 5 months after exposure to low radiation doses.<sup>55</sup> It is possible that free radical production during gamma irradiation is also dependent on the storage conditions (i.e. presence of water or air)<sup>56</sup>.

### *1.7.3 Current Good Manufacturing Practice*

A frequent hurdle when translating novel technology from academia to industry is that academic labs are not required to follow regulatory guidance and fail to consider the challenges a product might face if it needs to be scaled to a clinic-ready product. This causes a hurdle when translating a benchtop product to market. Before a product can be tested clinically, it must be produced in a good manufacturing practices (GMP) facility with an appropriate quality control unit. These regulations require a high degree of expertise. The Food and Drug Administration (FDA) oversees the manufacturing of pharmaceuticals in the United States.

Current Good Manufacturing Practice (CGMP) is defined in the Code of Federal Regulations (CFR) Title 21, which interprets the Federal Food, Drug and Cosmetic Act and other related statutes. The FDA gains its regulatory authority from the Federal Food Drug and Cosmetic Act. 21 CFR parts 210 and 211 detail the specifics of CGMP for pharmaceuticals. Failure

to comply with 21 CFR legally renders the product adulterated. 21 CFR 11 establishes the quality control unit as the responsible person or persons for maintaining GMP. 21 CFR 211 also covers the building, equipment, packaging, laboratory controls, and others.

#### *1.7.4 Clinical Trials*

Before a new drug delivery system can be sold in the United States, it must undergo several stages. First, the drug delivery system should be tested preclinically *in vitro* and in animal models to ensure safety. The drug delivery system's sponsor must file an investigational new drug (IND) application, then clinical trials are conducted in three phases. After clinical trials, the sponsor sends a new drug application (NDA). Only after approval of the NDA can the new drug delivery system be sold.

The IND is described in 21 CFR 312 and must detail the clinical trial plan for the new drug delivery system as well as any preclinical data to support the study design. 21 CFR 312.21 explains the phases of clinical trials necessary for approval. Phase I is a small-scale study (20-80 patients) that involves healthy volunteers and ensures the drug does not have any adverse effects. Phase II studies are larger (~100-300 subjects) and evaluate the efficacy of the drug for its indication. Phase III studies are very large (~300-3000) subjects and are designed to gather information about the overall benefits and risks of the new drug. These phases can overlap or be abbreviated. In the case of a drug delivery system that releases an approved pharmaceutical, an abbreviated clinical trial may be granted. In this case, the trial would be designed to ensure there were no adverse interactions with the drug delivery system and the active pharmaceutical ingredient. 21 CFR 314 explains the NDA. This is the final step before approval. One of the most important aspects of the NDA is drug labeling. This details how the drug is to be marketed, the warnings and contraindications, and the dosage.



## 1.8 Aims of the thesis project

Our current research endeavors to prepare the previously developed drug delivery systems for translation to the market. This includes controlling the manufacture of the systems, sterilization protocols, and shelf-life studies. The goal of these activities is to file for an IND and manufacture these products for clinical trials.

Primarily, the manufacture of these drug delivery systems must be controlled. First, the systems were tested for consistent drug loading between batches. The homogeneity of drug dispersal was also tested. Then the systems were tested for batch-to-batch variability with respect to the drug release.

Next, the drug delivery systems were compared before and after gamma sterilization. Previously, animal studies were performed with drug delivery systems that had been sterilized with UV light. This is not an acceptable sterilization technique for human use. It is important to understand the effect of a gamma sterilization protocol on the polymers. Any changes in the release can drastically affect the success of the product *in vivo*.

Finally, the shelf life of the drug delivery systems was examined. The product was stored at different temperatures and atmospheric conditions for a period of up to 3 months to determine the optimal state for product storage. PLGA is particularly susceptible to degradation during storage if free radicals generated by gamma irradiation or water from the manufacturing process are present.

Future research must be aimed at creating customizable drug delivery systems to give physicians greater control over the dosage and timing of administration. An injectable slow-release drug delivery system would give the physicians better control over drug administration. These would enable a physician to administer the antimetabolites to a patient if it appeared that they were having a stronger wound healing response. The results of these studies add to a

growing body of literature aimed at closing the gap between academic research and the healthcare market. Hopefully, this work can serve as a case study for the development of a drug delivery system.

## **Chapter 2 - AIM 1: Translating a p(HEMA)-based drug delivery system for good manufacturing practice (GMP)**

### **2.1 Introduction**

Glaucoma affects approximately 80 million people worldwide making it the primary cause of vision loss and the second leading cause of blindness.<sup>57</sup> The disease affects about 2.1% of the US population. However, glaucoma disproportionately affects African Americans at 3-4 times the rate of Caucasian Americans.<sup>58</sup> It is the leading cause of blindness among African Americans and is fifteen times more likely to cause blindness in African Americans than in Caucasians. Additionally, studies have shown that about half of people with glaucoma are unaware that they have the disease.<sup>59</sup>

Glaucoma is primarily characterized by an increase in intraocular pressure (IOP). Reducing IOP is the goal of most treatment paradigms.<sup>57</sup> Currently, topical treatments, such as prostaglandin analogs and  $\beta$ -blockers, are the first-line treatment for glaucoma. These treatments require the daily application of medicinal eye drops. These treatments may be poorly tolerated or have low patient compliance leading to a need for surgical intervention.<sup>60</sup>

There are two surgical options for glaucoma patients, trabeculectomy and tube shunt. Both have high failure rates after five years with almost 50 percent of surgeries requiring revision surgery.<sup>11</sup> The primary mode of failure for these surgeries is the formation of a fibrous capsule around the surgical site, occluding the flow of the aqueous humor, and causing the IOP to increase. To prevent fibrous scar tissue formation, mitomycin C, a DNA crosslinker that alkylates guanines and causes cell death in proliferating cells, is applied to the surgical site during the procedure.<sup>24</sup> However, delivery of anti-fibrotics in the days following the operation

rather than the time of surgery has been shown to be more effective as it aligns with the recruitment of fibroblasts to the surgical site during the wound healing process.<sup>17</sup>

2-Hydroxyethyl methacrylate (HEMA) and its polymer, poly(2-hydroxyethyl methacrylate) (p(HEMA)), were first described in 1936 by the E. I. du Pont de Nemours and Company (now DuPont). The biological applications of HEMA in hydrogels were first reviewed in 1960 when Wichterle and Lim described its use as an implantable biomaterial and as a transparent contact lens.<sup>61</sup> P(HEMA) is a promising biomaterial since it is biologically inert and its physical properties can be tailored to the specific application. For example, changing the water content during crosslinking leads to a corresponding change in hydrogel pore size, which translates to differences in biocompatibility.<sup>29</sup> P(HEMA) has been used as a platform for drug delivery since shortly after its discovery. Wichterle, Lim, and others applied it as an implantable reservoir for antibiotics and anticancer drugs.<sup>61</sup> P(HEMA) has also been proposed to be used as drug-loaded contact lenses to deliver corticosteroids, antibiotics, and  $\beta$ -blockers to the eye.<sup>62–65</sup>

Despite these advances, there are no commercially available p(HEMA)-based drug delivery systems. This could be due to any number of challenges arising from translating a drug or drug delivery system to the market, including gaps in funding, manufacturing challenges, and regulatory hurdles. In academia, after a product reaches the proof of concept stage, it is difficult to identify other funding opportunities for pursuing manufacture and subsequent tests of the product in clinical trials. These studies are usually funded by creating a start-up company or partnering with an established company. Such activities are time-consuming and not directly aligned with the goals of a research institution. There are also manufacturing challenges that beset a potential drug delivery system. It is often a non-trivial task to scale-up a product that was made in small batches in a laboratory setting to the full production batches that are required for clinical trials and commercial production. These challenges include sterilization,

process optimization, and the characterization required by the Food and Drug Administration (FDA) or other regulatory entities. The FDA oversees the clinical trials, marketing, and manufacture of drugs and drug device combination products. If the drug-device combination product is cutting edge, as in the case of drug-eluting contact lenses, a very rigorous and expensive series of clinical trials is necessary with many rounds of patient recruiting, patient follow-up, data collection, and analysis. Due to these challenges, many new products fall into the so-called “valley of death” where funding falls short of what is required to bring a product to market.

Blake, Ayyala, and John have previously developed an implantable p(HEMA) drug delivery system for use in glaucoma surgery.<sup>37,38</sup> This drug delivery system was cast in between sheets of glass and then cut into semi-circular disks before being loaded with mitomycin C. The system showed promise in both *in vitro* and *in vivo* models.<sup>39</sup> In the cited study, the group showed that mitomycin C exhibited sustained release over the first five days. Fibroblasts were inhibited in cell culture when treated with the eluted drug and were unaffected by a sham hydrogel with no drug. The p(HEMA) implant also showed a significant effect on the thickness of the fibrous capsule when compared to a sham PLGA control. However, there was a substantial time burden associated with creating these hydrogels. The casting took 24 hours and loading took an additional 10 days. Additionally, there were no established protocols for consistently ensuring the disk geometry or quantifying the amount of drug in an individual piece.

In this study, we established protocols and methods to improve the reproducibility and scalability of this product. We developed a method for quantifying the amount of drug in an individual piece and a method for producing uniform pieces. We reduced the casting and drug loading times, and we compared past and present methods to ensure comparability between studies.

## 2.2 Materials and Methods

### 2.2.1 Materials

2-hydroxyethyl methacrylate 99+% (Visomer<sup>®</sup>) was provided by Lintech International (Macon, GA). Methylene chloride (ACS grade) was acquired from Thermo Fisher Scientific (Waltham, MA). Mitomycin C (MMC) derived from *Streptomyces caespitosus*, neutral buffered formalin, N,N,N',N'-Tetramethylethylenediamine (TEMED), ammonium persulfate, and toluidine blue were from Sigma Aldrich Chemicals (St Louis, MO). N,N'-Methelyne-bisacrylamide (MBA) was acquired from Chem-Imprex International (Wood Dale, IL). 24-well Costar tissue culture plates (12.6 mm diameter) were purchased from Corning (Corning, NY). COS-1 cells were obtained from the American Type Culture Collection (Manassas, VA) and maintained in a humidified atmosphere of 5%CO<sub>2</sub>/95% air in Dulbecco's Modified Eagle's Medium (DMEM) (3.7 g/L sodium bicarbonate) supplemented with 10% fetal bovine serum, 1% 100 mM sodium pyruvate, and 1% of 100x antibiotic-antimycotic solution (10,000 units penicillin, 10 mg streptomycin and 25µg Amphotericin B per mL). DMEM, sodium pyruvate, antibiotic-antimycotic solution, and FBS were from Gibco (Part of Thermo Fisher Scientific). All chemicals were used as received, without further purification.

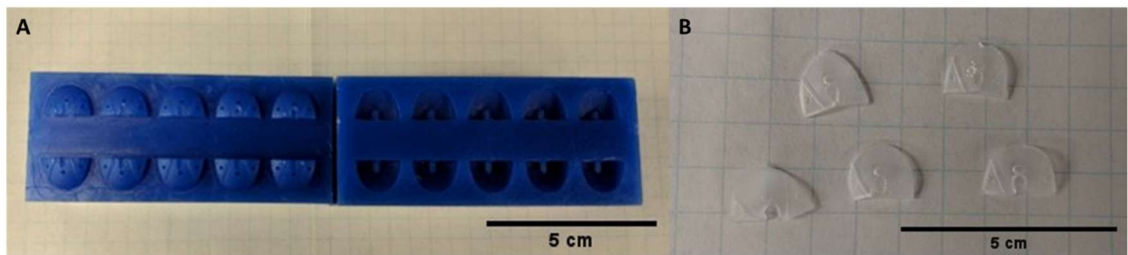


**Figure 2.1:** New molding method. A mold (A) was provided by New World Medical that enables us to cast HEMA into semicircular disks (B) that are compatible with the Ahmed valve.

### 2.2.2 Casting Hydrogel Disks

For these scale-up activities, it was necessary to reproduce past results and then improve on them by reducing the casting time and ensuring uniformity among lots. Casting the p(HEMA) hydrogel disks was performed as described previously<sup>37</sup>. Briefly, a 2-4 mm grease bead was placed around the perimeter of a glass slide. Then, 0.0508 g of MBA was mixed with 4 mL of water. Then, 0.0375 g of ammonium persulfate was mixed with 1 mL of water. TEMED (100  $\mu$ L) was added to 1 mL of the MBA solution followed by 1 mL of monomeric HEMA. The mixture was then vortexed for 10 seconds before adding 250  $\mu$ L of the ammonium persulfate solution to initiate the reaction. The reaction mixture was then poured onto the glass slide where the grease bead acted as a barrier. A second glass slide was placed on top of the reaction mixture carefully to minimize air bubbles. After the polymerization was complete, disks were cut into semicircles (measuring 13 x 6.5 mm) and washed in 50 mL of 50% ethanol five times for 3 hours to remove unreacted monomer.

For the new method, the reaction mixture was vortexed for 10 seconds after the addition of the ammonium persulfate and 110  $\mu$ L of the reaction mixture was subsequently added to each void in a custom-made mold. The mold was closed and the reaction was allowed to progress for 6 or 12 hours. The disks were then washed as described above. **Figure 2.1** shows the mold and resulting disks.



**Figure 2.2:** Drug loading set-up of p(HEMA) disks. Individual p(HEMA) disks, each in its own 20 mL vial, arranged in a single layer. This small portable vacuum oven can hold 70 vials in one layer, or the vials could be stacked to load up to 140 disks at one time.

### *2.2.3 p(HEMA) Disk Weight*

Batches of 6-hour cast and 12-hour mold-cast p(HEMA) disks were weighed to the tenth of a milligram on an analytical balance to see if there was a difference in polymer density due to the different polymerization times. Each individual piece was weighed and the resulting distributions were compared statistically using a Student's t-test.

### *2.2.4 Drug Loading*

To load a hydrogel with drug, it was placed in a glass vial and 10  $\mu$ L of ethanol with 6.5  $\mu$ g of MMC was added to each vial. Then the vial was placed in a vacuum oven at a pressure of 20 mbar for 2 days until the ethanol had evaporated. **Figure 2.2** shows the vials loaded into a vacuum oven. Sheet-cast and mold-cast polymers were loaded identically and then their loading efficiency was compared using a Student's t-test and an F-test to compare the variances.<sup>66</sup>

### *2.2.5 Drug Quantification*

To measure the amount of drug loaded into each disk, replicate disks (n=5) eluted in 5 mL of ethanol for 24 hours and the amount of MMC was measure using UV-Vis spectroscopy. The peak absorption was read at 365 nm and then the concentration calculated from a standard curve of MMC dissolved in ethanol. After measuring the amount of MMC in each disk, the distributions between 6-hour and 12-hour cast disks were compared using a Student's t-test.

### *2.2.6 PBS Release*

The time-dependent release of drug from the P(HEMA) from the disc was determined by placing each replicate disc (n=8) in a glass vial with 10 mL of PBS buffered to a pH of 7.4. The vials were then placed in a bead bath maintained at 37°C for 10 days. At 24 hour intervals, 1 mL of PBS was removed from each vial and replaced with 1mL of fresh PBS. The sample that was removed was analyzed via UV-Vis spectrophotometry at 365 nm and the MMC concentration was determined using a standard curve of MMC dissolved in PBS.



### 2.2.7 Cytotoxicity

To determine the MMC retained its activity, we performed a cytotoxicity assay. First, pHEMA disks were sterilized under UV light for 1 hour. The subsequent steps were performed in sterile conditions. The drug was eluted from the p(HEMA) disks (n=3) in 3mL of DMEM. The 3 mL of DMEM was replaced at 24-hour intervals and frozen until testing. COS-1 fibroblasts were seeded into a 24-well plate at 5000 cells/well in 0.5 mL of 3.5x cell culture media (35% FBS, 3.5% 100mM sodium pyruvate, and 3.5% 100Xantibiotic/antimycotic). The DMEM eluates (1.25 mL) from the p(HEMA) disks were added to each well of the plate, which the 3.5X media to 1x media (10% FBS, 1% sodium pyruvates, and 1% anti-anti). The cells were incubated undisturbed for 5 days at 37° C in a 5% CO<sub>2</sub>/95% air atmosphere. After 5 days, the wells were washed three times with 1 mL Dulbecco's PBS to remove any dead cells; the remaining cells were fixed with 0.5mL 10% neutral buffered formalin for 30 minutes before being stained with 0.5mL toluidine blue (0.5% w/v) for 1 hour. The plates were washed five times with 1 mL of deionized water and allowed to dry overnight. The toluidine blue stain was subsequently solubilized with 1 mL of 2% SDS and read on a plate reader at 650 nm. The percent effect was calculated based on the stain present in control wells that had no drug.<sup>37</sup>

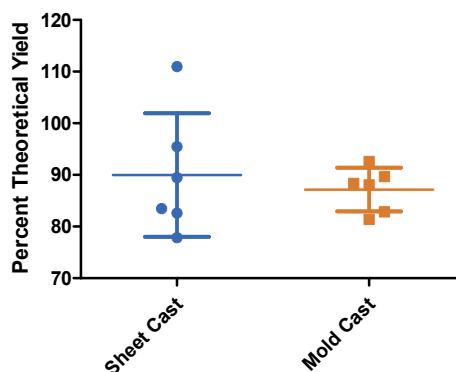


**Figure 2.3:** The percent theoretical yield for sheet and mold-cast pHEMA disks. The mean of the sheet-cast disks was  $89.98 \pm 11.96$  SD and the mean of the mold-cast disks was  $87.16 \pm 4.23$  SD. While a student's t-test showed that the yield was not significantly different, an F test showed that the variances were significantly different with a p value below 0.05. (n=5)

## 2.3 Results

### 2.3.1 Sheet vs Mold Cast Loading Efficiency

To show that there was no difference in loading efficiency between sheet and mold cast films, disks were loaded with 2 mg in each vial. The amount of drug in each disk was compared to the predicted amount loaded. **Figure 2.3** shows that the mold- and sheet-cast films had similar mean loading efficiency but statistically different variances. The mold-cast disks had a lower variance than the sheet-cast. A Student's t-test is used to determine if two samples have the

same mean where an f-test determines if they have the same variance.

### 2.3.2 6-hour vs 12-hour Weight

6-hour and 12-hour mold-cast pieces were weighed to determine if there was a difference in density due to casting times. **Figure 2.4** shows the distribution of weights for both groups. The mean weight of the 6-hour disks was  $36.37 \text{ mg} \pm 2.56 \text{ SD}$ . The mean weight of the 12-hour disks was  $39.76 \text{ mg} \pm 5.07 \text{ SD}$ . A Student's t-test determined that the difference in these means was statistically significant ( $p\text{-value} < 0.0001$ ) and an F-test to compare variances determined that the variances were also statistically different ( $p\text{-value} < 0.0001$ ).

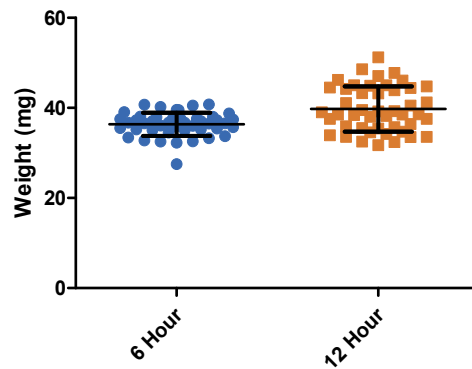


**Figure 2.4:** Weights of 6 and 12-hour p(HEMA) disks. 6- and 12-hour disks were washed and then dried before weighing to compare the consistency in their size. The 6-hour disks have more consistent sizing. The weight of each disk is plotted separately ( $n=46$  for each group) Error bars represent standard deviation. A Student's t-test found that there was a significant difference in the weights with the mean weight for the 6-hour disks being  $36.37 \pm 2.568$   $N=46$  and the mean weight for the 12-hour disks being  $39.76 \pm 5.01$   $N=46$  ( $p < 0.0001$ ). An F test found that the variances between the two were significantly different ( $P < 0.0001$ )

### 2.3.4 6-hour vs 12-hour Ethanol Quantification

Because there was a casting-time dependence on the p(HEMA) disk weight, we also performed a drug loading test on the two types of disks to determine if there was a difference in loading efficiency. The results were

calculated as percent theoretical yield.

**Figure 2.5** shows the comparison between the two. Here, the mean percent theoretical load for the 6-hour disks was  $69.16\% \pm 5.8$  SD, the mean percent theoretical for the 12-hour disks was  $75.19 \pm$

$9.7$  SD. A Student's t-test

determined that there was no statistically significant difference between the two means.

### 2.3.5 6-hour vs 12-hour PBS Release

We also compared an *in vitro* release of MMC of disks made using the 6- or 12-hour casting time. **Figure 2.6** shows the cumulative release MMC from the p(HEMA) disks into PBS over 10 days. The kinetics of the release between the two groups was not statistically different. Both disks would effectively release MMC over the course of 10 days.

### 2.3.6 6-hour v 12-hour Cytotoxicity

This assay measures the ability of a well-characterized fibroblast cell line, COS-1, to proliferate in the presence of MMS released from the p(HEMA) disk. Previous work has shown that when 5,000 cells are plated into each well of a 24 well plate, they will reach confluence after 5 days of culture with no medium changes.<sup>37</sup> Thus, we could compare the relative effect of

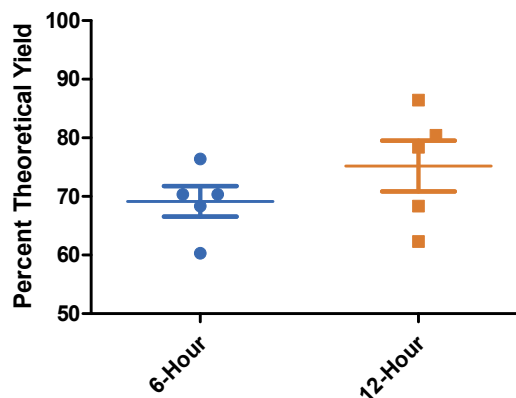


**Figure 2.5:** Drug yield of 6 and 12-hour p(HEMA) disks. p(HEMA) disks cured at 6 and 12 hours were placed in ethanol after loading with  $6.5 \mu\text{g}$  per disk. The amount of MMC was quantified using UV/vis and the two methods compared. The 6 hour had a lower error than the 12 hours but the means were not statistically significant. MMC from each disk is plotted separately, ( $n=5$ ). Error bars represent standard deviation.

MMC eluted into cell culture media on COS-1 fibroblasts to untreated cells. Prior work had shown that washed hydrogel with no MMC is not cytotoxic.<sup>37</sup> This ensures that the effect in the assay is a result of the MMC eluted into the cell culture media. **Figure 2.7** shows a representative example plate of stained COS-1 cells after 5 days of culture. The full concentration of MMC in this case was 10  $\mu\text{g}/\text{mL}$ . This illustrates the sensitivity limit of our cytotoxicity assay. To determine the activity of the MMC on fibroblasts, we performed a cytotoxicity study and

compared the 6-hour and 12-hour cast films. **Figure 2.8** shows that there was no significant difference between the cytotoxic activity of the disks over the course of 8 days.

## 2.4 Discussion

Previous methods described allowing the ethanol to evaporate under a hood for up to 10 days. This process is too time consuming for a manufacturing scale-up. Evaporating the ethanol under a vacuum reduced the time needed to load the MMC into the hydrogels by half and allowed the step to be taken without risk of light exposure, which can degrade the MMC.

Development of the ethanol drug quantification assay was crucial to manufacturing scale-up as we needed an assay to determine the actual drug load rather than simply relying on the theoretical load. This assay was critical in preparing the product for GMP manufacturing and allowed comparison between lots and casting methods.

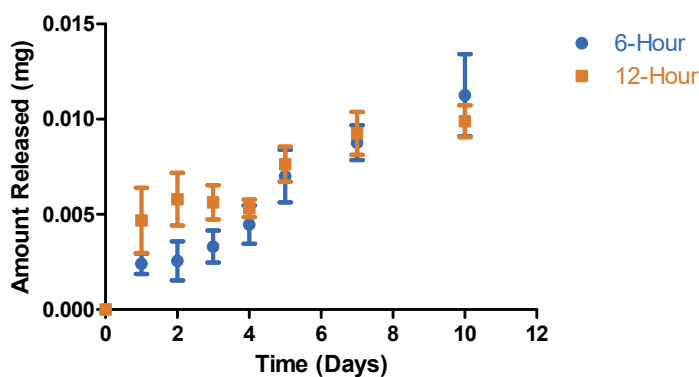


**Figure 2.6:** PBS release of 6 and 12-hour pHEMA disks. p(HEMA) disks cured at 6 and 12 hours, washed, and then loaded with 6.5  $\mu\text{g}$  of MMC. Disks were placed in 10 mL of PBS and eluted for 10 days as described in the text. Data are plotted as mean  $\pm$  SD (n=4).

The cytotoxicity assay helps show the effect the eluate has on proliferating cells. Diluting the MMC helped determine the sensitivity of the cytotoxicity assay. MMC effectively kills 100% of cells in concentrations as low as 1.65  $\mu\text{g}/\text{mL}$ . This dilution showed that no cells grow until  $\sim 0.5 \mu\text{g}/\text{mL}$  of MMC.

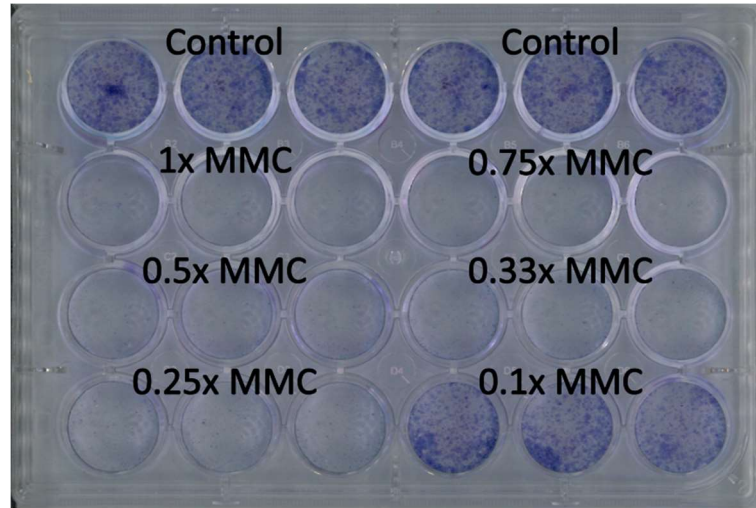


**Figure 2.7:** A representative plate of COS-1 staining. Here, MMC dilutions starting at 10  $\mu\text{g}/\text{mL}$  were tested in triplicate in wells B1-D6. A1-A6 were control wells with no treatment.

One of the key issues with scale-up for this p(HEMA) product was reducing the time required to produce each piece. By changing the casting method, casting time, and loading the disks under a vacuum, we were able to lower the production time by over 50% and increase uniformity in the product. Changing the casting method from a sheet to a mold reduced the number of steps necessary to produce these disks since we no longer had to cast the polymer in sheets of variable thickness and then cut the semicircles out of the p(HEMA) sheets. Demonstrating that there were no significant differences in the predicted drug load and the eluted drug load assured us that we had not changed the material significantly by casting it in the mold.

The mold-cast hydrogels were cast in a custom mold provided by New World Medical. The mold consists of two pieces that, when pressed together, formed 10 voids that allowed the hydrogel to cure into a shape that stacks well onto Ahmed glaucoma valves. Previously, we had reported a 12-hour casting time for the hydrogels cast into sheets. We wanted to determine if it

was possible to reduce this time to make more disks per day in the mold. We, therefore, made several mold-casted films for 6 and 12 hours, we weighed the pieces to determine if the differing casting time significantly altered the density. For this test, it was convenient that the mold ensured that each piece was created using the same amount of precursor solution.

The 6-hour cast pieces weighing less than the 12-hour pieces was initially concerning as we were uncertain if this would affect the loading efficiency, release kinetics, or the drug activity. We loaded both groups of hydrogels using identical techniques and measured the amount of MMC in each disk compared to the theoretical amount. The loading efficiency assay showed that there was no difference between the two casting times which is important as we must minimize the waste of costly MMC. The *in vitro* release showed that the release kinetics were unchanged by the different casting times. The cytotoxicity assay showed that the MMC activity was equivalent between the two groups. Thus, we determined that the differences in the 6-hour and 12-hour cast pieces would not affect the drug delivery and were equivalent to older casting methods.

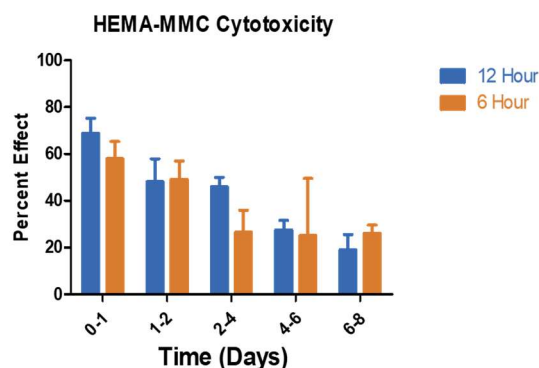


**Figure 2.8:** 12 and 6-hour disks loaded with 6.5  $\mu\text{g}$  of MMC were eluted into 3 mL of DMEM for the time periods indicated on the X-axis, for period encompassing 8 days. COS-1 fibroblasts were then allowed to grow for 5 days in the presence of the eluates and cell number was quantified and compared to a control with no MMC. There was no statistical difference in the cytotoxicity of drug eluted from the two types of disks. Data are plotted as mean  $\pm$  SD for each eluate (n=4).

## 2.5 Conclusion

Preparing this product for manufacturing required developing assays to understand how each step affected the final product. Using the drug quantification assays, we were able to compare between lots as well as between different methods of casting and loading. This

allowed us to determine the most important steps in manufacturing as well as determine the limits of our product. Using this assay, we reduced the manufacturing time of this product from 14 days to 7 days and achieved a 4-fold increase in the number of hydrogels that could be made in that time.

Additionally, in preparation for translating the product to GMP, it was important to formalize the manufacturing steps and finalize the procedure before producing a full-scale batch for clinical trials. We recorded all steps of the manufacturing process, drug quantification assay, *in vitro* release assay, and cytotoxicity assay as standard operating procedures (SOPs) for translation to a GMP facility. These SOP documents also will contribute to the Investigational New Drug (IND) submission to the FDA.

## **Chapter 3 - Aim 2: Translating a PLGA-based drug delivery system to a good manufacturing practice (GMP) facility**

### **3.1 Introduction**

Glaucoma is an insidious disease of the eye with a high toll on human welfare. In 2004, glaucoma caused an estimated \$2.9 billion economic burden in adults over the age of 40. Lower costs to the patient can be achieved through the use of outpatient procedures rather than using prescription medication.<sup>67</sup> Additionally, recent studies suggest that surgery has a lower failure rate in the first year compared to topical medication (24% failure rate for medication versus 12% for surgery).<sup>68</sup> These medications can fail for several reasons including patient compliance and lack of disease response to treatment. However, at 5 years, surgical interventions also have relatively high failure rates as a result of fibrous scar tissue forming around the surgical site or implant.<sup>11</sup> As a result, implantable drug delivery systems, both inert and biodegradable, have been proposed to combat these failures. Inert intraocular implants are invasive and come with an increased risk of hemorrhage.<sup>69</sup> Biodegradable implants reduce this risk by eroding after several weeks in the body.

Poly-lactic-co-glycolic acid (PLGA) is a biodegradable copolymer consisting of lactic and glycolic acid. It belongs to a group of esters known for their ability to hydrolytically degrade.<sup>35</sup> As the polymer degrades, it is reduced to monomers of lactic acid, which is cleared through the tricarboxylic acid cycle, and glycolic acid, which is metabolized and excreted in the kidney.<sup>33</sup> There are several PLGA-based drug delivery systems on the market and it has also been proposed as a biomaterial for tissue engineering.<sup>69,33</sup>



The Blake, John, and Ayyala group developed a PLGA-based drug delivery system in 2012 and tested the *in vitro* cytotoxicity of these films in 2014.<sup>44,40</sup> This system uses a breath figure morphology that is formed when the volatile solvent evaporates from a hydrophilic polymer causing the water vapor in the air to condense into a regular honeycomb pattern.<sup>41,42,70</sup> This breath figure enables a therapeutic to be surface-loaded into the pores of the PLGA as well as loaded into the bulk of the polymer. The research group loaded 5-flourouracil (5-FU) into the bulk of the polymer and mitomycin C into the pores. Figure 1.14 shows this drug delivery system attached to an Ahmed valve.

The Blake, John, and Ayyala group transitioned to PLGA from p(HEMA) based drug delivery system due to the biodegradability of PLGA. However, when compared to our earlier p(HEMA)-based drug delivery system, PLGA has additional advantages besides biodegradability. First, the raw materials are easier to procure as HEMA manufacturers usually sell barrels of material rather than the liter quantities required for lab testing. A drug can be loaded into the PLGA in multiple ways: suspended or dissolved in the bulk, or surface loaded into pores. Also, the loading of mitomycin C into the p(HEMA) system wasted much of the costly active ingredient whereas surface loading on the PLGA system reduces this waste.

The PLGA drug delivery system was tested in a lapine model for glaucoma drainage device surgery.<sup>39</sup> Here, six equal groups (n=8) of New Zealand white rabbits were treated with PLGA-based drug delivery devices with various amounts of 5-FU and MMC. In the group treated with a PLGA wafer loaded with 0.65 µg of MMC and 0.45 mg of 5-FU, a 40% reduction in the thickness of the fibrous capsule surrounding the drainage device was shown compared to a sham PLGA control.

After this promising study, the wafer drug delivery product required scale up for translation to a good manufacturing practice (GMP) facility. This required characterization of the

product and the formalization of the manufacturing protocols. The Food and Drug Administration (FDA) regulates the manufacture of drug products and requires that a product be produced and analyzed in commercial-scale batches before clinical trials.

In the present study, we describe the process of scaling up the production of PLGA films. This includes creating an assay to quantify the amount of drug in each wafer, modifying the manufacturing controls for quality assurance, and reproducing the product in large batches to ensure consistency between lots.

### **3.2 Materials and Methods**

#### *3.2.1 Materials*

Poly(D, L-lactide-co-glycolide) (PLGA 50:50) polymers, Resomer RG 504, and Resomer RG 502 were purchased from Evonik (Essen, Germany). Methylene chloride (ACS grade) was procured from Thermo Fisher Scientific (Waltham, MA). MMC (derived from *Streptomyces caespitosus*), 5-flourouracil (5-FU), neutral buffered formalin, dichloromethane (DCM), tetrahydrofuran (THF), and toluidine blue were from Sigma Aldrich Chemicals (St. Louis, MO). 24-well Costar tissue culture plates (15.6 mm diameter) were purchased from Corning (Corning, NY). COS-1 cells were obtained from the American Type Culture Collection (Manassas, VA) and maintained at 37°C in a humidified atmosphere of 5% CO<sub>2</sub>/95% air in Dulbecco's Modified Eagle's Medium (DMEM) (3.7 g/L sodium bicarbonate) supplemented with 10% fetal bovine serum, 1% 100 mM sodium pyruvate, and 1% 100x antibiotic-antimycotic. DMEM, antibiotic-antimycotic solution, sodium pyruvate, and FBS were from Gibco (Part of Thermo Fisher). PBS (137 mM NaCl, 3 mM KCl, 10 mM phosphate, pH 7.4) was prepared in-house. All chemicals were used as received, without further purification.

### 3.2.2 Drug Quantification

To measure the amount of 5-FU in cast films, we developed an extraction method for dissolving a PLGA wafer in an organic solvent and extracting the 5-FU into an immiscible ammonium hydroxide layer. First, a PLGA wafer was placed into a glass vial with 2 mL of dichloromethane (DCM). Then, 2 mL of 1 M ammonium hydroxide was added. The vial was capped and vortexed for 60 seconds until an unstable emulsion had formed. The suspension separated after 24 hours and the 5-FU partitioned into the top ammonium hydroxide layer. The concentration of 5-FU in the ammonium hydroxide layer could then be quantified using UV-Vis spectrophotometry. The results were analyzed using a Student's t-test to determine if the value was statistically different from the desired loading or among different lots.

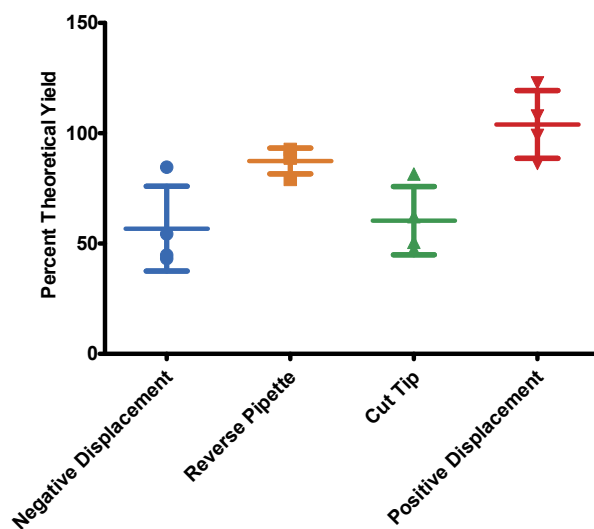


**Figure 3.1:** Determining the best pipetting method for use in casting a PLGA solution. A drug quantification assay was performed on films prepared using four different pipette techniques: negative displacement, reverse pipetting, cutting the pipette tip, and using a positive displacement pipette. A total of four films were examined for each method. Plotted points represent the value for each film; the long line represents the mean; shorter lines represent the upper and lower bound of the SD. A Tukey's multiple comparison test showed that the positive displacement differed from each of the three other groups. Additionally, a t-test showed that positive displacement was the only group that was not statistically different from the theoretical value of 100. The means were: Negative displacement  $56.75 \pm 19.22$ ; Reverse pipette  $87.43 \pm 5.848$ ; Cut tip  $60.39 \pm 15.47$ ; Positive displacement  $104 \pm 15.34$ . Results are reported as mean  $\pm$  standard deviation.

### 3.2.3 Pipette Test

Using the drug quantification assay described above, we determined which of four pipette techniques was most accurate for casting the volatile, viscous PLGA solution. Typical pipettes use negative displacement, where the vacuum formed from the pipette piston causes the solution to aspirate. Here, a typical user depressed the piston to the first stop, aspirates the liquid by allowing the spring-loaded piston to rise, and then depresses the piston to the second stop to dispense all of the liquid. Reverse pipetting uses negative displacement but requires the user to depress the pipette to the second stop before aspirating the liquid and then only depressing to the first stop to dispense the liquid. Cut tip pipetting, commonly used for viscous liquids, utilizes pipette tips that have had the first 2-3 millimeters removed to create a larger opening at the tip. Positive displacement pipettes use a microsyringe in the pipette tip to displace the liquid. For these experiments, we used a Microman E M250E positive displacement pipette from Gilson (Middleton, WI).

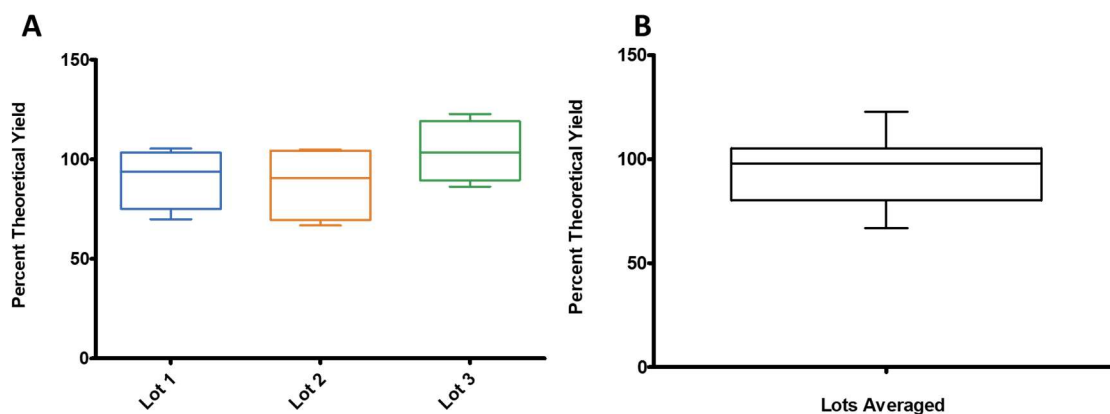


**Figure 3.2:** Drug quantification study with (A) lots compared and (B) lots averaged. Films were dissolved in DCM and the 5-FU was extracted into ammonium hydroxide. The means for Lots 1, 2, and 3 were  $1.63 \pm .27$  SD,  $1.58 \pm .33$  SD, and  $1.87 \pm .27$  SD. The mean for the lots averaged together was  $1.68 \pm .29$  SD. One-way ANOVA confirmed that the three lots were not significantly different from each other and one-sample t-tests confirmed that the lots individually and averaged are not significantly different than the theoretical value of 1.8. Boxes represent the middle quartiles and whiskers show the minimum and maximum values. The horizontal line represents the mean.

We made a 12.5% w/v solution of Resomer RG 504 in DCM with 0.9 mg/mL of 5-FU and used each technique to pipette 200  $\mu$ L of the solution. We then compared the results to a theoretical yield using a Student's t-test and compared amongst groups using one-way ANOVA.

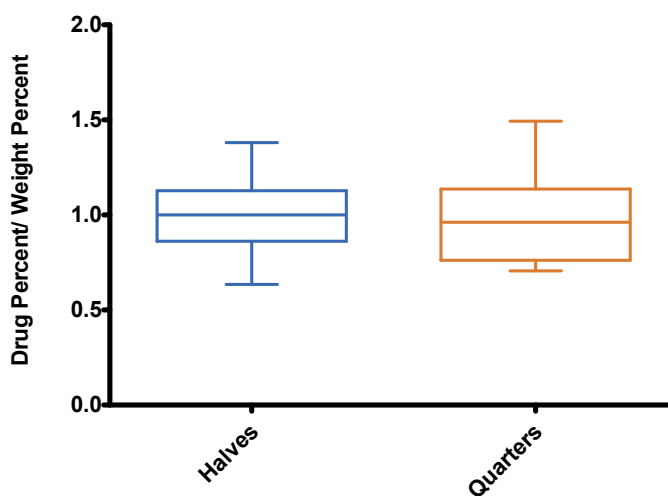


**Figure 3.3:** 5-FU is homogeneously dispersed in the films. Films from each lot were cut into pieces (either halves or quarters) and weighed. The pieces were then quantified using extrusion in ammonium hydroxide. If the drug is distributed homogeneously, the percent of drug in each piece should be the same as the percent weight of each piece. Thus, the percent drug was divided by the percent weight of each piece and the means were then compared to a theoretical value of 1.00 using a one-sample t-test. The means for the half-pieces were  $0.99 \pm 0.18$  SD and for the quarter pieces, it was  $0.99 \pm 0.12$  SD. Neither group showed a statistically significant difference from the theoretical mean of 1.00.

#### 3.2.4 Casting the Films

5-FU was ground to a fine powder (particle diameter approximately 10-100 $\mu$ m) using a mortar and pestle. A positive displacement pipette was used to cast the films for the rest of the studies. First, a 12.5% w/v solution of Resomer RG 504 in DCM with 0.9 mg/mL of 5-FU was made. The suspension was vortexed and then bath sonicated for 10 minutes. During the casting process, the solution was vortexed for 10 seconds in between each casting to maintain an even distribution of 5-FU in the polymer solution. Then, 200  $\mu$ L of the solution was pipetted onto a 0.5-inch diameter Teflon disk. The films were allowed to dry overnight at room temperature. For the second layer, a solution of 15% w/v Resomer RG 502 PLGA in DCM was prepared. The first

layer was placed in a spin-coater and 150  $\mu\text{L}$  of the Resomer RG 502 PLGA solution was dispensed on top before spinning at 1000 rpm for 25 seconds. The disk was then placed in a humid environment (60-70% relative humidity) to dry.

To load the MMC, a solution of 0.13 mg/mL of MMC in a 5:1 solution of DCM:THF was prepared; then 10  $\mu\text{L}$  of this solution was added to the top of each film, effectively loading 1.3  $\mu\text{g}$  of MMC on each wafer. Films were stored in a dark place at room temperature to avoid photo-degradation of the MMC.

For lot-to-lot variation studies, we produced 100 films on three separate days and sampled these lots for drug quantification (described above), and homogeneity and release kinetics (described below).

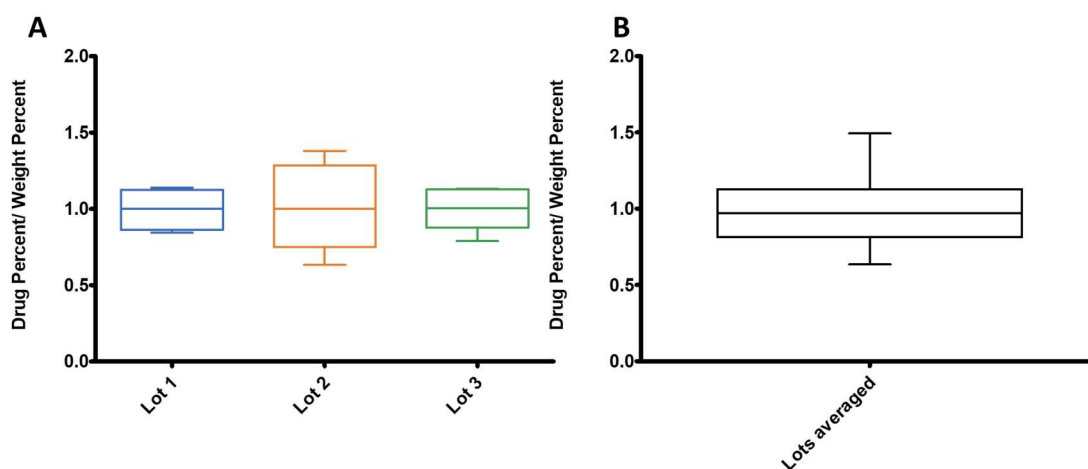


**Figure 3.4:** The 5-FU is homogeneously dispersed in the films. Lot-to-lot homogeneity study with (A) lots compared ( $n=10$  pieces for each lot) and (B) lots averaged ( $n=30$  pieces). Boxes represent the middle quartiles and whiskers show the minimum and maximum values. The horizontal line represents the mean. The mean values for lots 1 2 and 3 were  $0.995 \pm 0.12$ ,  $1.01 \pm 0.28$  and  $0.994 \pm 0.14$  respectively. The mean for all of the lots in aggregate was  $0.99 \pm 0.21$ .

### 3.2.5 Homogeneity

We wanted to determine if the 5-FU was homogeneously dispersed in the films for the anticipated use case of the films being cut by the end-user to change to dosage. Films were cut

into halves or quarters and each piece was weighed individually. The weights of the pieces were divided by the total weight of the wafer to determine the weight percent of each half or quarter. Then, the amount of 5-FU in each piece was measured using the drug quantification assay described above. The total amount of 5-FU was summed to determine the percent of the total 5-FU represented by each piece. The ratio of drug percent to weight percent was also determined for each half or quarter. Theoretically, if the drug is homogeneously dispersed the ratio of weight percent to drug percent should be 1.

### *3.2.6 Kinetics of drug release into PBS*

To determine the drug-release kinetics of the films, we conducted a study in PBS. Each PLGA disk, with Teflon still on the bottom, was placed into a glass vial with 10 mL of PBS pH 7.4. The vials were kept in a bead bath at 37° C for 30 days. At days 1, 3, 6, 8, 10, 13, 15, 17, 21, 24, 27, and 30, 1 mL of PBS was removed from the vial and 1 mL of fresh PBS was added to maintain the sink conditions. The sample was read on the UV-Vis spectrophotometer and the amount of 5-FU released was calculated from the absorbance at 266 nm, as determined from a standard curve of 5-FU prepared in PBS.

### *3.2.7 Cytotoxicity*

As reported in the previous chapter, the activity of the 5-FU and MMC was determined using a cell-based assay.<sup>40</sup> PLGA wafers were sterilized under UV light for 1 hour. Subsequent steps were performed in sterile conditions. DMEM without antibiotic-antimitotic, sodium pyruvate, and FBS was used to elute the drug from the wafers. Each wafer was placed in 3 mL of this incomplete DMEM, then placed into an incubator at 37° C 5% CO<sub>2</sub>. The entire volume of DMEM was removed at various intervals (1 to 3 days), replaced, and stored in a freezer until use. The eluate was then used to treat COS-1 fibroblasts. This cell line (5,000 cells in 0.5 mL) were seeded into the wells of 24-well plates DMEM with 3.5x anti-anti, FBS, and sodium

pyruvate. The cells were allowed to incubate for 1 hour before being treated with 1.25 mL of the eluate. The control well was treated with 1.25 mL of incomplete DMEM. The cells were incubated undisturbed for 5 days. After 5 days, the cells were gently washed three times with 1 mL Dulbecco's PBS and fixed with 0.5 mL 10% neutral buffered formalin for 30 minutes. The formalin was subsequently removed and 0.5 mL of 0.5% w/v toluidine blue in 10 % formalin was used to stain the cells (1 hour at 25°C). The stain was removed and the wells were gently washed four times with deionized water. The plates air dried overnight. The stain was solubilized with 0.5 mL of 2% w/v SDS in deionized water and quantified in triplicate in a 96-well plate using a plate reader at 650 nm.

### 3.3 Results

#### 3.3.1 Determining the best pipetting technique for casting PLGA films

Using the drug quantification assay, we were able to determine that positive displacement pipetting yielded the most accurate results for the loading of 5-FU into the disks. We performed the assay on PLGA disks prepared by the four methods (n=4 for each method). The negative displacement method yielded disks that contained 56.76 % (19.22 SD) of the theoretical drug yield, while the yield for the reverse pipette method was 87.43% (5.84 SD), the cut tip method 60.39% (15.47 SD), and the positive displacement pipette method was 104% (15.34 SD). Using a one-sample t-test we determined that **only the positive displacement pipette method** provided a drug yield that was not statistically different from the theoretical yield of 100%. **Figure 3.1** shows the data from disks cast using the different methods, plotted with mean and SD. Based on these data, we used the positive displacement pipetting method for all subsequent PLGA casting.



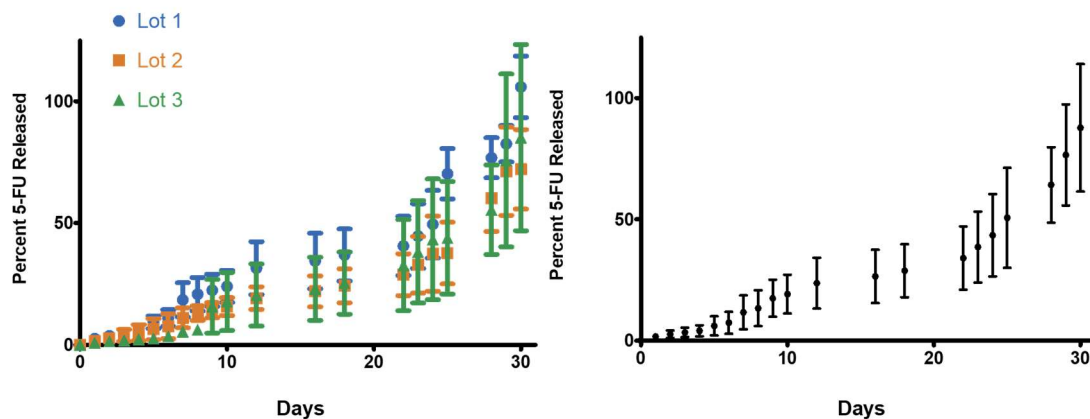


**Figure 3.5:** The release profiles of films n=9 with (A) the lots compared and (B) the lots averaged. Films were placed in 10 mL of PBS for 30 days. Samples were taken at regular intervals and read on a spectrophotometer. There is a delayed burst in the first 10 days and the drug is released at a relatively steady rate as the polymer begins to degrade after day 23. Values are plotted as mean  $\pm$  SD.

### 3.3.2 Lot-to-Lot Drug Quantification

We compared the drug quantification among three lots of PLGA films produced on separate days. We took 4 samples from each lot and quantified the amount of 5-FU in each film. **Figure 3.2** demonstrates that we were able to obtain the theoretical yield of 100% reproducibly among manufacturing lots. The means of the sample lots were  $90.75\% \pm 15.09$  SD,  $\pm 88.21\% \pm 18.77$  SD, and  $104\% \pm 15.35$  SD, respectively. A one-sample t-test determined that none of these lots were statistically different from the theoretical yield of 100%. The amount of MMC in each piece is 1.3  $\mu$ g. This is below the sensitivity of our spectrophotometer. We have shown the effectiveness of adding MMC to the system in previous cytotoxicity studies.<sup>44</sup>

### 3.3.4 Homogeneity Study

The homogeneity study was conducted by cutting the films into halves or quarters and weighing each piece. The weight was converted to a percentage of the total film weight by comparing it to the other pieces from the same films. Then, the drug content in each piece was quantified using our drug quantification assay. We were able to determine homogeneity by

comparing the ratio of the percent drug in each film over the percent weight to the theoretical value of 1. If the drug is homogeneously distributed within the films, the weight percent of the piece will be equal to the percentage of drug in that piece.

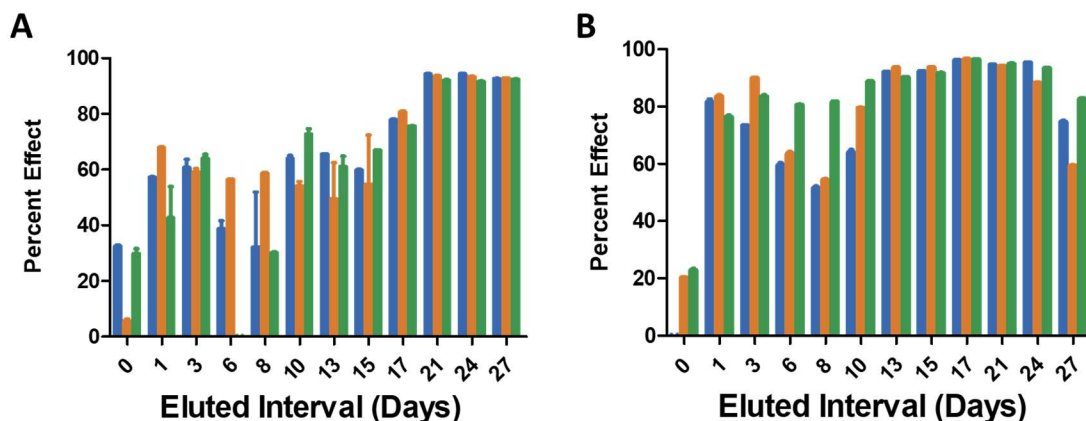


**Figure 3.6:** Cytotoxicity of (A) 5-FU and (B) 5-FU with MMC in PLGA films. Films were eluted in incomplete DMEM for intervals of 1-3 days. The eluate was then used to treat COS-1 fibroblasts. Percent effect refers to the ratio of stain in treated wells compared to the control wells with no treatment. 100% indicates no stain present and therefore 100% cell death. Here, individual samples are plotted in triplicate to illustrate the non-homogeneity of the assay.

**Figure 3.3** shows the homogeneity of wafers split into halves and quarters ( $n=18$  halves and  $n=12$  quarters). The pieces split into halves had a mean drug percent to weight percent ratio of  $0.999 \pm 0.18$  SD. The pieces split into quarters had a mean ratio of  $0.988 \pm 0.26$  SD. **Figure 3.4** depicts the lot-to-lot homogeneity for halved wafers from three separate lots ( $n=6$  from each lot). Lot 1, lot 2, and lot 3 had mean drug percent to weight percent ratios of  $0.995 \pm 0.12$  SD,  $1.01 \pm 0.28$  SD, and  $0.994 \pm 0.14$  SD, respectively. A one-sample t-test confirmed that none of the groups was statistically different from the theoretical mean of 1.

### 3.3.5 Kinetics of drug release into PBS

**Figure 3.5** shows the release kinetics of 5-FU from PLGA films derived from three different manufactured lots. A total of three films were used from each lot and **Panel A** compares the release between the three lots. **Panel B** presents the data from all nine films as

mean  $\pm$  SD. The Teflon reduced the initial burst of 5-FU escaping from the surface of the PLGA, then a sharp increase of 5-FU was noted around Day 25 when the PLGA is subject to bulk erosion. There was no difference in the release profile among lots; thus, lot-to-lot variations in drug release were within acceptable tolerances.

### *3.3.6 Cytotoxicity*

We determined the cytotoxic activity of the drugs released from these films using a cell-based assay. **Figure 3.6, Panel A**, shows the results of a cytotoxicity assay performed using films made only with 5-FU incorporated into the bulk PLGA. **Panel B** shows the cytotoxicity of films prepared with both bulk-loaded 5-FU and surface-loaded MMC. The bars on the graph represent individual samples to illustrate the heterogeneity in this assay. The addition of MMC raised the average percent effect to 65% for the first 10 days as opposed to 45% in the sample without MMC.

## **3.4 Discussion**

The first step towards making the PLGA films a viable product was revising and perfecting the published protocols. To ensure production reproducibility, we developed a drug quantification protocol that can determine the quantity of drug in each wafer. We used this assay to determine the best method for accurately dispensing equivalent amounts of the viscous PLGA/DCM solution during the casting step. In a traditional negative displacement pipette, the volatile solution affects the vacuum and causes the solution to leak from the tip during aspirating and dispensing. Additionally, DCM can corrode the rubber gasket on pipettes and prevent a seal from forming. In positive displacement pipettes, this problem is solved by using microsyringes as the pipette tips. In positive displacement pipettes, a disposable piston displaces the liquid and prevents the vapor from a volatile solution from affecting the vacuum. Casting the PLGA films using a positive displacement pipet allowed us to manufacture the PLGA

films with a high degree of consistency. The use of a positive displacement pipette in all later manufacturing greatly decreased the lot-to-lot variability of the drug content in our manufactured films.

Because the clinician may wish to cut the PLGA wafers into smaller segments before implantation, the next set of experiments was performed to determine if 5-FU was homogeneously deposited within the PLGA wafers. The drug percent to weight percent ratio creates a critical number that simplifies the results of the drug quantification assay and enables quick comparison among lots. We were able to show that not only were the films homogeneous, but they were also reproducibly homogeneous among manufacturing lots.

We used similar techniques to characterize the kinetics of drug release among different manufacturing lots. Here, we compared the lot-to-lot variation to that of the total production run. These release kinetics graphs show how the PLGA degrades in bulk, as there is a large burst drug release near the end of the study, signifying the bulk degradation of PLGA. The shape of these figures could be modified by changing the ratio of lactic acid to glycolic acid monomers, or by modifying the molecular weight of the PLGA. We were also able to demonstrate reproducibility amongst lots for the PBS release.

We also measured the activity of the 5-FU and MMC in cytotoxicity assays to ensure that the manufacturing process had not affected their anti-fibrotic effect. The toluidine blue assay enables quick measurement of cell presence and allows for rapid comparison between films. Films loaded with just MMC or just 5-FU can be used to quantify the effect of just one of the active ingredients. **Figure 3.6** demonstrates the smoothing effect MMC has on the initial few days of release. This is due to the surface-loaded MMC being released within the first 5 days before the 5-FU is released.<sup>44</sup>

### 3.6 Conclusion

Using PLGA for our ocular drug delivery device allays concerns of the long-term effects as the polymer erodes into biocompatible lactic and glycolic acid which can be harmlessly absorbed by the body. However, PLGA poses a challenge in scale-up due to the need for organic solvents to produce the breath figure morphology essential for the dual drug loading. Characterizing this product for translation to a GMP facility involved developing assays that were inexpensive and easy to perform in a laboratory setting. The solvent extraction drug quantification assay enabled us to rigorously interrogate each step of our manufacturing process. The assay allowed us to compare between pipette techniques and determine that a positive displacement pipette was the most effective way to produce consistently loaded wafers and reduce lot-to-lot variability. The drug quantification assay also allowed us to determine that the 5-FU was homogeneously dispersed within the films. This is important as a clinician may wish to modulate the dosage by cutting the film into smaller pieces.

Our PBS release study demonstrated reproducibility between large batches of films. Previously, films were made specifically for each study with no consideration for variability between days or issues with scaling up the manufacturing process. Producing 100 of these films on three separate days and then randomly sampling the lots ensured confidence in the manufacturing process.

The cytotoxicity assay provides an inexpensive way to determine the cytotoxic effect of the active ingredients and allows us to compare the effect between individual PLGA films. Here, we were able to demonstrate that the addition of MMC is effective in maintaining cytotoxic activity for 30 days before it is degraded and reabsorbed by the body.

In preparing this product for translation to a GMP facility, we also formalized the manufacturing steps to ensure reproducibility between lots regardless of manufacturer. These

standard operating procedures (SOPs) were recorded and delivered to the GMP facility and contributed to the investigational new drug (IND) submission with the FDA.

## **Chapter 4 - Aim 3: Sterilization and storage considerations for novel pHEMA and PLGA-based drug delivery systems**

### **4.1 Introduction**

The average time between an experimental discovery and patient-use of products successfully translated to market is 17 years.<sup>46</sup> Many inventions fail to achieve success, falling into the so-called “valley of death” where they lack the funding and resources necessary to achieve market penetration.<sup>71</sup> One challenge for novel drug delivery products is that there is seldom consideration for sterilization and storage during the inception of the innovative product. These hurdles can become insurmountable for small university spin-outs or clinicians who desire to bring their products to market.

Sterilization is required for products that are implanted in humans to ensure that there are no pathogens on the product from human contact during the manufacturing process. In this chapter, we describe a study that compares gamma and e-beam irradiation for sterilization of our p(HEMA)- and PLGA-based devices. Typically, and in our proceeding studies, we have used gamma irradiation sterilization with cobalt-60 as the emitting isotope. During decay, the cobalt-60 atoms consistently and continually emit one low energy electron (0.3 Mega Electron Volts, MeV) and two gamma rays at energies of 1.17 MeV and 1.33 MeV. E-beam radiation is produced using an electron accelerator. These accelerated electrons have a photon energy of around 10 MeV. This source is higher energy, but the resulting particles are less penetrative than the gamma rays produced by Co-60 decay. The result of this higher photon energy is that less exposure time is required to achieve the same dosage.

Any given radiation technique can have an unpredictable effect on polymers.<sup>49</sup> For instance, depending on the polymer type, chain length can be reduced or increased by gamma irradiation.<sup>51,72-74</sup> The number average molecular weight of polymer chains and the weight average molecular weight of the chains can be divided to give a measure of the variation in the molecular weights known as the polydispersity index (PDI). A higher PDI indicates more variation in the sizes of polymer chains.

It has been shown that irradiation, either by gamma or E-beam can cause chain scission in PLGA, reducing the molecular weight and increasing the PDI.<sup>73,75</sup> If radiation causes chain scission in a drug delivery system, it could reduce the molecular weight of all molecules in the system resulting in a similar release profile with a faster release; or it could reduce the molecular weight for some of the molecules causing a higher PDI and changing the release profile. In most cases, radiation will cause a combination of the two.

Alternatively, gamma or e-beam irradiation can cause crosslinking in p(HEMA) resulting in higher molecular weight and smaller pore size in the hydrogel.<sup>50,76,77</sup> When hydrogels crosslink, the molecular weight increases, and the drug release would be slowed. In the present study, we devise experiments to understand and control the effect of sterilization on our drug-releasing products.

In addition to sterilization, it is also important to understand how storage conditions affect the stability of our product before clinical trials are initiated. Herein we review the effect of lyophilization on our products. Lyophilization, also known as freeze-drying, is a process of removing moisture from a product at a low temperature. First, the product is frozen, then the pressure is reduced so that the ice sublimates from the product.<sup>78</sup> It had been used effectively in pharmaceutical applications to preserve biologically active ingredients.<sup>79</sup> We hypothesize that lyophilization will improve the long-term stability of our products. It is important to study the



stability of new polymeric drug delivery systems before clinical trials. The drug delivery system must behave the same way for each patient for the duration of the clinical trials and after the product reaches the market. Additionally, 21 CFR 312 delineates the requirements for submission of an Investigational New Drug (IND) application and requires that the product is stability-tested before clinical trials.<sup>80,81</sup> In this present study, we explore the effect of sterilization and storage on our polymer drug delivery systems.

## **4.2 Materials and Methods**

### *4.2.1 Materials*

2-hydroxyethyl methacrylate 99+% (Visomer<sup>®</sup>) was provided by Lintech International (Macon, GA). Poly(D, L-lactide-co-glycolide) (PLGA 50:50) polymers, Resomer RG 504, and Resomer RG 502 were purchased from Evonik (Essen, Germany). N,N'-Methylene-bisacrylamide (MBA) was acquired from Chem-Imprex International (Wood Dale, IL). Methylene chloride (ACS grade) was procured from Thermo Fisher Scientific (Waltham, MA). Mitomycin C (MMC) derived from *Streptomyces caespitosus*, N,N,N',N'-Tetramethylethylenediamine (TEMED), ammonium persulfate, 5-fluorouracil (5-FU), neutral buffered formalin, dichloromethane (DCM), tetrahydrofuran (THF), and toluidine blue were from Sigma Aldrich Chemicals (St. Louis, MO). 24-well Costar tissue culture plates were purchased from Corning (Corning, NY). COS-1 cells were obtained from the American Type Culture Collection (Manassas, VA) and maintained in a humidified atmosphere of 5%CO<sub>2</sub>/95% air in Dulbecco's Modified Eagle's Medium (DMEM) (3.7 g/L sodium bicarbonate) supplemented with 10% fetal bovine serum, 1% 100 mM sodium pyruvate, and 1% of 100x antibiotic-antimycotic. DMEM, sodium pyruvate, antibiotic-antimycotic solution, sodium pyruvate, and FBS were from Gibco (Part of Thermo Fisher Scientific). All chemicals were used as received, without further purification.

#### 4.2.2 Casting of *p*(HEMA) Disks

*p*(HEMA) disks were cast using the improvements described in Chapter 2. Briefly, 0.0508 g of MBA was mixed with 4 mL of water. Then, 0.0375 g of ammonium persulfate was mixed with 1 mL of water. 100  $\mu$ L of TEMED was added to 1 mL of the MBA solution followed by 1 mL of monomeric HEMA. The mixture was then vortexed for 10 seconds before initiating the reaction by adding 250  $\mu$ L of the ammonium persulfate solution. The mixture was vortexed again for 10 seconds before 110  $\mu$ L of the reaction mixture was added to each void in a custom-made mold. The mold was closed and the reaction was allowed to progress for 6 hours. The polymer pieces were removed and subjected to 5 sequential, 3-hour washes in 50 mL of 50:50 ethanol:water.

#### 4.2.3 Casting of PLGA Wafer

5-FU was ground to a fine powder (particle diameter approximately 10-100 $\mu$ m) using a mortar and pestle. PLGA wafers were cast with the improvements described in Chapter 3. A positive displacement pipette was used to cast the wafers. For the first layer, 12.5% w/v solution of Resomer RG 504 in DCM with 0.9 mg/mL of 5-FU was prepared. The solution was vortexed and then bath sonicated for 10 minutes. During the casting process, the solution was vortexed for 10 seconds in between each casting to maintain an even distribution of 5-FU within the polymer solution. Then, 200  $\mu$ L of this suspension was pipetted onto a 0.5-inch diameter Teflon disk. The wafers were allowed to dry overnight at room temperature. For the second layer, a solution of 15% w/v Resomer RG 502 PLGA in DCM was prepared. The single layered wafer containing 5-FU was placed in a spin-coater and 150  $\mu$ L of the Resomer RG 502 PLGA solution was dispensed on top of the wafer before spinning at 1000 rpm for 25 seconds. The disk was then placed in a humid environment (60-70% relative humidity) to dry. To load the MMC, a solution of 0.13 mg/mL of MMC in a 5:1 solution of DCM:THF was freshly prepared. This solution

(10 µL) was added to the top of each wafer, effectively loading 1.3 µg of MMC onto each wafer.

Wafers were stored in the dark at room temperature to avoid degradation of the MMC.

#### *4.2.4 Comparison of UV and Gamma Sterilization of PLGA*

Our initial experiments sought to compare previously published UV sterilization techniques with the industry-standard gamma irradiation. To UV sterilize, the wafers were placed in a chamber illuminated with UV light (~250nm). The samples were approximately 6 inches from the light source and were left exposed for 1 hour. For the initial gamma irradiation studies, samples were shipped to Sterigenics in Corona, CA. The product was gamma-irradiated with a target dose of 20 kGy and a range of 18-22 kGy. After sterilization wafers were stored at room temperature in a dry, dark place.

#### *4.2.5 Longitudinal Study Storage Conditions and Sterilization*

We performed a longitudinal storage study with the gamma-irradiated PLGA wafers. Wafers were made either with 5-FU only, with 5-FU and MMC, or with MMC only. Four storage conditions were studied: atmospheric pressure at both room temperature and 4° C; vacuum at both room temperature and 4° C . Vacuum-stored wafers were prepared by placing groups of wafers in a 40 mL amber vial with a rubber septum; the air was subsequently evacuated with a 20-gauge needle attached to the house vacuum that pulled to 20 mbar. All other samples were stored in the same vials without the application of vacuum. These samples were not lyophilized.

Wafers were sent to Sterigenics in Corona, CA for gamma irradiation. The product was gamma-irradiated with a target dose of 20 kGy and a range of 18-22 kGy. After sterilization, the wafers were stored according to the conditions described above: atmospheric pressure at both room temperature and 4° C; vacuum at both room temperature and 4° C . Both *in vitro* drug release into PBS and a cell-based cytotoxicity study were conducted at three time intervals to

determine the effect of storage time on the drug release properties: immediately after gamma irradiation; after 1 month of storage: and after 3 months of storage.

#### *4.2.6 GMP Manufacturing and Packaging*

PLGA and p(HEMA) disks were also manufactured at a GMP facility (a requirement for subsequent clinical trials) at Maitland Labs, in Maitland, FL. In this series of experiments, we explored lyophilization as a process to remove residual water from the devices before sterilization. The p(HEMA) and PLGA products were packaged in 10 mL amber bottles from Gurrusheimer Queretaro (Santiago De Queretaro, Mexico) stoppered with 20mm 2-leg lyophilization stoppers from Voigt Global Distribution Inc (Lawrence, KS). The 2-leg stoppers allow for a vacuum to be applied to the vial before the stoppers are fully depressed and sealed using a foil crimp. The lyophilization was performed using a VirTis 35L Ultra XL-70 Lyophilizer from SP Scientific (Gardiner, NY). The samples are loaded into a chamber and then the temperature is lowered to  $\sim -50^{\circ}\text{C}$  and the air is removed from the chamber to a vacuum pressure of 100 mTorr. After the water has evaporated and the samples are dry, the stoppers on the vials are depressed using a hydraulic system that seals the vials.

#### *4.2.7 GMP Product Gamma vs. E-Beam Sterilization Run*

The lyophilized GMP-manufactured samples were subsequently shipped to Sterigenics in Corona, CA for either gamma or E-Beam sterilization. The gamma sterilization run had a target dose of 15 kGy with a minimum reported dose of 14.3 kGy and a maximum dose of 16.2 kGy. The e-beam sterilization run had a target dose of 10.5 kGy with a minimum dose of 8 kGy and a maximum dose of 12 kGy. The irradiated wafers were shipped back to the Blake Lab and stored at ambient temperature in a dark place.

#### 4.2.8 PBS Release Studies

Drug release into PBS was performed as described previously. Each disk, with Teflon still on the bottom in the case of the PLGA wafers, was placed into a glass vial with 10 mL of PBS, pH 7.2. The vials were kept in a bead bath at 37° C for 30 days. At days 1, 3, 6, 8, 10, 13, 15, 17, 21, 24, 27, and 30, 1 mL of PBS was removed from the vial and 1 mL of fresh PBS was added to maintain the sink conditions. The sample was read on the UV-Vis spectrophotometer and the amount of drug released was quantified from the extinction coefficient at the absorption maximum (365 nm for MMC and 266 nm for 5-FU).

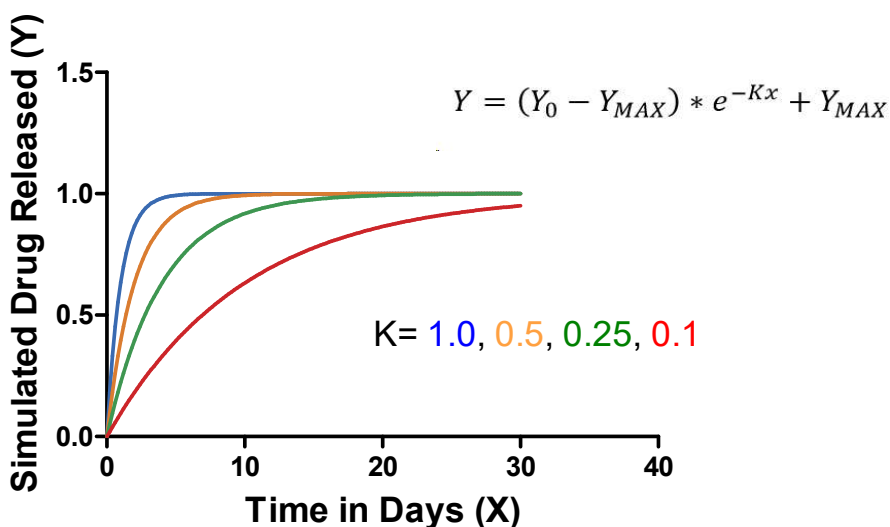


**Figure 4.1:** Theoretical *in vitro* release of the MMC from the p(HEMA) fitted to the exponential decay equation. This graph shows theoretical curves of the exponential decay equation with  $Y_0$  and  $Y_{max}$  values fixed at 0 and 1, respectively. The K values set to 1.0, 0.5, 0.25 and 0.1. These k values correspond to days of 50% release of 1, 1.5, 3, and 7, respectively.

#### 4.2.9 Cytotoxicity Study

As described in previous chapters, the activity of the 5-FU and MMC was determined using an *in vitro* cytotoxicity assay. Sterilized wafers with 5-FU only, 5-FU and MMC, or MMC only were eluted in incomplete DMEM in sterile conditions. The eluate was frozen until use. COS-1 fibroblasts seeded in 0.5 mL of 3.5x media were treated with 1.25 mL eluate and then the cells were fixed in stained after 5 days in culture. In previous reports, the pH of the eluate was

balanced to 7.4 before treating cells.<sup>40</sup> This technique was not used in these studies. For comparing the cytotoxicity studies, the mean cytotoxicity was calculated by averaging all time points in a single study. This number allowed for ease of comparison between study groups.

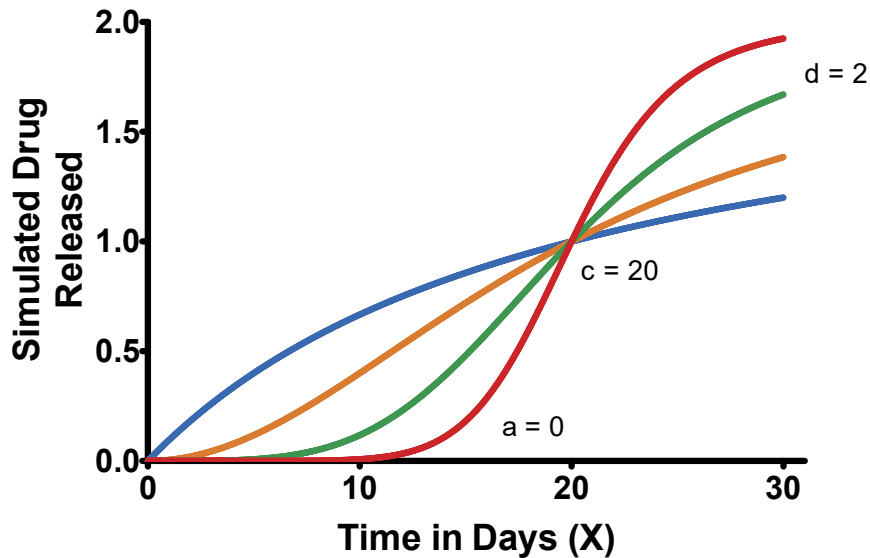


**Figure 4.2.** Example of Hill equation for release analysis: The *in vitro* release curves for the 5-FU released from PLGA were fit to the Hill equation above. In this example, the x-value at point c coefficient represents the time that 50% of the drug has been released. Here, we've set it to 20 days. Additionally, we've shown how the shape of the graph changes as you increase the b coefficient.

#### 4.2.10 Statistical Analysis and Curve Fit

The *in vitro* release profiles of the PLGA disks were fit to the Hill equation (**Equation 1**) so that curves could be compared between storage conditions and time points. In the Hill equation, the A and D coefficients determine the start and end values for Y. The b coefficient is a measure of the sigmoidicity of the graph. The lower the b coefficient, the more gradual the release of drug from the matrix. The c coefficient indicates the day of 50% release on the curve.

**Figure 4.1** shows a set of theoretical curves from the Hill equation with the A values set to 0, the D values set to 2, and the c values set to 20. The b values are set at 1, 2, 4, and 8. Each release

was fit to the Hill Equation and then the b and c coefficients were compared between each group.

$$Y = d + \frac{a - d}{1 + \left(\frac{X}{c}\right)^b}$$

**Equation 1: The Hill Equation**

The *in vitro* release of the MMC from the PHEMA could be fit an exponential decay equation (**Equation 2**). Here, Y represents the amount of drug released, X represents days *in vitro*, and k is a rate constant. Dividing the max value for Y by 2 and solving for X gives the day of 50% release for the MMC. **Figure 4.2** shows a set of theoretical curves from the exponential decay with the  $Y_0$  values set to 0, the  $Y_{max}$  value set to 1, and the K values set to 1.0, 0.5, 0.25, and 0.1.

$$Y = (Y_0 - Y_{MAX}) * e^{-Kx} + Y_{MAX}$$

**Equation 2: Exponential Decay**

## 4.3 Results

### 4.3.1 Preliminary UV and Gamma Irradiation Test

To compare the previous UV sterilization technique to gamma irradiation, films were sterilized in UV and also gamma irradiated. Then, an *in vitro* release was performed and the curves were fit to **Equation 1**. **Figure 4.3** shows the release curves for both groups at months 0 and 6. The  $r^2$  values for the UV curves at 0 and 6 months were 0.84 and 0.95, respectively. The  $r^2$  values for the gamma sterilized curves were 0.94 at 0 months and 0.98 at 6 months. The mean value for the sigmoidicity (b coefficient) of UV sterilized films was  $16.09 \pm 3.5$  at month 0 and  $8.59 \pm 1.4$  at month 6. The mean values for the sigmoidicity of gamma-sterilized films at months 0 and 6 were  $15.88 \pm 4.7$  and  $10.20 \pm 1.25$ , respectively. A two-way ANOVA determined that

there was no significant interaction between time and the sterilization technique and a Bonferroni post-test showed no statistically significant difference between the sigmoidicity coefficients between the groups at 0 and 6 months (**Figure 4.4**). The mean values for the c coefficient of UV sterilized films at months 0 and 6 were  $23.33 \pm 0.45$  and  $18.69 \pm 0.46$ , respectively. The mean values for the c coefficient of gamma-sterilized films at months 0 and 6 were  $19.49 \pm 0.18$  and  $19.49 \pm 0.40$ , respectively. A two-way ANOVA determined that there was significant variation caused by the sterilization technique and a Bonferroni post-test showed a statistically significant difference ( $p < 0.001$ ) between the two groups at both 0 and 6 months (**Figure 4.5**).

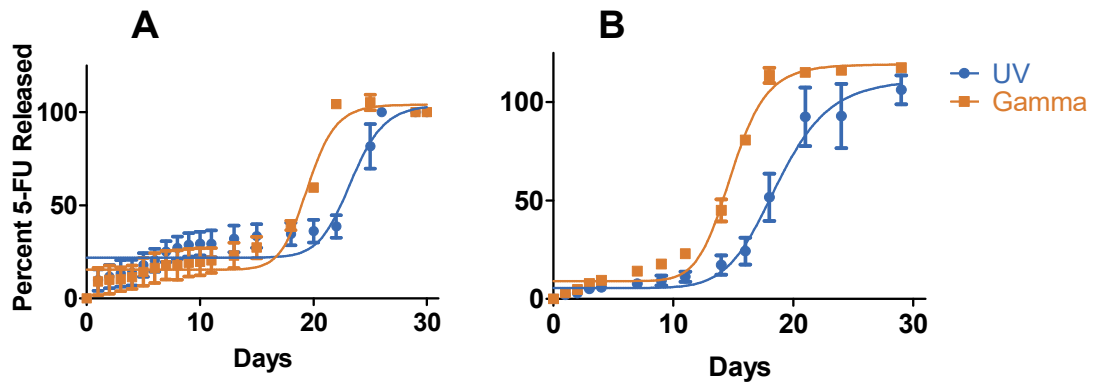


**Figure 4.3.** UV and gamma-sterilized films shown (A) immediately after and (B) 6 months after sterilization. Gamma sterilization causes a noticeable change in the release profile and both groups degraded over 6 months when stored in glass vials at room temperature in dark conditions. (n=3 for all groups)



#### 4.3.2 Longitudinal Storage Study in vitro Release after Gamma Irradiation

For the PLGA wafers stored in either cold or room temperature and under vacuum or in atmospheric conditions, a PBS release was performed at 0 months, 1 month, and 3 months after

sterilization and the curves

were fit to **Equation 1**. The  $r^2$

values range from 0.63 to

0.87 and the fit values for

each group can be found in

the supplementary

information. **Figure 4.6**

shows the release profiles of

the films kept at room

temperature under vacuum

at 0, 1, and 3 months. The

curves for the other storage conditions can be found in **Table S.1** in the supplementary

information. **Figure 4.7** shows the sigmoidicity coefficient for all 4 storage conditions at each

time point. **Figure 4.8** shows the day of 50% release for all 4 storage conditions at each time

point. The values of the b coefficient and c coefficient were plotted and compared using two-

way ANOVA. For the sigmoidicity b coefficient, the two-way ANOVA found significant ( $p < 0.0001$ )

interaction between storage condition and time since release indicating a decrease in both

values for all storage conditions over time. The results of the Bonferroni post-tests can be found

in **Table S.2** in the supplementary information. For the 50% release c coefficient, two-way

ANOVA found significant ( $p < 0.0001$ ) interaction between the storage condition and time. The

results of the Bonferroni post-tests can be found in **Table S.3** in the supplementary information.

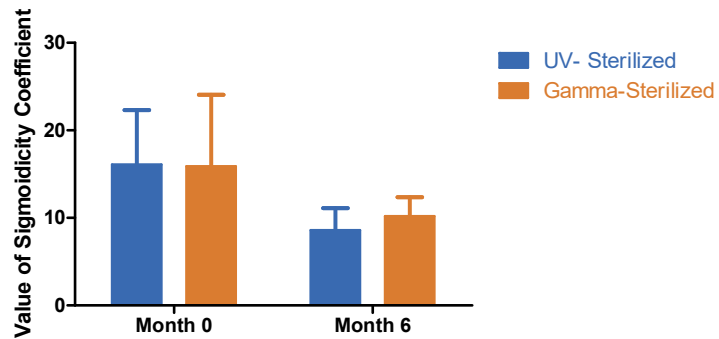


**Figure 4.4.** The sigmoidicity coefficients from the releases decrease as the films are stored for longer. Here, the b coefficients from the curves of each sample are plotted by sterilization technique. There is no statistical difference between sigmoidicity from either group between time points though there is a difference from month 0 to month 6. The lower sigmoidicity indicates a more gradual release of 5-FU. The mean values for the sigmoidicity of UV sterilized films at month 0 and 6 were  $16.09 \pm 3.5$  and  $8.59 \pm 1.4$ , respectively. The mean values for the sigmoidicity of gamma-sterilized films at month 0 and 6 were  $15.88 \pm 4.7$  and  $10.20 \pm 1.25$  respectively.

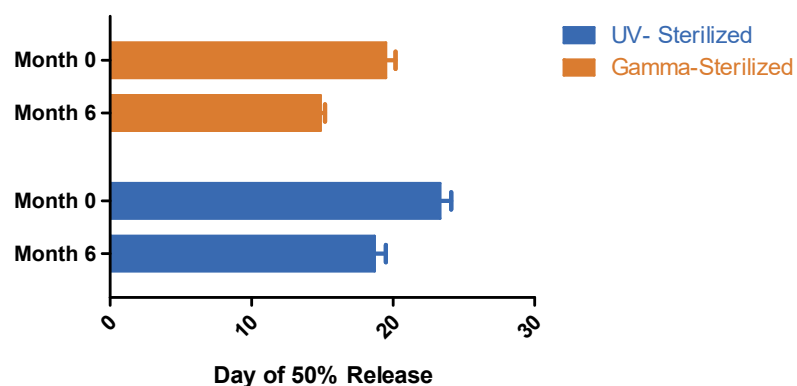


**Figure 4.5.** This graph depicts the *C* coefficient (day of 50% release) from the curve fits of each data set. There was a statistically significant difference between UV and gamma-sterilized groups at each time point. This shows that the films are degrading with storage and that gamma sterilization accelerates the degradation. The mean values for the *c* coefficients of UV sterilized films at months 0 and 6 were  $23.33 \pm 0.45$  and  $18.69 \pm 0.46$ , respectively. The mean values for the *c* coefficients of gamma-sterilized films at months 0 and 6 were  $19.49 \pm 0.18$  and  $15.49 \pm 0.40$ , respectively.

#### 4.3.3 Longitudinal Storage Study Cytotoxicity Assay after Gamma Irradiation

After gamma irradiation, the wafers were eluted into cell culture media after being held in the various storage conditions for 0, 1, and 3 months after irradiation. **Figure 4.9** shows the cytotoxicity assay results for PLGA wafers stored under our most stringent storage conditions (4°C under vacuum). **Tables S.4-S.7** in the supplementary information shows the results for all four storage conditions at all three time points. We ran a one-way ANOVA to compare storage conditions between months and drug loading types (5-FU only, 5-FU + MMC, and MMC only) and performed a Tukey’s multiple comparison post-test to determine if there was a difference in the mean cytotoxicity for the assays between each storage condition. The ANOVA found that there was no statistical difference between all groups at month 0 and 3. At month 1 for the 5-FU only groups, Tukey’s multiple comparison test found a difference in the cold-vacuum and room-vacuum storage conditions as well as between the room-vacuum and cold-atmosphere storage conditions. At month 1 for the 5-FU+MMC group, Tukey’s multiple comparisons showed a significant difference ( $p < 0.001$  between the cold-vacuum and room vacuum storage as well as

the room-vacuum and room-atmosphere storage. These differences led to the ANOVA indicating a difference in the mean cytotoxicity for Month 1 of the 5-FU and 5-FU+MMC groups. Full results of Tukey's multiple comparison post-test can be found in **Tables S.8-16** in the supplementary information.

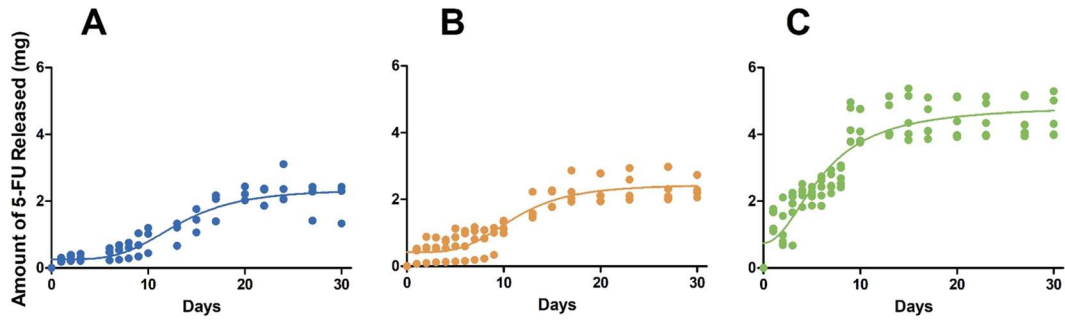


**Figure 4.6.** The release profile of the PLGA wafers in PBS changes after 3 months in storage. PLGA wafers were stored in four different conditions: in room temp or at 4° C, and under vacuum or in atmospheric pressure. Above are three exemplary release curves at (A) 0 months, (B) 1 month, and (C) 3 months of storage from the room-vacuum condition. The release curves visibly shift after being in storage. (n=4) for all groups

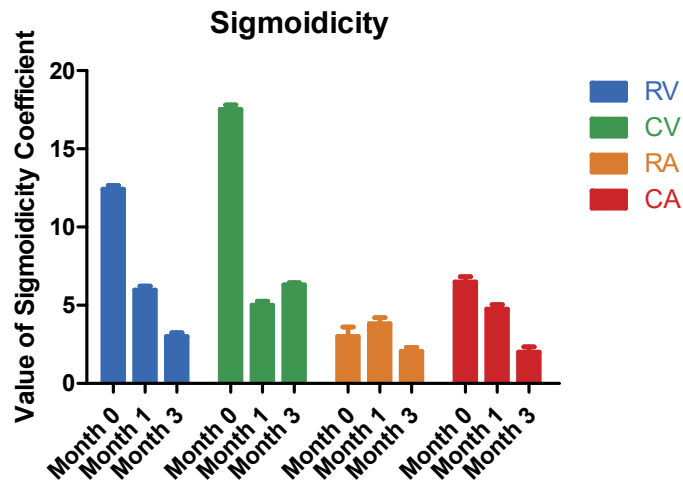


**Figure 4.7.** The sigmoidicity from the curves of the releases decrease as the films are stored for longer. Here, the b coefficients from the curve fits of each sample are plotted by the storage condition. You can see that while the vacuum-sealed wafers performed better initially than the atmospheric wafers, all groups had degraded significantly after 1 month of storage.

It seems that cold storage does not mitigate this degradation. RV=room temperature, vacuum; CV=cold storage, vacuum; RA=room temperature, atmospheric pressure; CA=cold storage, atmospheric pressure.

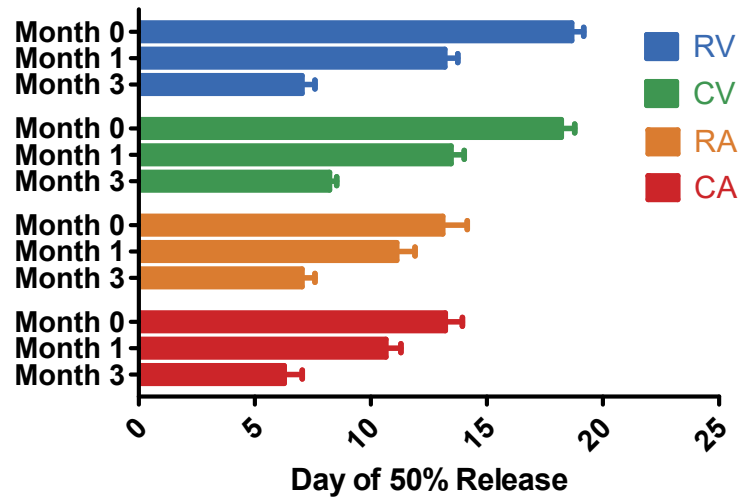


**Figure 4.8.** The curves show the time in the 50% release happening earlier with longer storage. Here, we depict the c coefficients from the curves of each data set. There was no significant difference between room temperature storage and cold storage groups. There is a significant difference between the vacuum and atmosphere stored groups. There was no significant difference among all the groups by 3 months of storage. This signifies that the product had degraded by month 3 regardless of storage condition. RV=room temperature, vacuum; CV=cold storage, vacuum; RA=room temperature, atmospheric pressure; CA=cold storage, atmospheric pressure.

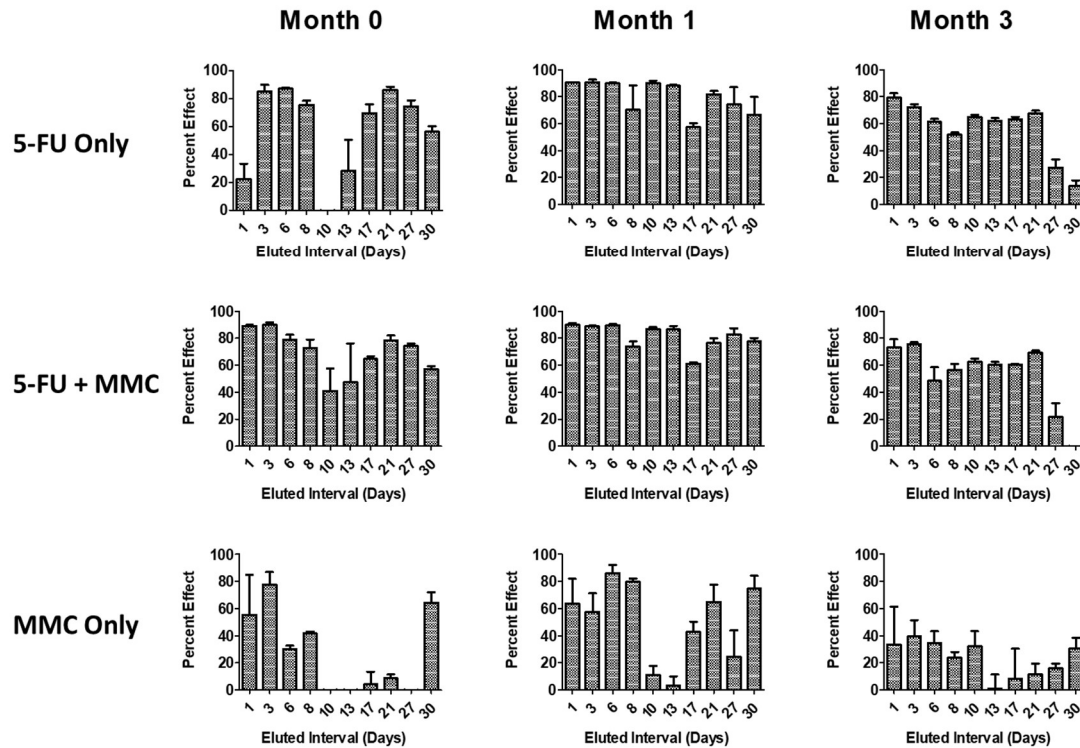


**Figure 4.9:** Cytotoxicity data from PLGA wafers stored under the most stringent storage conditions (4°C under vacuum). A table of example graphs showing the cold-vacuum storage condition for all three film types, 5-FU only, 5-FU+MMC, and MMC only at month 0, month 1, and month 3. One-way ANOVA showed no statistically significant difference between storage conditions for months 0, 1, and 3 for all three film types. (n=3 for all groups). All graphs can be found in the supplementary info.

#### 4.3.4 GMP Manufactured and Sterilized PLGA Wafers

After manufacturing and lyophilization, PLGA wafers were sent to California for either gamma sterilization or e-beam sterilization. We performed a PBS release on three groups: unsterilized, gamma sterilized, and e-beam sterilized. **Figure 4.10** shows the release curves of the three groups fitted to the Hill equation (**Equation 1**). The calculated day of 50% release and sigmoidicity coefficients was compared amongst curves. The  $r^2$  value of unsterilized was 0.66, for gamma sterilized was 0.66 and for e-beam sterilized was 0.67. The mean values of the b coefficient for sigmoidicity of the unsterilized, gamma sterilized or e-beam sterilized samples were  $7.92 \pm 1.60$ ,  $6.32 \pm 1.49$ , and  $4.57 \pm 0.88$ , respectively. (**Figure 4.11**) There was no

statistically significant difference between the unsterilized and gamma groups but the unsterilized and gamma sterilized groups both differed significantly from the e-beam sterilized group. The mean values of the c coefficient for 50% release of the unsterilized, gamma sterilized

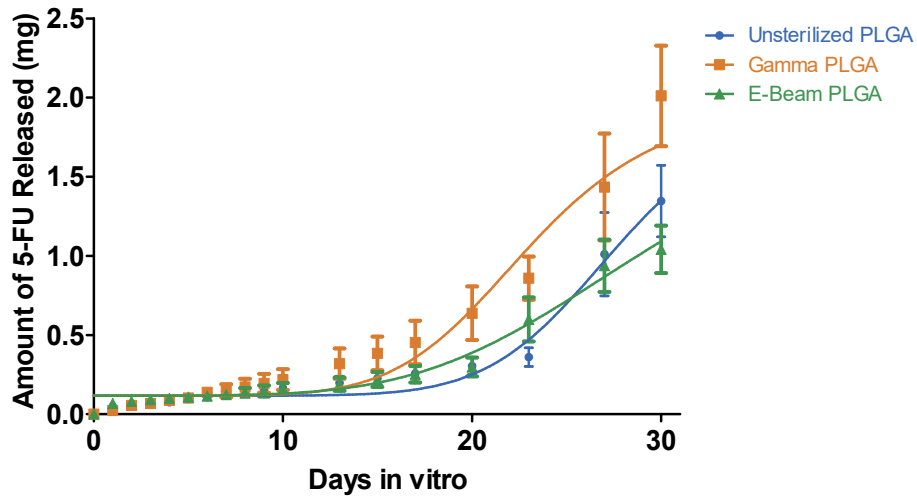


**Figure 4.10.** The release profile of the PLGA wafers in PBS changes under three sterilization conditions, unsterilized, gamma sterilized and e-beam sterilized. Above are the three release curves fitted with the Hill equation. The  $r^2$  value for unsterilized was 0.66, for gamma sterilized was 0.66 and for e-beam was 0.67. (n=8) ADD error bars. Try a refit to a different model.

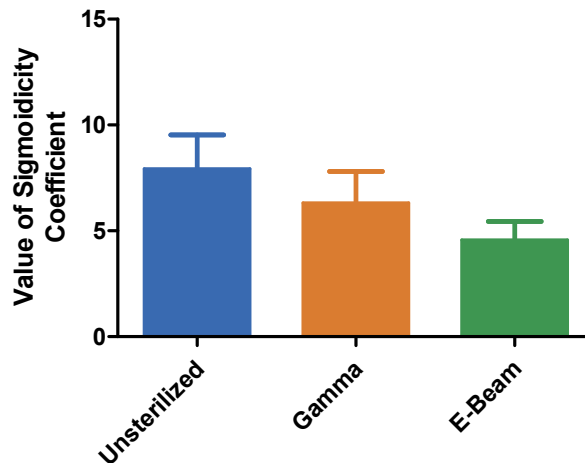


**Figure 4.11.** The sigmoidicity from the curves of the unsterilized, gamma sterilized, and e-beam sterilized films. This graph depicts the b coefficients from the curve fits of each sterilization technique. The mean values for unsterilized, gamma sterilized or e-beam sterilized samples were  $7.92 \pm 1.60$ ,  $6.32 \pm 1.49$ , and  $4.57 \pm 0.88$ , respectively (n=8). There was no statistically significant difference between the unsterilized and gamma groups but the unsterilized and gamma groups both differed significantly from e-beam.

or e-beam sterilized samples were  $27.67 \pm 1.33$ ,  $23.04 \pm 1.58$ , and  $29.55 \pm 2.25$  respectively.

(**Figure 4.12**) There was no statistically significant difference between the unsterilized and e-beam groups but the unsterilized and e-beam both differed significantly from gamma.

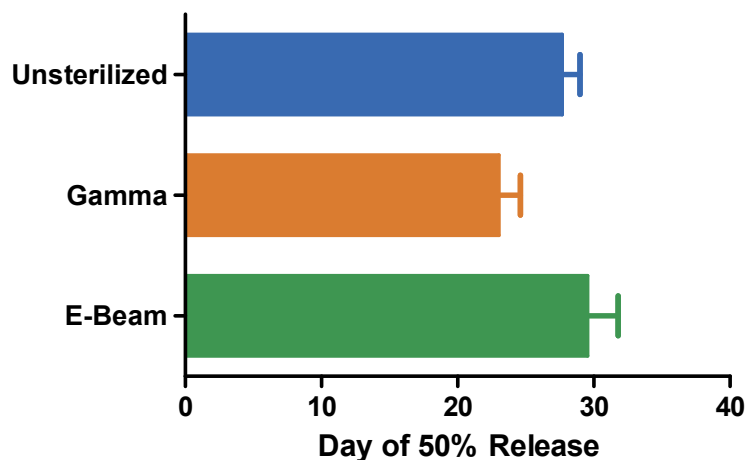


**Figure 4.12.** The day of 50% drug release for the unsterilized, gamma sterilized and e-beam sterilized films. Depicted here are the c coefficients from the curves of each data set. The mean values for unsterilized, gamma sterilized or e-beam sterilized samples were  $27.67 \pm 1.33$ ,  $23.04 \pm 1.58$ , and  $29.55 \pm 2.25$ , respectively ( $n=8$ ). There was no statistically significant difference between the unsterilized and e-beam groups but the unsterilized and e-beam both differed significantly from gamma.

#### 4.3.5 GMP Manufactured and Sterilized p(HEMA) Disks

After manufacturing and lyophilization, p(HEMA) disks were sent for either gamma sterilization or E-beam sterilization. We performed a PBS release on three groups, unsterilized, gamma sterilized, and e-beam sterilized. **Figure 4.13** shows the release curves of the three groups fitted to the exponential decay equation (**Equation 2**) and their day of 50% release was compared amongst curves. The  $r^2$  values for the unsterilized, gamma, and e-beam curves were 0.92, 0.94, and 0.88, respectively. The calculated day of 50% release determined by the fit was  $2.12 \pm 0.016$  days for the unsterilized group,  $5.79 \pm 0.007$  days for the gamma sterilized group, and  $4.17 \pm 0.013$  for the e-beam group. Thus the sterilized devices are releasing

## 4.4 Discussion

### 4.4.1 Comparison of UV and Gamma Sterilized PLGA Wafers

We performed a comparison of UV and gamma-sterilized films immediately after and 6 months after sterilization. The films were tested by determining the kinetics of drug release into PBS and the resulting curve was fit to the Hill equation. PLGA degrades in the presence of water. The water penetrates the matrix and hydrolyzes the ester bonds, reducing the molecular weight of the PLGA. A lower molecular weight leads to a more gradual release as shown by a decrease in sigmoidicity and a faster day of 50% release. Sigmoidicity can be related to the polydispersity index (PDI) of the polymer, with a lower PDI meaning a steeper release curve and a higher PDI meaning a more gradual release curve. A lower PDI indicates more uniform molecular weights which would lead to uniform degradation. Higher the PDI means more disparate molecular weights of individual polymer chains. These chains degrade at the same rate but smaller chains become soluble more quickly leading to a breakdown in the bulk of the polymer disks. **Figure 4.4** shows the release curves for the UV and gamma sterilized products at months 0 and 6. **Figure 4.5** shows the sigmoidicity coefficients for both groups at months 0 and 6. **Figure 4.6** plots the day that 50% of the drug had been released from the PLGA films subjected to different sterilization regimes, immediately after the process and after 6 months of storage at ambient temperature. This initial test showed that gamma irradiation sped up the release of 5-FU from our PLGA product. At month 0 and at month 6, the gamma-irradiated product had a sooner day of 50% release compared to the UV product.

Immediately after sterilization, the gamma sterilized group had released 50% of the 5-FU after 19.5 days *in vitro* compared to 23.33 days for the UV sterilized group which were significantly different ( $p < 0.0001$ ). After 6 months of storage, the day of 50% release was 18.7 for the gamma sterilized group compared to 19.49 for the UV sterilized group which were



significantly different ( $p < 0.0001$ ). Both groups showed an earlier day of 50% release after 6 months in storage. There was no statistically significant difference in sigmoidicity ( $p > 0.5$ ) between the groups immediately after storage and after 6 months of storage. However, both groups showed a decrease in sigmoidicity after 6 months in storage. These results showed that the product was degraded after gamma irradiation and that it continues during storage regardless of the sterilization technique.

#### 4.4.2 Longitudinal Storage Study of Gamma Sterilized PLGA Wafers

Based on the previous results, we devised an experiment to test if changing the storage condition of our product could mitigate the degradation we observed over time. In the new study, we stored the PLGA wafers under 4 different conditions: in 4° C and at room temperature, and with and without vacuum. We chose these conditions as they were easy to create in a laboratory setting and they are common methods for storing degradable products. These four groups were sterilized as before and then tested using both an assay that measured the kinetics of *in vitro* drug release PBS release as well as an assay that assessed the drug's cytotoxicity. The curves of drug release into PBS were fit to the Hill Equation. The *in vitro* release results show that vacuum storage mitigated the degradation caused by gamma irradiation but after 3 months in storage all groups showed similar degradation. It is possible that pulling a vacuum on the product did not adequately remove water from the system. Moisture is the main cause of PLGA degradation through hydrolysis. Additionally, it did not appear that keeping the product in cold storage had any effect on the PBS release. This is good news for commercialization as cold chain storage is expensive and limits access in underdeveloped nations.

For the cytotoxicity assay, films were made with 5-FU only, 5-FU + MMC, and MMC only. The mean cytotoxic effect was compared between storage conditions for each drug type and

storage condition at each time point. **Figure 4.10** shows the cytotoxicity profiles for all three film types stored under a vacuum and at 4° C. A one-way ANOVA showed that there was no difference in the activity of the drugs amongst storage conditions at months 0, 1, and 3. This signifies that irradiation does not affect drug activity. This is beneficial for the commercial product as it indicates that the drugs will be active regardless of the sterilization technique.

#### *4.4.3 Comparison of Gamma and E-beam Sterilization Techniques with GMP Manufactured PLGA Wafers*

To improve the shelf life of our PLGA product, we lyophilized our PLGA wafers after manufacturing them in a GMP facility. Then we compared the effects of gamma sterilization and e-beam sterilization. E-beam sterilization has a less energetic source of radiation and we hypothesized that this would cause less degradation of our product. In PLGA degradation by radiation could cause the production of free radicals at the chain ends of the polymer. These radicals could accelerate the degradation process. The results indicate that e-beam did cause less degradation with the day of 50% release happening later than the gamma sterilized product. However, the e-beam also showed a more gradual release as it has a significantly lower sigmoidicity. This gradual release indicates a lower PDI for the PLGA matrix. However, a gradual release could be desirable if it is controlled and does not lead to further degradation with storage. It will be important to perform a stability test on these products to determine if the lyophilization improved the stability of the product over time as our initial tests without lyophilization created products that were unsuitable for commercialization.

#### *4.4.4 Comparison of Gamma and E-beam sterilization with GMP Manufactured p(HEMA)*

The p(HEMA) disks were made in a GMP facility and then lyophilized. After lyophilization, the disks were separated into three groups: unsterilized, gamma sterilized and e-beam sterilized and drug release into PBS was quantified over 30 days. The exponential curve fit

procedure describes above allowed for ease of comparison among the three groups. **Figure 4.13** shows the drug release into PBS. The e-beam sterilization has a less penetrating particle source (accelerated electrons) and was predicted to cause less crosslinking in the hydrogel matrix. Crosslinking in the matrix would result in a slower release as it would take longer for the MMC to diffuse out of the hydrogel. Indeed, the e-beam sterilized films showed a faster release than the gamma sterilized product and both released more slowly than the unsterilized group. In the case of the p(HEMA), a slower release is not necessarily undesirable. This is because fibroblasts are recruited between days 3-10 during the wound healing process, and a slower delivery would allow drug release to better coincide with fibroblast appearance at the site of GDD implantation. Reducing the number of fibroblasts recruited into the surgical site will improve the outcome of the surgery by lowering the number of cells that synthesize and secrete extracellular matrix in the bleb wall. It will be important to test these p(HEMA) delivery devices again after several months to see if the release curves are unchanged after storage.

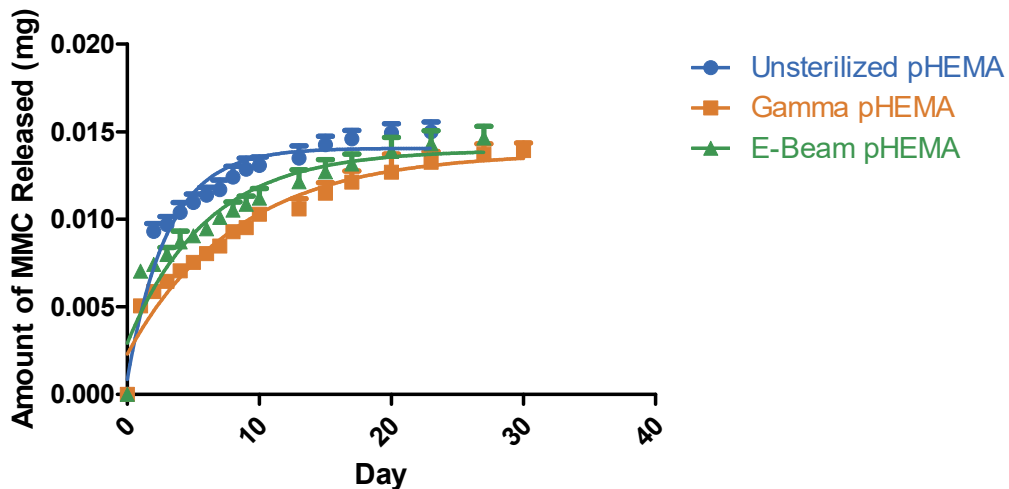


**Figure 4.13:** *In vitro* release of MMC from pHEMA disks. The release follows a one-phase exponential decay (see Eq 1 in text). The  $r^2$  values for the unsterilized, gamma, and e-beam curves were 0.92, 0.94, and 0.88, respectively. The calculated days of 50% release determined by the fit were 2.12, 5.79, and 4.17 for unsterilized, gamma, and e-beam, respectively. (n=8)

#### 4.5 Conclusion

Because UV sterilization is not an accepted sterilization technique by the FDA, other sterilization and packaging procedures needed to be developed for our drug delivery devices. Our preliminary trials with gamma irradiation showed that sterilization degraded our PLGA product in an undesirable way. Our subsequent attempts to slow down product degradation (storage under vacuum or at 4°C) had no lasting effect on product stability and only improved the degradation for the first time point after sterilization (1 month). While the kinetics of drug release changed after storage, the cytotoxicity studies show that the activity of the drugs in the PLGA wafer did not significantly degrade after storage and retained their anti-fibrotic effects.

We then lowered the target dosage of radiation from 20 kGy to 15 kGy and introduced e-beam radiation as a lower energy option. Additionally, we lyophilized our products, both to remove additional water and to more closely mimic the GMP manufacturing process.

In the p(HEMA)-based drug delivery device, e-beam treated product showed a faster release than the gamma-irradiated material and both sterilization techniques produced films with faster releases than the unsterilized product. This is a result of chain crosslinking that occurs in p(HEMA) after radiation. The crosslinking causes smaller pores in the hydrogel matrix and increases the time it takes for MMC to diffuse out of the bulk of the polymer. The slower release caused by gamma irradiation could be beneficial if it can be controlled and the degradation does not continue during storage.

For the PLGA, the e-beam sterilized product had a slower release than the gamma-irradiated product. This is because the high-energy sterilization in the gamma produces chain scission in the PLGA. The lower molecular weight PLGA then releases 5-FU more rapidly. All three groups that were manufactured at the GMP facility and lyophilized performed better than the previous storage condition study when compared at the initial time point. The could be an

early indication that lyophilization improves the degradation. However, to fully determine if the lyophilization reduces degradation, we will have to perform these studies again after at least a month in storage.

The p(HEMA) and PLGA products now have a clear path forward for clinical trials, with a few follow up studies necessary to determine the stability of the products. It appears that the initial degradation of the PLGA product has been mitigated and a simple stability study will show whether lyophilization will improve the shelf life of the product. For in-human clinical trials, the products can now be reliably made in a GMP facility as the FDA requires.

## Chapter 5 - Glaucoma Market Landscape and Challenges

This work has been a part of an ongoing effort by a Tulane University spin-out, Elutimed, to develop a solution to poor patient outcomes in glaucoma surgery. Elutimed is currently in the process of assembling an Investigational New Drug (IND) filing for submission to the Food and Drug Administration (FDA), which is the final checkpoint before clinical trials. The global glaucoma market is poised for growth and is projected to reach \$3 billion dollars by 2023.<sup>82</sup> Elutimed enters into a fragmented market with much competition and a high barrier to entry. This increased competition, however, indicates the urgent need for solutions in this field. Indeed, patient and physician surveys indicate a desire for improved outcomes.<sup>83</sup>

The glaucoma market's growth is driven by an aging population, an increase in disposable income, and technological change. From 2014-2019 there was a 3.6% annual growth in number of older adults (65+ years old) and this number is set to increase year over year until 2030.<sup>84</sup> Additionally, the per capita disposable income has increased by 2.5% annually for that same time period. Patients with more disposable income are at an increased likelihood of resolving vision impairments.<sup>85</sup> These market drivers create a healthy market for Elutimed and the technological innovations in the market increase the probability of acceptance for Elutimed's products.

**Table 5.1** show a list of companies creating drug release products for glaucoma. The FDA recently approved Durysta, the first of many drug delivery systems in the pipeline for glaucoma treatment. Many of these competitor's products focus on minimally invasive injectable systems that attempt to reduce intraocular pressure (IOP). Few of these products are biodegradable, however, and none combat scar tissue formation after glaucoma surgery.<sup>86</sup> This

competition indicates a fragmented field with many vying for market share. Elutimed has differentiated itself by targeting a patient population that has already undergone surgery.

Recent patient surveys indicate a desire for new drug delivery options if they reduce the dependence on eye drops. In one survey, 61% of patients studied indicated acceptance of subconjunctival sustained release device given the chance to prevent blindness.<sup>83</sup> Among those that indicated acceptance, 78.6% said they would be willing to pay an equal or higher cost compared to their current eye drop treatment.<sup>87,88</sup> The challenge for Elutimed will be regulatory rather than market-based.

Table 5.1: Competitors						
Competitor	Product	Material	Minimally Invasive	Biodegradable	Anti-fibrotic	Approval Status
Abbvie	Durysta	Gelatin cross-linked with glutaraldehyde	Yes	Yes	No	FDA approved
Mati Therapeutics	Evolute	Polymer	Yes	No	No	Phase II
Ocular Therapeutix	OTX-TP	Polymer	Yes	No	No	Phase III
EyePoint Pharmaceuticals	Durasert	Polymer	Yes	Yes	No	Phase I
Glaukos	iDose	Titanium	Yes	No	no	Phase II
Elutimed	Elutiglass	PLGA	No	Yes	Yes	Pre-clinical

Elutimed, and other glaucoma start-ups like it, face steep regulatory hurdles to reach approval by the FDA. The current state of the ophthalmologic device field makes it unclear if a product like Elutimed’s drug delivery system would be treated as a drug or as a device-drug combination product.<sup>81</sup> An additional financial hurdle is that complete product development must abide by current Good Manufacturing Practices (GMP).<sup>89</sup> The company must report how they intend to fulfill cGMP requirements through an IND filing.<sup>80</sup>

Current Good Manufacturing Process (cGMP) are the rules and guidelines laid out in the code of federal regulations (Title 21 CFR Part 210). 21 CFR 310, details how to document these

practices as it relates to filing an investigational new drug (IND) application with the FDA. As stated previously, the IND delineates the chemistry, manufacturing, and controls of a drug product. Composition, toxicology, pharmacokinetics, pharmacodynamics, dosage form, stability, and description of active and inactive ingredients all fall under the heading of chemistry. Manufacturing is described as the machinery, processes, and location of each step of the production of a drug substance or drug product. This includes the packaging, labeling, and sterilization of the product. The controls described in this section are stability, identity, and degradation tests, as well as quality assurance/quality controls that are required in cGMP.

With drug release systems and other complex drug products, it is hard to predict how requirements like sterilization will affect the final product. The two polymer-based products in our study responded differently to irradiation with our p(HEMA)-based hydrogel crosslinking and our PLGA-based system undergoing chain scission. Understanding the reaction of these polymers is critical to the commercial success of the drug product. We also did not fully understand the impact of various packing techniques on the drug products. These types of activities are costly in time and money for university spin-outs who have little of both.

The scale-up from a laboratory setting to this manufacturing setting is onerous and comes with a large capital requirement. One study estimated the cost of bringing a product through IND submission as \$3.2 million. With the IND preparation costing \$780,000 of that total. For a drug delivery platform, the authors predicted that number to lower to \$2.35 million.<sup>90</sup> This process is anticipated to take 3-5 years from clinical formulation development to IND filing. This timeline, however, counts on strategizing early about cGMP chemistry manufacturing and controls. This is where finding strategic partners early can bolster the chance of a product's success. After IND filing, clinical trials can take another 2-3 years before completion and then approval by the FDA.



The IND also details the protocols that will be followed for in-human clinical trials. Here, a sponsor needs to detail the study sites and how the trial will be blinded if applicable. They also will detail the number of patients, and admission criteria into the trial. Sponsors will also include information on data collection and analysis including trial endpoints.

To date, Elutimed has raised seed funds to translate its product to a GMP facility and to complete pre-clinical testing of its device. The company will need another round of approximately \$3 million in funding to perform first in human trials. The most likely exit for Elutimed would be acquisition by a major player in the glaucoma space. Potential buyers include Abbvie, who recently acquired Allergan and its Durysta implant; Alcon, who holds a 52.2% market share in the glaucoma market; and J&J which has a track record of purchasing high-tech biopharma start-ups. To make itself an attractive target for such an acquisition, Elutimed should seek to derisk its products by completing the IND filing.

## Chapter 6 - Conclusion and Future Work

Many innovations in academia halt their growth after the initial proof of concept studies. Commercialization is not a core tenant of academic philosophy; the academic goal of free information exchange seemingly conflicts with creating a product to compete in a marketplace. Participating in a commercial endeavor, however, may be the key to disseminating technological innovations more broadly. The Bayh-Dole Act, which gave research institutions the right to patented inventions funded by government grants, passed through Congress in 1980 to encourage the broader use of university innovations. Universities have traditionally relied on licensing their innovations to established companies in the 40 years since the Bayh-Dole Act, though this last decade has seen a new focus on investigator-led start-ups carrying the burden of commercialization. As we saw in chapter 5, the majority of new products in the ocular drug delivery space are led by start-ups. With the landscape in academia shifting, it is important to study an innovation's life cycle to de-risk it for the market. New projects should consider the scale-up necessary for manufacturing, the packaging and storage, and the regulatory hurdles a new product might face.

We applied this strategy to our polymer-based drug delivery systems. We were able to redesign the manufacturing process of the poly(Hydroxyethyl methacrylate)-based drug delivery system and test its properties after sterilization. The resulting scale-up more than halved the time to create a single mitomycin C-loaded hydrogel. We also introduced a method using a vacuum chamber that allowed for hundreds of these hydrogels to be loaded simultaneously. We demonstrated the reaction of the p(HEMA) hydrogel to gamma and e-beam radiation and how both slowed the release of mitomycin C from the hydrogel matrix. Future work will consider the

stability of the hydrogel and active ingredient by employing a forced-degradation study. Also, reducing the waste of the active ingredient during loading will drastically improve any potential margins for the product.

For the poly(lactic-co-glycolic acid)-based drug delivery system, we created a manufacturing process that could scale-up and reproducibly make hundreds of wafers in a week. We developed a method for quantifying the amount of drug in a whole wafer or a piece of a wafer. We tested the long-term stability of the films in various storage conditions. We also showed how the product reacts after sterilization. We plan to repeat the phosphate-buffered saline release with the lyophilized product after six months in storage to ensure stability. Additional future studies include using mass spectroscopy to characterize the byproducts of degradation. Potentially, the degradation products of 5-fluorouracil may appear in our release assay but are not biologically active. Automating more of the manufacturing process would drastically improve reproducibility and reduce the time necessary to make each product.

The next iterations of these drug delivery systems will benefit from the know-how reported in this document. The next step for these products is to develop a minimally invasive version of the product. The competitors in this market all seem to focus on injectable drug delivery systems. No product yet exists for a sustained release on antifibrotics after glaucoma surgery. Our preliminary results indicate that this is a feasible route of delivery though proof of concept has yet to be established in an animal model (see appendix).

These drug delivery systems are close to being registered as an investigational new drug with the FDA, which would signify the final step before moving into in-human clinical trials. This is a tremendous hurdle for a new product. It is unlikely that an established company would have invested the intellectual and material capital necessary to bring these products to this stage had the academic research effort ended with the initial proof of concept studies. The presented

studies have increased the potential impact of these products and improved their chances of being translated to the market. The clinical trials will ensure the safety of the drug delivery systems and show if they improve upon the current best practices utilized during glaucoma surgery.

## References

1. Allingham, R. *et al.* Shields' Textbook of Glaucoma. in (2020).
2. Reddy, V. N. Dynamics of transport systems in the eye. Friedenwald lecture. *Investig. Ophthalmol. Vis. Sci.* (1979).
3. Worthen, D. M. Histology of the Human Eye. *Arch. Ophthalmol.* (1972)  
doi:10.1001/archopht.1972.01000030236034.
4. McLaren, J. W. Measurement of aqueous humor flow. *Experimental Eye Research* (2009)  
doi:10.1016/j.exer.2008.10.018.
5. Radenbaugh, P. A. *et al.* Concordance of aqueous humor flow in the morning and at night in normal humans. *Investig. Ophthalmol. Vis. Sci.* (2006) doi:10.1167/iovs.06-0154.
6. Sit, A. J., Nau, C. B., McLaren, J. W., Johnson, D. H. & Hodge, D. Circadian variation of aqueous dynamics in young healthy adults. *Investig. Ophthalmol. Vis. Sci.* (2008)  
doi:10.1167/iovs.07-1139.
7. Nemesure, B., Honkanen, R., Hennis, A., Wu, S. Y. & Leske, M. C. Incident Open-angle Glaucoma and Intraocular Pressure. *Ophthalmology* (2007)  
doi:10.1016/j.ophtha.2007.04.003.
8. Heijl, A., Bengtsson, B., Hyman, L. & Leske, M. C. Natural History of Open-Angle Glaucoma. *Ophthalmology* (2009) doi:10.1016/j.ophtha.2009.06.042.
9. Ahmed Glaucoma Valve | World's Leading Glaucoma Drainage Device.  
<https://www.newworldmedical.com/ahmed-glaucoma-valve/> (2020).
10. Suzuki, R. & Susanna, R. Early transconjunctival needling revision with 5-fluorouracil versus medical treatment in encapsulated blebs: A 12-month prospective study. *Clinics*

- 68, 1376–1379 (2013).
11. Gedde, S. J., Singh, K., Schiffman, J. C. & Feuer, W. J. The Tube Versus Trabeculectomy Study: Interpretation of results and application to clinical practice. *Current Opinion in Ophthalmology* vol. 23 118–126 (2012).
  12. Atkinson, J., Boden, T., Mocho, J. P. & Johnson, T. Refining the unilateral ureteral obstruction mouse model: No sham, no shame. *Lab. Anim.* **0**, 1–9 (2020).
  13. Sgalla, G., Franciosa, C., Simonetti, J. & Richeldi, L. Pamrevlumab for the treatment of idiopathic pulmonary fibrosis. *Expert Opin. Investig. Drugs* **29**, 771–778 (2020).
  14. Caja, L. *et al.* TGF- $\beta$  and the tissue microenvironment: Relevance in fibrosis and cancer. *Int. J. Mol. Sci.* **19**, (2018).
  15. Khaw, P. T. *et al.* Modulation of wound healing after glaucoma surgery. *Curr. Opin. Ophthalmol.* **12**, 143–148 (2001).
  16. Witte, M. B. & Barbul, A. General principles of wound healing. *Surg. Clin. North Am.* **77**, 509–528 (1997).
  17. Chang, L., Crowston, J. G., Cordeiro, M. F., Akbar, A. N. & Khaw, P. T. The role of the immune system in conjunctival wound healing after glaucoma surgery. *Surv. Ophthalmol.* **45**, 49–68 (2000).
  18. Cabourne, E., Clarke, J. C. K., Schlottmann, P. G. & Evans, J. R. Mitomycin C versus 5-Fluorouracil for wound healing in glaucoma surgery. *Cochrane Database Syst. Rev.* **2015**, (2015).
  19. Longley, D. B., Harkin, D. P. & Johnston, P. G. 5-Fluorouracil: Mechanisms of action and clinical strategies. *Nat. Rev. Cancer* **3**, 330–338 (2003).
  20. van Groeningen, C. J. *et al.* pharmacokinetics of 5-fluorouracil assessed with a sensitive mass spectrometric method in patients on a dose escalation schedule. *Cancer Res.* **48**,

- 6956–6961 (1988).
21. Stevens, C. L. *et al.* Chemistry and Structure of Mitomycin C. *J. Med. Chem.* **8**, 1–10 (1965).
  22. Yosizawa, Z., Sato, T. & Schmid, K. Hydrazinolysis of  $\alpha$  1 -acid glycoprotein. *BBA - Gen. Subj.* **121**, 417–420 (1966).
  23. Verweij, J. & Pinedo, H. M. Mitomycin C: mechanism of action, usefulness and limitations. *Anticancer. Drugs* **1**, 5–13 (1990).
  24. Amoozgar, B., Lin, S. C., Han, Y. & Kuo, J. A role for antimetabolites in glaucoma tube surgery: Current evidence and future directions. *Curr. Opin. Ophthalmol.* **27**, 164–169 (2016).
  25. Grover, D. S., Kornmann, H. L. & Fellman, R. L. Historical Considerations and Innovations in the Perioperative Use of Mitomycin C for Glaucoma Filtration Surgery and Bleb Revisions. *J. Glaucoma* **29**, 226–235 (2020).
  26. Wu, Z., Li, S., Wang, N., Liu, W. & Liu, W. A comparative study of the safety and efficacy effect of 5-fluorouracil or mitomycin C mounted biological delivery membranes in a rabbit model of glaucoma filtration surgery. *Clin. Ophthalmol.* **7**, 655–662 (2013).
  27. Fredenberg, S., Wahlgren, M., Reslow, M. & Axelsson, A. The mechanisms of drug release in poly(lactic-co-glycolic acid)-based drug delivery systems - A review. *International Journal of Pharmaceutics* vol. 415 34–52 (2011).
  28. Sharma, P., Negi, P. & Mahindroo, N. Recent advances in polymeric drug delivery carrier systems. *Adv. Polym. Biomed. Appl.* 369–388 (2018).
  29. Kopeček, J. Hydrogels: From soft contact lenses and implants to self-assembled nanomaterials. *J. Polym. Sci. Part A Polym. Chem.* **47**, 5929–5946 (2009).
  30. Reddy, D. V. N. & Kinsey, V. E. Composition of the Vitreous Humor in Relation to That of

- Plasma and Aqueous Humors. *AMA. Arch. Ophthalmol.* **63**, 715–720 (1960).
31. Davis, S. S. Drug delivery systems. *Interdiscip. Sci. Rev.* **25**, 175–183 (2000).
  32. Porter, T. L., Stewart, R., Reed, J. & Morton, K. Models of hydrogel swelling with applications to hydration sensing. *Sensors* **7**, 1980–1991 (2007).
  33. Gentile, P., Chiono, V., Carmagnola, I. & Hatton, P. V. An overview of poly(lactic-co-glycolic) Acid (PLGA)-based biomaterials for bone tissue engineering. *Int. J. Mol. Sci.* **15**, 3640–3659 (2014).
  34. Lyu, S. & Untereker, D. Degradability of polymers for implantable biomedical devices. *International Journal of Molecular Sciences* vol. 10 4033–4065 (2009).
  35. Makadia, H. K. & Siegel, S. J. Poly Lactic-co-Glycolic Acid (PLGA) as Biodegradable Controlled Drug Delivery Carrier. *Polymers (Basel)*. **3**, 1377–1397 (2011).
  36. Ayyala, D., Blake, D. A., John, V. T. & Ayyala, R. S. A glaucoma drainage device incorporating a slow-release drug delivery system for the management of fibrosis. *Biomaterials and Regenerative Medicine in Ophthalmology: Second Edition* 349–367 (2016) doi:10.1016/B978-0-08-100147-9.00014-6.
  37. Blake, D. A. *et al.* Inhibition of cell proliferation by mitomycin C incorporated into P(HEMA) hydrogels. *J. Glaucoma* **15**, 291–298 (2006).
  38. Sahiner, N. *et al.* Creation of a Drug-Coated Glaucoma Drainage Device Using Polymer Technology. *Arch. Ophthalmol.* **127**, 448–453 (2009).
  39. Schoenberg, E. D. *et al.* Effect of Two Novel Sustained-Release Drug Delivery Systems on Bleb Fibrosis: An In Vivo Glaucoma Drainage Device Study in a Rabbit Model. *Transl. Vis. Sci. Technol.* **4**, 4 (2015).
  40. Ponnusamy, T., Yu, H., John, V. T., Ayyala, R. S. & Blake, D. A. A novel antiproliferative drug coating for glaucoma drainage devices. *J. Glaucoma* **23**, 526–534 (2014).



41. Zhang, A., Bai, H. & Li, L. Breath Figure: A Nature-Inspired Preparation Method for Ordered Porous Films. *Chem. Rev.* **115**, 9801–9868 (2015).
42. Madej, W., Budkowski, A., Raczowska, J. & Rysz, J. Breath figures in polymer and polymer blend films spin-coated in dry and humid ambience. *Langmuir* **24**, 3517–3524 (2008).
43. Park, M. S. & Kim, J. K. Breath figure patterns prepared by spin coating in a dry environment. *Langmuir* **20**, 5347–5352 (2004).
44. Ponnusamy, T. *et al.* In vitro degradation and release characteristics of spin coated thin films of PLGA with a “breath figure” morphology. *Biomatter* **2**, 77–86 (2012).
45. Swann, F. B. *et al.* Effect of 2 Novel Sustained-release Drug Release Systems on Bleb Fibrosis: An in Vivo Trabeculectomy Study in a Rabbit Model. *J. Glaucoma* **28**, 512–518 (2019).
46. Morris, Z. S., Wooding, S. & Grant, J. The answer is 17 years, what is the question: Understanding time lags in translational research. *J. R. Soc. Med.* **104**, 510–520 (2011).
47. Health Economics Research Group, B. U., Office of Health Economics & Europe, R. Medical Research: What’s it worth? Estimating the economic benefits of research in the UK. 1–108 (2008).
48. Osawa, Y. & Miyazaki, K. An empirical analysis of the valley of death: Large-scale R&D project performance in a Japanese diversified company. *Asian J. Technol. Innov.* **14**, 93–116 (2006).
49. Abuhanoğlu, G. & Özer, A. Radiation sterilization of new drug delivery systems. *Interv. Med. Appl. Sci.* **6**, 51–60 (2014).
50. Galante, R., Pinto, T. J. A., Colaço, R. & Serro, A. P. Sterilization of hydrogels for biomedical applications: A review. *J. Biomed. Mater. Res. - Part B Appl. Biomater.* **106**,

- 2472–2492 (2018).
51. Hill, D. J. T., O'Donnell, J. H., Pomery, P. J. & Saadat, G. Degradation of poly(2-hydroxyethyl methacrylate) by gamma irradiation. *Radiat. Phys. Chem.* **48**, 605–612 (1996).
  52. Montanari, L. *et al.* Gamma irradiation effects on poly(DL-lactide-co-glycolide) microspheres. *J. Control. Release* **56**, 219–229 (1998).
  53. Sayin, B. & Çaliş, S. Influence of accelerated storage conditions on the stability of vancomycin-loaded poly(D,L-lactide-co-glycolide) microspheres. *Fabad J. Pharm. Sci.* **29**, 111–116 (2004).
  54. Fonte, P. Optimization of Lyophilization Parameters of Polymeric Nanoparticles for Delivery of Therapeutic Proteins. (2015).
  55. de Oliveira, A. R. *et al.* Monitoring structural features, biocompatibility and biological efficacy of gamma-irradiated methotrexate-loaded spray-dried microparticles. *Mater. Sci. Eng. C* **80**, 438–448 (2017).
  56. Davison, L., Themistou, E., Buchanan, F. & Cunningham, E. Low temperature gamma sterilization of a bioresorbable polymer, PLGA. *Radiat. Phys. Chem.* **143**, 27–32 (2018).
  57. Conlon, R., Saheb, H. & Ahmed, I. I. K. Glaucoma treatment trends: a review. *Can. J. Ophthalmol.* **52**, 114–124 (2017).
  58. Johnson, L. N. Glaucoma: our role in reducing the burden of blindness. *J. Natl. Med. Assoc.* **94**, 908–911 (2002).
  59. Friedman, D. S. Prevalence of Open-Angle Glaucoma among Adults in the United States. *Arch. Ophthalmol.* **122**, 532–538 (2004).
  60. Lusthaus, J. & Goldberg, I. Current management of glaucoma. *Med. J. Aust.* **210**, 180–187 (2019).

61. Wichterle, O. & Lim, D. Hydrophilic Gels for Biological Use. *Nature* **185**, 117–118 (1960).
62. García-Millán, E., Koprivnik, S. & Otero-Espinar, F. J. Drug loading optimization and extended drug delivery of corticoids from pHEMA based soft contact lenses hydrogels via chemical and microstructural modifications. *Int. J. Pharm.* **487**, 260–269 (2015).
63. Kapoor, Y. & Chauhan, A. Ophthalmic delivery of Cyclosporine A from Brij-97 microemulsion and surfactant-laden p-HEMA hydrogels. *Int. J. Pharm.* **361**, 222–229 (2008).
64. Li, C. C., Abrahamson, M., Kapoor, Y. & Chauhan, A. Timolol transport from microemulsions trapped in HEMA gels. *J. Colloid Interface Sci.* **315**, 297–306 (2007).
65. Ciolino, J. B. *et al.* A drug-eluting contact lens. *Investig. Ophthalmol. Vis. Sci.* **50**, 3346–3352 (2009).
66. Box, G. E. . Non-Normality and Tests on Variances. **40**, 318–335 (1953).
67. Rein, D. B. *et al.* The economic burden of major adult visual disorders in the United States. *Arch. Ophthalmol.* **124**, 1754–1760 (2006).
68. Lichter, P. R. *et al.* Interim clinical outcomes in the collaborative initial glaucoma treatment study comparing initial treatment randomized to medications or surgery. *Ophthalmology* **108**, 1943–1953 (2001).
69. Short, B. G. Safety Evaluation of Ocular Drug Delivery Formulations: Techniques and Practical Considerations. *Toxicol. Pathol.* **36**, 49–62 (2008).
70. Bunz, U. H. F. Breath figures as a dynamic templating method for polymers and nanomaterials. *Adv. Mater.* **18**, 973–989 (2006).
71. Butler, D. Crossing the valley of death. *Nature* **453**, 840–842 (2008).
72. Davison, L., Themistou, E., Buchanan, F. & Cunningham, E. Low temperature gamma sterilization of a bioresorbable polymer, PLGA. *Radiat. Phys. Chem.* **143**, 27–32 (2018).

73. Hausberger, A. G., Kenley, R. A. & DeLuca, P. P. Gamma Irradiation Effects on Molecular Weight and in Vitro Degradation of Poly(D,L-Lactide- CO-Glycolide) Microparticles. *Pharm. Res. An Off. J. Am. Assoc. Pharm. Sci.* **12**, 851–856 (1995).
74. Sakar, F. *et al.* Nano drug delivery systems and gamma radiation sterilization. *Pharm. Dev. Technol.* **22**, 775–784 (2017).
75. Türker, N. S., Özer, A. Y., Çolak, Ş., Kutlu, B. & Nohutçu, R. ESR investigations of gamma irradiated medical devices. *Appl. Radiat. Isot.* **130**, 121–130 (2017).
76. Brígido Diego, R., Salmerón Sánchez, M., Gómez Ribelles, J. L. & Monleón Pradas, M. Effect of  $\gamma$ -irradiation on the structure of poly(ethyl acrylate-co-hydroxyethyl methacrylate) copolymer networks for biomedical applications. *J. Mater. Sci. Mater. Med.* **18**, 693–698 (2007).
77. Montheard, J. P., Chatzopoulos, M. & Chappard, D. 2-Hydroxyethyl methacrylate (hema): Chemical properties and applications in biomedical fields. *J. Macromol. Sci. Part C* **32**, 1–33 (1992).
78. Smith, T. A History of Lyophilization in Pharmaceutical Applications..pdf. *Pharm. Technol.* 44–49 (2004).
79. Wang, B., McCoy, T. R., Pikal, M. J. & Varshney, D. *Lyophilization of Therapeutic Proteins in Vials: Process Scale-Up and Advances in Quality by Design. Lyophilized Biologics and Vaccines* (2015). doi:10.1007/978-1-4939-2383-0\_7.
80. Ali, Y. & Lehmuusaari, K. Industrial perspective in ocular drug delivery. *Adv. Drug Deliv. Rev.* **58**, 1258–1268 (2006).
81. Novack, G. D. Ophthalmic drug delivery: Development and regulatory considerations. *Clin. Pharmacol. Ther.* **85**, 539–543 (2009).
82. Mccarthy, B. C. Glaucoma market to grow to \$ 3 billion by 2023 PRODUCTS SOLD. *Optom.*

*Times* **7**, 5 (2015).

83. Varadaraj, V., Kahook, M. Y., Ramulu, P. Y. & Pitha, I. F. Patient Acceptance of Sustained Glaucoma Treatment Strategies. *J. Glaucoma* **27**, 328–335 (2018).
84. Iriondo, J. & Jordan, J. Older people projected to outnumber children for first time in U.S. history. (2018).
85. Curran, J. Looking up : An aging population and higher disposable income will bolster revenue Ophthalmic Instrument Manufacturing in the US About this Industry. 1–39 (2019).
86. Schweitzer, J. New Drugs and Delivery Options In Glaucoma. *Mod. Optometry* 22–24 (2020).
87. Chan, H. H., Wong, T. T., Lamoureux, E. & Perera, S. A Survey on the Preference of Sustained Glaucoma Drug Delivery Systems by Singaporean Chinese Patients: A Comparison between Subconjunctival, Intracameral, and Punctal Plug Routes. *J. Glaucoma* **24**, 485–492 (2015).
88. Wang, B. B., Lin, M. M., Nguyen, T. & Turalba, A. V. Patient attitudes toward novel glaucoma drug delivery approaches. *Digit. J. Ophthalmol. DJO* **24**, 16–23 (2018).
89. Kaufman, B. & Novack, G. D. Compliance issues in manufacturing of drugs. *Ocul. Surf.* **1**, 80–85 (2003).
90. Strovel, J. *et al.* Early Drug Discovery and Development Guidelines: For Academic Researchers, Collaborators, and Start-up Companies. *Assay Guid. Man.* 1–35 (2004).

## Supplementary Information

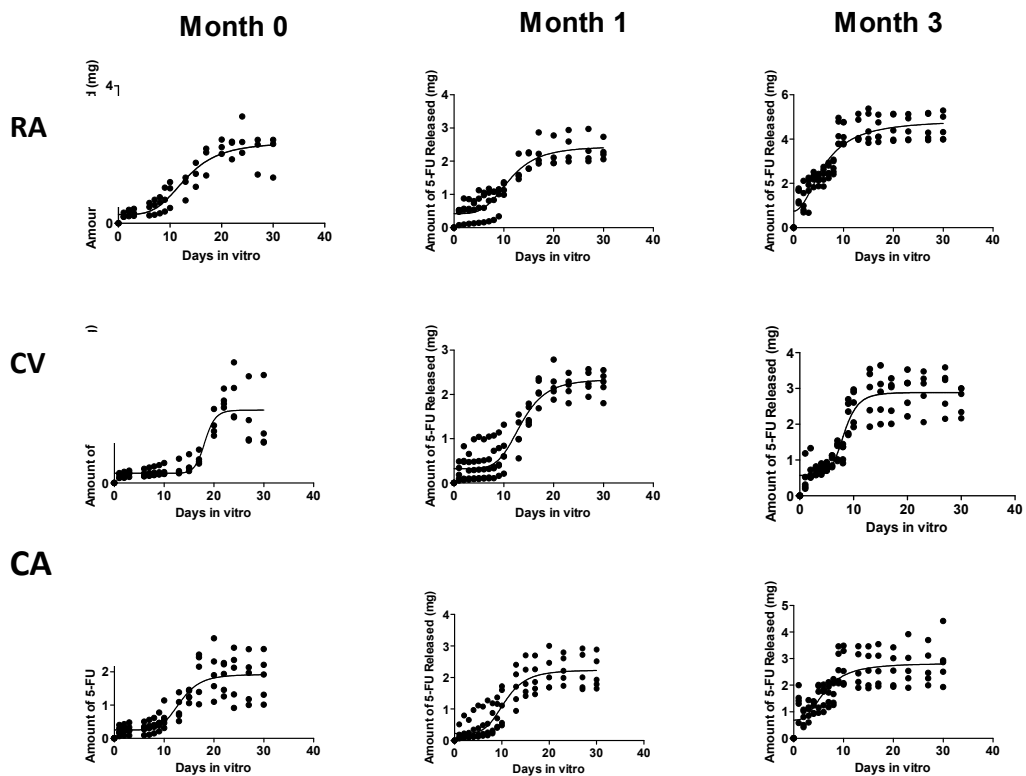


**Table S.1** Curves fit to the PBS releases of the gamma-sterilized PLGA in different storage conditions. The curves are Room-atmosphere(RA), Cold-vacuum (CV) and Cold-Atmosphere (CA) groups at months 0, 1 and 3. The RV curves can be found in Figure 4.6

R <sup>2</sup> Values For Curve fit to Hill Equation			
	Month 0	Month 1	Month 3
Cold-Vacuum (CV)	0.80	0.87	0.85

<b>Room-Vacuum (RV)</b>	0.83	0.85	0.71
<b>Cold-Atmosphere (CA)</b>	0.76	0.81	0.63
<b>Room-Atmosphere (RA)</b>	0.86	0.84	0.84

<b>Table S.2: p Values of Bonferroni Post-tests for 50% Coefficient on Curve Fits</b>				
	<b>RV</b>	<b>RA</b>	<b>CV</b>	<b>CA</b>
<b>RV0</b>		<b>0.001</b>	ns	<b>0.001</b>
<b>RV1</b>		<b>0.001</b>	ns	<b>0.001</b>
<b>RV3</b>		ns	<b>0.05</b>	ns
<b>RA0</b>	<b>0.001</b>		<b>0.001</b>	ns
<b>RA1</b>	<b>0.001</b>		<b>0.001</b>	ns
<b>RA3</b>	ns		<b>0.05</b>	ns
<b>CV0</b>	ns	<b>0.001</b>		<b>0.001</b>
<b>CV1</b>	ns	<b>0.001</b>		<b>0.001</b>
<b>CV3</b>	<b>0.05</b>	<b>0.05</b>		<b>0.001</b>
<b>CA0</b>	<b>0.001</b>	ns	<b>0.001</b>	
<b>CA1</b>	<b>0.001</b>	ns	<b>0.001</b>	
<b>CA3</b>	ns	ns	<b>0.001</b>	

<b>Table S.3: p Values of Bonferroni Post-tests for Sigmoidicity Coefficient on Curve Fits</b>				
	<b>RV</b>	<b>RA</b>	<b>CV</b>	<b>CA</b>
<b>RV0</b>		ns	<b>0.001</b>	ns
<b>RV1</b>		<b>0.001</b>	ns	<b>0.05</b>
<b>RV3</b>		<b>.001</b>	<b>0.001</b>	<b>0.001</b>
<b>RA0</b>	ns		<b>0.001</b>	<b>0.001</b>
<b>RA1</b>	<b>0.001</b>		<b>0.05</b>	ns
<b>RA3</b>	<b>0.001</b>		<b>0.001</b>	ns
<b>CV0</b>	<b>0.001</b>	<b>0.001</b>		<b>0.001</b>
<b>CV1</b>	ns	<b>0.05</b>		ns
<b>CV3</b>	<b>0.001</b>	<b>0.001</b>		<b>0.001</b>
<b>CA0</b>	ns	<b>0.001</b>	<b>0.001</b>	
<b>CA1</b>	<b>0.05</b>	ns	ns	

CA3	0.001	ns	0.001	
-----	-------	----	-------	--

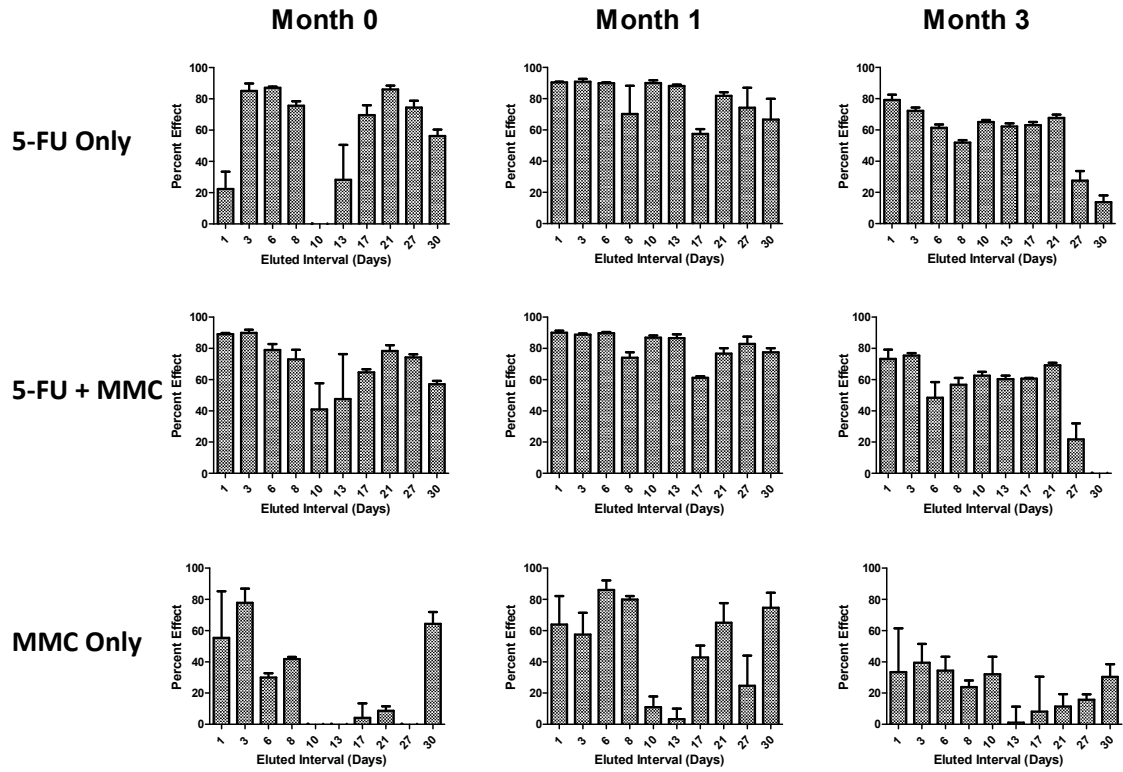


Figure S.4: Assay results for the cytotoxicity studies for the Cold-vacuum group of films.



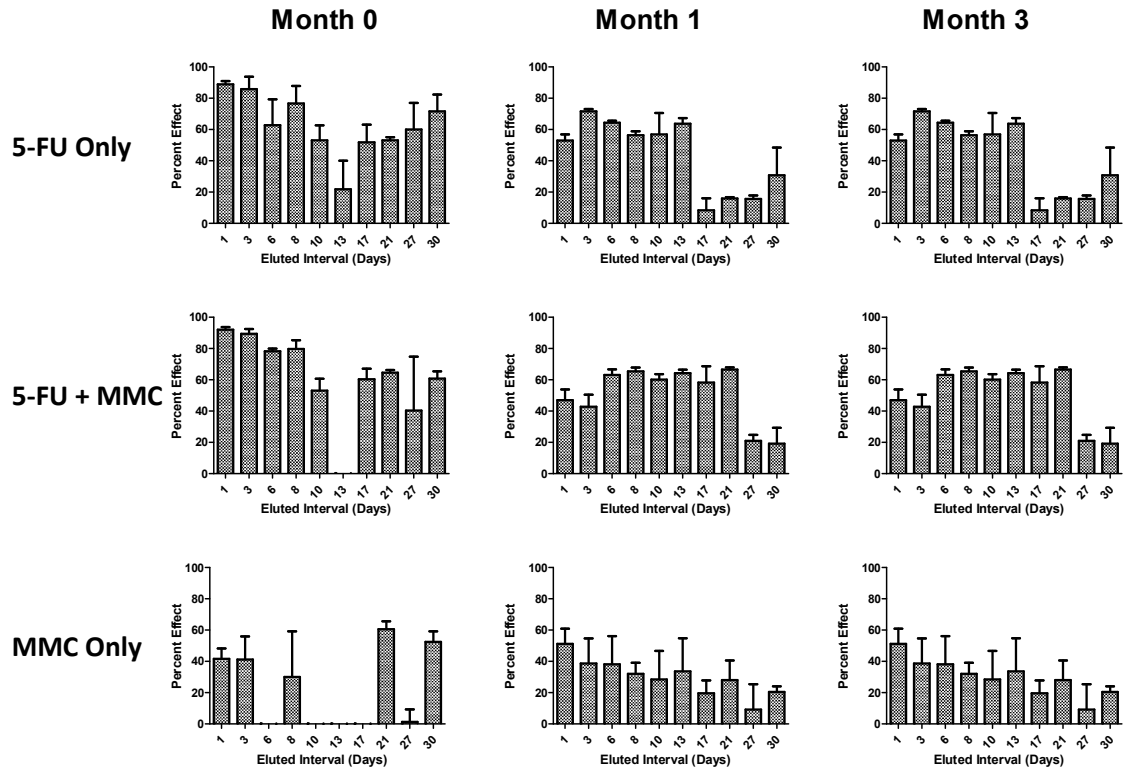


Figure S.5 Assay results for the cytotoxicity studies for the room-vacuum group of films.

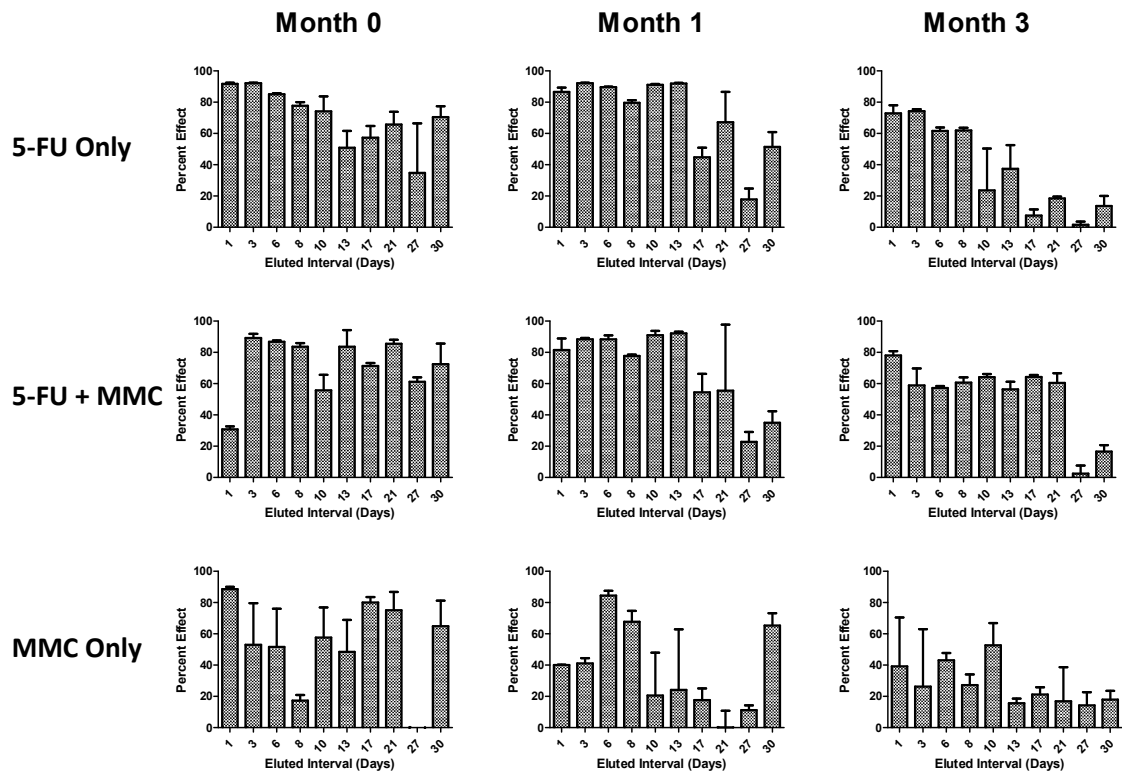


Figure S.6 Assay results for the cytotoxicity studies for the Cold-atmosphere group of films.

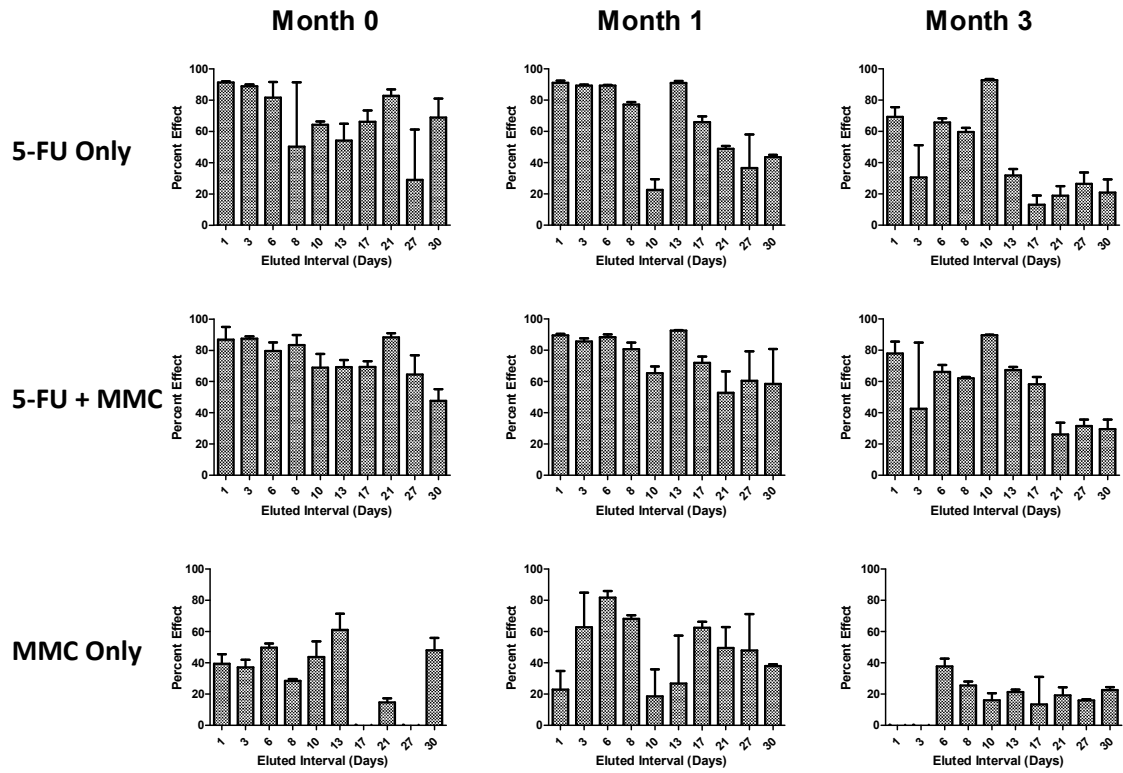


Figure S.7 Assay results for the cytotoxicity studies for the Room-atmosphere group of films.

Table S.8 Tukey's Post-test for 5-FU only Films at Month 0					
Groups Compared	Mean Diff.	q	Significant? P < 0.05?	Summary	95% CI of diff
CV0 50 vs RV0 50	-4.791	0.6519	No	ns	-32.81 to 23.23
CV0 50 vs CA0 50	-12.26	1.668	No	ns	-40.28 to 15.76
CV0 50 vs RA0 50	-9.949	1.354	No	ns	-37.97 to 18.07
RV0 50 vs CA0 50	-7.47	1.016	No	ns	-35.49 to 20.55
RV0 50 vs RA0 50	-5.157	0.7017	No	ns	-33.18 to 22.87
CA0 50 vs RA0 50	2.312	0.3146	No	ns	-25.71 to 30.34

Table S.9 Tukey's Post-test for 5-FU + MMC Films at Month 0					
Groups Compared	Mean Diff.	q	Significant? P < 0.05?	Summary	95% CI of diff
CV0 5M vs RV0 5M	10.67	1.495	No	ns	-16.54 to 37.89
CV0 5M vs CA0 5M	-2.574	0.3606	No	ns	-29.79 to 24.64
CV0 5M vs RA0 5M	-5.017	0.7028	No	ns	-32.23 to 22.20
RV0 5M vs CA0 5M	-13.25	1.856	No	ns	-40.46 to 13.97
RV0 5M vs RA0 5M	-15.69	2.198	No	ns	-42.90 to 11.53
CA0 5M vs RA0 5M	-2.443	0.3422	No	ns	-29.66 to 24.77

Table S.10 Tukey's Post-test for MMC only Films at Month 0					
Groups Compared	Mean Diff.	q	Significant? P < 0.05?	Summary	95% CI of diff
CV0 MO vs RV0 MO	-5.544	0.4873	No	ns	-48.92 to 37.83
CV0 MO vs CA0 MO	-39.56	3.478	No	ns	-82.94 to 3.809
CV0 MO vs RA0 MO	-12.03	1.058	No	ns	-55.41 to 31.34
RV0 MO vs CA0 MO	-34.02	2.990	No	ns	-77.39 to 9.353
RV0 MO vs RA0 MO	-6.489	0.5704	No	ns	-49.86 to 36.88
CA0 MO vs RA0 MO	27.53	2.420	No	ns	-15.84 to 70.91

Table S. 11 Tukey's Post-test for 5-FU only Films at Month 1					
Groups Compared	Mean Diff.	q	Significant? P < 0.05?	Summary	95% CI of diff
CV1 50 vs RV1 50	36.37	5.116	Yes	**	9.264 to 63.48
CV1 50 vs CA1 50	8.819	1.240	No	ns	-18.29 to 35.93
CV1 50 vs RA1 50	14.51	2.041	No	ns	-12.59 to 41.62
RV1 50 vs CA1 50	-27.55	3.875	Yes	*	-54.66 to -0.4455
RV1 50 vs RA1 50	-21.86	3.074	No	ns	-48.97 to 5.250
CA1 50 vs RA1 50	5.695	0.8010	No	ns	-21.41 to 32.80

Table S.12 Tukey's Post-test for 5-FU + MMC Films at Month 1					
Groups Compared	Mean Diff.	q	Significant? P < 0.05?	Summary	95% CI of diff
CV1 5M vs RV1 5M	30.70	5.484	Yes	**	9.358 to 52.04
CV1 5M vs CA1 5M	12.78	2.284	No	ns	-8.557 to 34.12
CV1 5M vs RA1 5M	6.897	1.232	No	ns	-14.44 to 28.24
RV1 5M vs CA1 5M	-17.92	3.201	No	ns	-39.26 to 3.426
RV1 5M vs RA1 5M	-23.80	4.252	Yes	*	-45.14 to -2.461
CA1 5M vs RA1 5M	-5.887	1.052	No	ns	-27.23 to 15.45

Table S.13 Tukey's Post-test for MMC only Films at Month 1					
Groups Compared	Mean Diff.	q	Significant? P < 0.05?	Summary	95% CI of diff
CV1 MO vs RV1 MO	21.02	2.837	No	ns	-7.229 to 49.28
CV1 MO vs CA1 MO	13.71	1.850	No	ns	-14.54 to 41.96
CV1 MO vs RA1 MO	3.081	0.4158	No	ns	-25.17 to 31.33
RV1 MO vs CA1 MO	-7.311	0.9866	No	ns	-35.56 to 20.94
RV1 MO vs RA1 MO	-17.94	2.421	No	ns	-46.19 to 10.31
CA1 MO vs RA1 MO	-10.63	1.435	No	ns	-38.88 to 17.62

Table S.14 Tukey's Post-test for 5-FU only Films at Month 3					
Groups Compared	Mean Diff.	q	Significant? P < 0.05?	Summary	95% CI of diff
CV3 5O vs RV3 5O	12.79	1.624	No	ns	-17.23 to 42.81
CV3 5O vs CA3 5O	19.15	2.432	No	ns	-10.87 to 49.17
CV3 5O vs RV3 5O	13.53	1.718	No	ns	-16.49 to 43.55
RV3 5O vs CA3 5O	6.360	0.8077	No	ns	-23.66 to 36.38
RV3 5O vs RV3 5O	0.7398	0.09395	No	ns	-29.28 to 30.76
CA3 5O vs RV3 5O	-5.620	0.7138	No	ns	-35.64 to 24.40

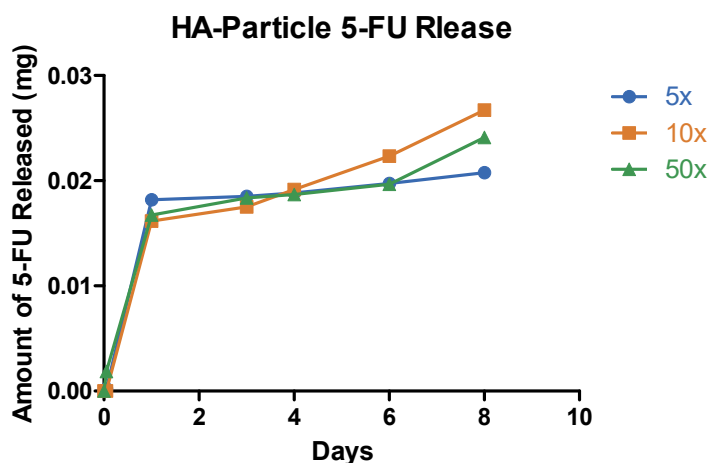
Table S.15 Tukey's Post-test for 5-FU + MMC Films at Month 3					
Groups Compared	Mean Diff.	q	Significant? P < 0.05?	Summary	95% CI of diff
CV3 5M vs RV3 5M	-4.832	0.5391	No	ns	-39.01 to 29.34
CV3 5M vs CA3 5M	-5.980	0.6671	No	ns	-40.15 to 28.19
CV3 5M vs RV3 5M	-9.153	1.021	No	ns	-43.33 to 25.02
RV3 5M vs CA3 5M	-1.147	0.1280	No	ns	-35.32 to 33.03
RV3 5M vs RV3 5M	-4.321	0.4821	No	ns	-38.49 to 29.85
CA3 5M vs RV3 5M	-3.174	0.3541	No	ns	-37.35 to 31.00

Table S.16 Tukey's Post-test for MMC only Films at Month 3					
Groups Compared	Mean Diff.	q	Significant? P < 0.05?	Summary	95% CI of diff
CV3 MO vs RV3 MO	-6.854	1.611	No	ns	-23.08 to 9.368
CV3 MO vs CA3 MO	-4.322	1.016	No	ns	-20.54 to 11.90
CV3 MO vs RV3 MO	8.216	1.931	No	ns	-8.006 to 24.44
RV3 MO vs CA3 MO	2.532	0.5951	No	ns	-13.69 to 18.75
RV3 MO vs RV3 MO	15.07	3.542	No	ns	-1.151 to 31.29
CA3 MO vs RV3 MO	12.54	2.947	No	ns	-3.683 to 28.76

## Appendix - Injectable drug delivery systems

### A.1 Hyaluronic acid particles

We have also begun work on creating an injectable version of this drug delivery system. In our first attempts, we loaded porous hyaluronic acid (HA) particles have been made by the Sahiner Lab in Turkey with 5-FU or MMC. The micro particles have different crosslinking densities. Higher crosslinking density leads to smaller the pores in the material and likely slower release times. We loaded 5x, 10x, and 50x crosslinked particles with either 5-Fluorouracil (5-FU) or mitomycin C (MMC) for use as an injectable therapeutic.



**Figure A.1.** 5-FU release from 5x, 10x, and 50x HA particles. Data are plotted as mean  $\pm$  SD (n=3).

HA particles (0.025 g) were placed in 5mL of dimethyl sulfoxide (DMSO) containing 0.1 mg/mL of either 5-FU or MMC. The particles were allowed to swell overnight before centrifuging them at 10,000 RPM and removing the supernatant. Drying attempts failed as DMSO has a very high boiling point (189°C). Further work is needed to find an alternative solvent for particle loading. The particles containing DMSO and drug were placed in 5mL of 7.2 pH PBS and kept in a

water bath at 37° C. An aliquot (1 mL) of eluate was removed at various time points and replaced with fresh PBS. The eluate was read spectrophotometrically and the results are shown in **Figures A.1** and **A.2**.

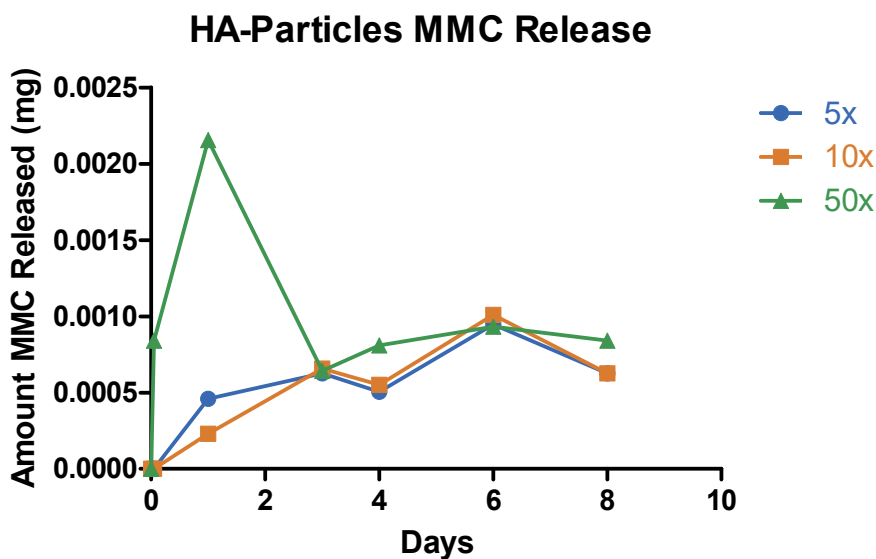


**Figure A.2** MMC released from 5x, 10x, and 50x HA particles. Data are plotted as mean  $\pm$  SD (n=3).

The release from the 5-FU particles was well defined. Most of the drug came out in the first day followed by a slow release for the next week. The amount of MMC released was very small and the results are unreliable. MMC is not stable in solution and is challenging to measure over long periods. We may need to adjust our release protocol to account for MMC degradation. The DMSO loading is not a viable option moving forward as the DMSO is nearly impossible to remove and is toxic to human cells. Further work will center on finding a water miscible solvent that will solubilize the 5-FU or MMC, preserve drug activity and HA particle structure, and be volatile enough to remove from the particles after drug loading.



## A.2 Physical conjugation of MMC to hyaluronic acid

Based on the difficulty of loading MMC into HA particles, we attempted the covalent conjugation of MMC to hyaluronic acid (HA). We used a 10-molar excess (as carboxyl groups) of 1-ethyl-3-(3-dimethylaminopropyl)carbodiimide (EDC) to activate the carboxyl groups of the HA.

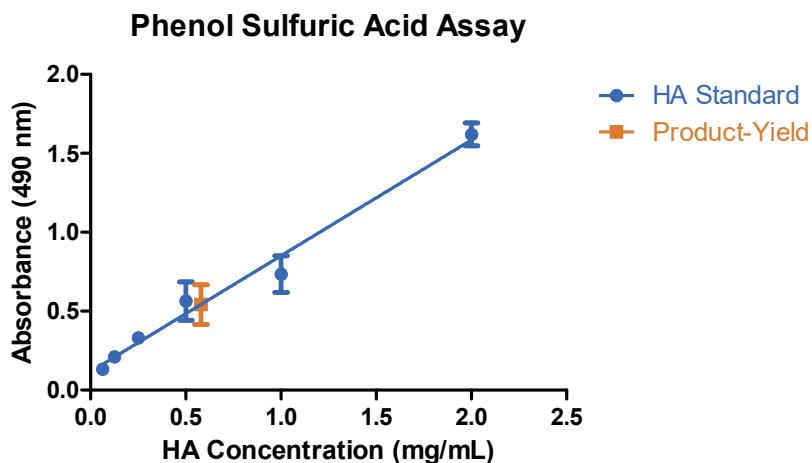


**Figure A.3:** Phenol-sulfuric acid assay to determine the yield of our conjugation experiment.

The approximate yield was 0.63 mg. Data are represented as mean  $\pm$  SD (n=3)

After 15 minutes, we added a 5 molar excess of MMC to the activated HA and allowed the reaction to progress of 2 h. The MMC-HA product was purified by dialysis against PBS, we characterized the product by measuring the amount of HA in the dialyzed product using the phenol sulfuric acid assay (Masuko 2005), using HA as a standard. **Figure A.3** shows the standard curve for HA (Blue Circles) and the amount of the HA in the dialyzed product (Orange Square). Total yield of HA in the dialyzed product was 63%.

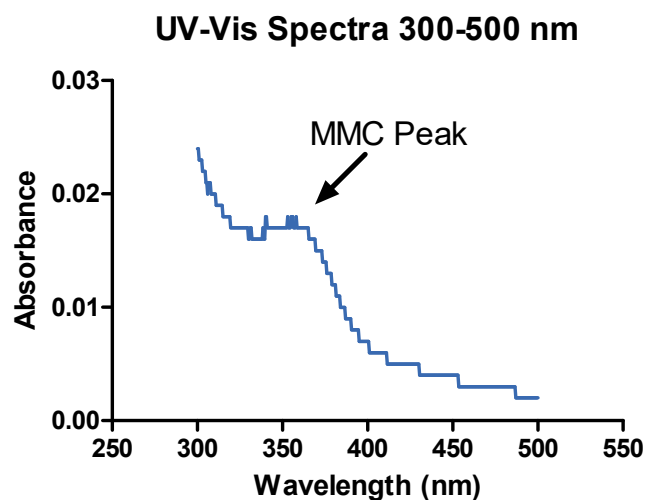


**Figure A.4:** a UV-Vis spectra of the reaction product showing a peak at 360 which corresponds with the presence of MMC. This spectra was collected using the dialysate to blank the spectrophotometer.

MMC in the dialyzed product was determined via UV-Vis spectroscopy as shown in **Figure A.4**. The UV-Vis spectra shows the characteristic peak of MMC as 360 nm. Coupling efficiency was low; in this experiment we conjugated 0.3 $\mu$ g of MMC to 6.3mg of HA. **Figure A.5** shows that the MMC-HA conjugate, even at the low levels of coupling achieved in this preliminary study, retained the ability to inhibit the proliferation of COS-1 cells. Controls in the cytotoxicity test included no additives, PBS, the dialysate from the MMC-HA conjugation, and hyaluronic acid present at an approximate concentration in the conjugate. Now that we have developed all the assays for characterization of the conjugate, we will concentrate on increasing the efficiency of our conjugation procedures.

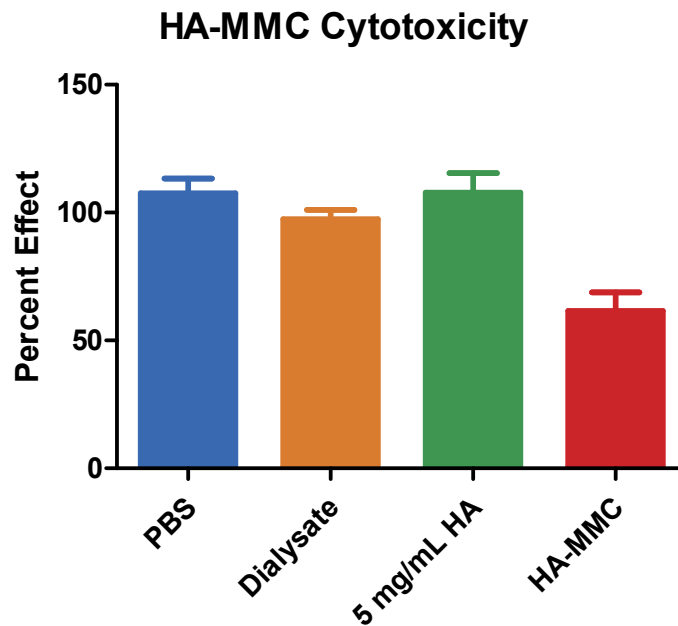


**Figure A.5:** COS-1 cells were treated with the reaction product to determine if the MMC present was still reactive. The HA-MMC conjugate was compared to PBS, the Dialysate, an equivalent amount of hyaluronic acid with no MMC, and no treatment. There was a significant decrease in cell viability when treated with the HA-MMC conjugate. Data are represented as mean  $\pm$  SD (n=3)

These preliminary results are very encouraging and could lead to new intellectual property for Elutimed. Further work needs to be done to make the reaction more efficient. The next milestone for this project is to increase the amount of MMC loaded onto the hyaluronic acid. Then we will attempt to conjugate the MMC to hyaluronic acid particles provided by Dr. Sahiner. Then, the release rate of MMC from the hyaluronic acid will be determined and possibly tuned by increasing the cross link density of the particles. Ideally, this product could be administered once post-operatively and remain in the bleb for 5-10 days before being absorbed.

## **Biography**

Mitchell Fullerton was born with his twin brother and near-constant companion in Lubbock, TX in 1990. The son of an Air Force pilot, Mitchell moved frequently, living in eight different cities before graduating high school in Dover, DE. Growing up, Mitchell benefited from parents who made scholastic success a priority for him and his siblings. Mitchell participated in marching band, track and field, and drama in high school before heading the Clemson University in South Carolina for a degree in Biomedical Engineering. While in undergrad, Mitchell participated in research projects in imaging, atomic force microscopy, genetics, and biomechanics. He was an active member of Clemson Wesley, serving as the President in his senior year. Mitchell studied abroad at Nanyang Technological Institute in Singapore.

After completing his degree, Mitchell was accepted into the Bioinnovation Program at Tulane University where he participated in research rotations in the labs of Dr. Dianne Blake, Dr. Jeff Gimble, and Dr. Kristin Miller. He spent his first summer of graduate school interning at the Food and Drug Administration before rejoining Dr. Blake's lab to work on a collaboration with Dr. Ramesh Ayyala and Dr. Vijay John. While completing his studies, Mitchell volunteered for Great Minds in STEM's STEM Showdown with local high schools and lead two teams to victory. He also organized a regular game night with fellow graduate students and friends. During his research, Mitchell was able to set up a GMP manufacturing site for Dr. Ayyala's start-up, Elutimed, and contribute to the process of writing an investigational new drug filing with the Food and Drug Administration. Mitchell has started his career in technology transfer at Columbia University and is excited to start a life in New York with his wife, Devon Bowser.